OXIDATIVE CHEMISORPTION OF SO_2 ON γ - Al_2O_3 AND DEPOSITION OF H_2–PERMSELECTIVE SiO_2 FILMS

Thesis by

Suk Woo Nam

In Partial Fulfillment of the Requirements

for the Degree of

Doctor of Philosophy

California Institute of Technology

Pasadena, California

1989

(Submitted May 30, 1989)

To my parents

and

parents-in-law

ACKNOWLEDGEMENTS

I wish to thank Professor George R. Gavalas for his support throughout this work. He has been a good mentor. His scholarship and creativity have been a constant source of inspiration.

I'd like to thank Dr. Yesinowski in Chemistry for making it possible for me to use the FTIR spectrometer in Crellin. James Hansen helped me to use the FTIR instrument. I thank Donna Johnson for typing my manuscripts. I enjoyed my life here with many good friends and have appreciated their moral support.

I graciously acknowledge financial support from the Korean Government and the Chemical Engineering Department at CalTech.

I am very lucky to have a stable source of love and support from a very special family. I thank my parents, parents-in-law and all other family members for all their love. Special thanks goes to Sun Shin, my sister-in-law, for caring and supporting my family. She provided everything we needed.

Words do not justify in describing what SunSook's caring and understanding have meant to me. She has been my best friend since we met. Her patience and encouragement made all things possible. Daniel (KiHeon) and Michael (KiUng) were born here and have given us wonderful moments.

ABSTRACT

The interaction of SO_2 with $\gamma - Al_2O_3$ and the deposition of H_2 permselective SiO_2 films have been investigated. The adsorption and oxidative adsorption of SO_2 on $\gamma - Al_2O_3$ have been examined at temperatures 500-700°C by Fourier transform infrared spectroscopy (FTIR) and thermogravimetric analysis (TGA). At temperatures above 500°C most of SO_2 adsorbed on the strong sites on alumina. The adsorbed SO_2 species was characterized by an IR band at 1065 cm^{-1}. The equilibrium coverage and initial rate of adsorption decreased with temperature suggesting a two-step adsorption. When $\gamma - Al_2O_3$ was contacted with a mixture of SO_2 and O_2, adsorption of SO_2 and oxidation of the adsorbed SO_2 to a surface sulfate characterized by broad IR bands at 1070 cm^{-1}, 1390 cm^{-1} took place. The results of a series of TGA experiments under different atmospheres strongly suggest that surface SO_2 and surface sulfate involve the same active sites such that SO_2 adsorption is inhibited by already formed sulfate. The results also indicate a broad range of site strengths.

The desorption of adsorbed SO_2 and the reductive desorption of oxidatively adsorbed SO_2 have been investigated by microreactor experiments and thermogravimetric analysis (TGA). Temperature programmed reduction (TPR) of adsorbed SO_2 showed that SO_2 was desorbed without significant reaction with H_2 when H_2 concentration was low while considerable reaction occurred when 100% H_2 was used. SO_2 adsorbed on the strong sites on alumina was reduced to sulfur and H_2S. The isothermal reduction experiments of oxidatively adsorbed SO_2 reveal that the rate of reduction is very slow below 550°C even with 100% H_2. The reduction product is mainly composed of SO_2. TPR experiments of oxidatively adsorbed SO_2 showed that H_2S arose from a sulfate

strongly chemisorbed on the surface.

Films of amorphous SiO_2 were deposited within the walls of porous Vycor tubes by SiH_4 oxidation in an opposing reactants geometry : SiH_4 was passed inside the tube while O_2 was passed outside the tube. The two reactants diffused opposite to each other and reacted within a narrow front inside the tube wall to form a thin SiO_2 film. Once the pores were plugged the reactants could not reach each other and the reaction stopped. At 450°C and 0.1 and 0.33 atm of SiH_4 and O_2, the reaction was complete within 15 minutes. The thickness of the SiO_2 film was estimated to be about 0.1μm. Measurements of H_2 and N_2 permeation rates showed that the SiO_2 film was highly selective to H_2 permeation. The H_2:N_2 flux at 450°C varied between 2000-3000.

Thin SiO_2 films were heat treated in different gas mixtures to determine their stability in functioning as high-temperature hydrogen-permselective membranes. The films were heat-treated at 450 - 700°C in dry N_2, dry O_2, N_2-H_2O, and O_2-H_2O mixtures. The permeation rates of H_2 and N_2 changed depending on the original conditions of film formation as well as on the heat treatment. Heating in dry N_2 slowly reduced the permeation rates of both H_2 and N_2. Heating in a N_2-H_2O atmosphere led to a steeper decline of H_2 permeability. But the permeation rate of N_2 increased or decreased according to whether the film deposition had been carried out in the absence or presence of H_2O vapor, respectively. Thermal treatment in O_2 caused rapid decline of the permeation rates of H_2 and N_2 in films that were deposited under dry conditions. The decline was moderate in films deposited under wet conditions.

TABLE OF CONTENTS

LIST OF TABLES

Chapter I

Chapter II

Chapter IV

LIST OF FIGURES

Chapter I

Chapter II

Chapter III

CHAPTER I

Introduction

1.1 Control of Sulfur Oxide Emissions

Atmospheric sulfur oxide is a principal cause of acid deposition, frequently referred to as acid rain. A major source of SO_2 is combustion of sulfur-containing coal. Considerable amounts of sulfur oxide are also emitted from fluid catalytic cracking unit in petroleum refineries.

Sulfur dioxide from combustion of coal can be reduced by switching to lower sulfur coal or to processes that remove sulfur from coal before, during, or after combustion [1,2]. Physical coal cleaning is a currently available technology capable of removing 10-30% of sulfur from coal before combustion. The removal of SO_2 by injection of calcium-based sorbents into existing, coal-fired power plants has received much attention. Under certain combustion conditions these sorbents can achieve SO_2 control by forming solid sulfate, which is collected at the furnace outlet [3]. SO_2 reduction can also be achieved by fluidized-bed combustion (FBC) of coal mixed with sorbents (limestone, dolomite) [4].

The highest levels of SO_2 removal are currently achieved by postcombustion flue gas desulfurization (FGD) processes. Among many FGD systems, wet chemical processes that use lime or limestone as a reagent are by far the most prevalent. A typical system achieves 90% of sulfur removal and employs forced oxidation of reaction products to yield a solid waste consisting primarily of calcium sulfate. In recent years, dry FGD systems that use lime spray dryers for SO_2 removal have received considerable attention [5]. Both wet and dry FGD systems produce solid waste.

Regenerable sorbents eliminate the extensive solid disposal requirement associated with "throwaway" sorbents and, under suitable conditions, produce elemental sulfur as a useful product. The materials investigated as regenerable

sorbents are alkalized alumina [6,7], molten alkali carbonates [8], and metal oxides supported on alumina [9,10]. These sorbents react with SO_2 to form stable sulfates and can be regenerated by reduction of sulfates. The regenerable sorbents can be used in an unsteady way, with a two-step cycle of oxidative adsorption and reductive regeneration.

Steady removal of sulfur oxide from flue gas can be accomplished using a catalyst based on alumina. The well-known Claus reaction is carried out on activated alumina at moderate temperatures. The direct catalytic reduction of SO_2 by CO, H_2 and CH_4 on alumina-based catalysts has been extensively investigated [11-15].

The removal of sulfur oxide from fluid catalytic cracking (FCC) units has received considerable attention over the past few years. The source of sulfur oxide is organo-sulfur compounds contained in hydrocarbon feedstocks for FCC units. When this feedstock is cracked in the FCC units reactor, about 45-55 % of feed sulfur is converted to H_2S, about 35-45 % remains in the liquid products, and about 5-10 % is deposited on the catalyst in the coke [16]. During the coke-burning step in the FCC regenerator, the sulfur in the coke is oxidized to SO_2 or SO_3 (SO_x). The amount of SO_x emitted from the regenerator depends on the quantity of sulfur in the feed, coke yield, and conversion.

SO_x emissions are considerable in amount and are increasingly becoming the target of regulation. There are many ways to reduce SO_x emissions from the FCC. Flue gas scrubbing and feedstock hydrodesulfurization are effective means of SO_x control but are expensive. The least costly approach is the use of a SO_x-reduction catalyst or a transfer catalyst as an additive to the FCC catalyst inventory.

The mechanism for operation of a transfer catalyst has been discussed by others [17,18]. A schematic of a generally accepted mechanism is shown in Figure 1. In the regenerator, the coke on the spent cracking catalysts is burned to give a regenerated cracking catalyst. During the coke burning, the sulfur in the coke is converted to sulfur oxide. The transfer catalyst, metal oxide(MO), oxidatively captures SO_2 and forms surface metal sulfate.

$$S(\text{coke}) + O_2 \longrightarrow SO_2$$

$$SO_2 + \frac{1}{2}O_2 + MO \longrightarrow MSO_4$$

The regenerated cracking catalyst and the SO_x transfer catalyst then move to the reactor. In the reactor, the cracking catalyst cracks the hydrocarbon feedstock to lighter hydrocarbon and produces H_2, H_2S and sulfur-containing coke. At the same time, the metal sulfate on the surface of the SO_x catalyst is reduced by H_2 to metal sulfide or to metal oxide to release H_2S in the reactor.

$$MSO_4 + 4H_2 \longrightarrow MS + 4H_2O$$

$$MSO_4 + 4H_2 \longrightarrow MO + H_2S + 3H_2O$$

The spent catalysts then move to the stripper where they are treated with steam to flush out the volatile hydrocarbons. The steam also hydrolyzes the metal sulfide, making metal oxide and releasing H_2S.

$$MS + H_2O \longrightarrow MO + H_2S$$

The FCC units regenerator operates at temperatures about 670-730°C, while the reactor and stripper operate at about 480-540°C. A SO_x transfer catalyst has two functions: oxidative chemisorption and reductive decomposition. A number of studies have been made, to design a suitable SO_x transfer

catalyst. The important elements and compounds in a transfer catalyst (from the literature) are alumina, rare earth, platinum and magnesia.

Alumina-based catalysts have been used as regenerable SO_2 sorbents and a SO_x transfer catalysts. Alumina plays an important role in SO_2 adsorption and reduction steps as a sorbent and a catalyst. Much of the previous work on the fundamental adsorption and reduction reactions on alumina surfaces was carried out at temperatures below 500°C with a focus on the Claus reaction. The objective of the research described in the first part of this thesis is to determine the mechanism and kinetics of the interaction of SO_2 with γ-alumina at temperatures above 500°C. Adsorption and oxidative adsorption of SO_2 on alumina have been investigated with thermogravimetric analysis and Fourier transform infrared spectroscopy and are presented in Chapter II. In Chapter III the results on the reduction of adsorbed SO_2 and surface sulfates are presented.

1.2 Inorganic Membranes for Gas Separation

Membranes made from inorganic materials have received growing attention over the past few years. Comprehensive reviews of inorganic membranes can be found elsewhere [19]. These membranes have thermal, structural and chemical stabilities that the most well-established polymeric membranes do not have. Thus inorganic membranes can be used for gas separation at high temperatures or under corrosive conditions. One example is the recovery of hydrogen from the purge stream of ammonia synthesis reactors. This recovery is practiced today using hollow fiber polymeric membranes operating at ambient temperatures. Conducting this recovery with inorganic membranes, which can selectively permeate hydrogen at the temperature of ammonia synthesis, about 450°C, would improve the thermal efficiency of the overall process. In addition to their use

in separation, these membranes can be used both as separators and reactors in a single unit operation for some catalytic reactions, to increase yield and selectivity due to equilibrium displacement by continuous removal of one or more products, or suppression of undesirable side reactions by the controlled addition of the reactants [20].

Both microporous and nonporous inorganic membranes have been considered in gas separation application. Some nonporous materials are known to be permeable only to certain gases. Palladium and its alloys have been studied extensively in connection with hydrogen separation in certain dehydrogenation reactions [21,22]. Nonporous silver is selectively permeable to oxygen and has been studied with oxidation reactions [23]. Zirconium is known to be permeable to hydrogen [24]. Besides metals, silica glass is known to be highly selective for hydrogen permeation [25,26]. This selectivity towards hydrogen is due to the relatively easy permeation of small hydrogen molecules through openings in the glass network. Certain oxides like ZrO_2 and Bi_2O_3 are good conductors of oxygen and have been studied as solid-oxide electrolytes [27,28]. The low permeation rate of gases through nonporous membranes, however, limited their commercial usage.

Commercial microporous membranes made from metals, zirconia, alumina, silica have consistent quality and narrow pore size distribution nowadays and have been applied mainly to liquid separations. These porous inorganic membranes can be prepared in various ways and details are summarized in reference [19]. For gas separation the microporous inorganic membranes have not been used on a production scale. Porous glass and alumina membranes have been considered for gas separation and applied to the catalytic decomposition of H_2S

with simultaneous H_2 separation [29,30]. Operating at 800°C with MoS_2 and WS_2 catalysts, conversion twice as the reaction equilibrium conversion have been obtained. Shown in Table 1 are studies using inorganic membranes for H_2-N_2 separation. The separation selectivity of a microporous membrane is governed by Knudsen diffusion and is insufficient for gas separation and membrane reactors.

The selectivity of the microporous membranes can be increased by applying thin films of selective materials in or on a thick porous support using various film deposition techniques. Chapter IV describes deposition of SiO_2 films to increase the selectivity of H_2 permeation in a porous glass tube. Chemical vapor deposition of SiO_2 was chosen since it can be easily applied to porous substrates. Using silane oxidation reaction, thin films of SiO_2 were deposited within the walls of the porous Vycor tube. Since deposited SiO_2 was densified by H_2O, stability of the films was also examined.

REFERENCES

[1] E. S. Rubin, M. A. Cushey, R. J. Marnicio, N. Bloyd and J. F. Skea, *Environ. Sci. Technol.*, **20**, 960 (1986).

[2] "Clean Coal Use Technologies," DOE/S-0036, Energy Research Advisory Board, Department of Energy, Washington, D.C., Vols. I and II. (1985).

[3] G. H. Newton, D. J. Harrison, G. D. Silcox and D. W. Pershing, *Environmental Progress*, **5**, 140 (1986).

[4] E. J. Badin and G. C. Frazier, *Environ. Sci. Technol.*, **19**, 894 (1985).

[5] C. Jorgensen, J. C. S. Chamg and T. G. Brna, *Environmental Progress*, **6**, 26 (1987).

[6] J. W. Town, J. I. Paige and J. H. Russel, *Chem. Eng. Progr. Symposium Series*, **66**, 261 (1970).

[7] M. D. Schlesinger and E. G. Illig, *Chem. Eng. Progr. Symposium Series*, **67**, 46 (1971).

[8] R. D. Oldenkamp and E. D. Margolin, *Chem. Eng. Progress*, **65**, 73 (1969).

[9] R. F. Vogel, B. R. Mitchell and F. E. Massoth, *Environ. Sci. Technol.*, **8**, 432 (1974).

[10] G. R. Gavalas, S. Edelstein, M. Flytzani-Stephanopoulos and T. A. Weston, *A.I.Ch.E. J.*, **33**, 258 (1987).

[11] S. E. Kkalafalla, E. F. Foerster and L. A. Hass, *I&EC Prod. Res. Dev.*, **10**, 133 (1971).

[12] S. E. Kkalafalla and L. A. Hass, *J. Catal.*, **24**, 115 (1972).

[13] R. Querido and W. L. Short, *I&EC Prod. Res. Dev.*, **12**, 10 (1973).

[14] V. C. Okay and W. L. Short, *I&EC Prod. Res. Dev.*, **12**, 291 (1973).

[15] W. D. Hunter,Jr., J. C. Fedoruk, A. W. Michener and J. E. Harris, in "Sulfur Removal and Recovery," *Adv. Chem Ser. No. 139*, p. 23, ACS (1975).

[16] M. E. T. Habib,Jr., *Oil Gas J.* Aug. 8, 111 (1983).

[17] J. W. Byrne, B. K. Spernello and E. L. Leuenberger, *Oil Gas J.* Oct. 15, 101 (1984).

[18] J. D. Wall, *Hydrocarbon Processing* Oct. 45 (1984).

[19] H. P. Hsieh, *A.I.Ch.E. Symp. Series*, **84** 1 (1988).

[20] H. P. Hsieh, Paper presented at A.I.Ch.E. Meeting, Washington D.C. (1988).

[21] H. Nagamoto and H. Inouye, *Chem. Eng. Commun.*, **34** 315 (1985).

[22] N. Itoh, *A.I.Ch.E. J.*, **33** 1576 (1987).

[23] V. M. Gryaznov, V. I. Vedernikov and S. G. Gul'ysnova, *Kinet. Katal*, **27** 142 (1986).

[24] C. Hsu and R. E. Buxbaum, Paper presented at A.I.Ch.E. Meeting, New York (1987).

[25] V. O. Altemose, Paper presented at 7th Symposium on the Art of Glass Blowing, (1962).

[26] D. C. Boyd and D. A. Thompson, "Glass," in Encyclopedia of Chemical Technology, Vol. 11, p. 807 (1980).

[27] M. F. Carolan and J. N. Michaels, *Solid State Ionics*, **25** 207 (1987).

[28] A. O. Isenberg, *Solid State Ionics*, **3** 431 (1981).

[29] T. Kameyama, K. Fukuda, M. Fujushige, H. Yokohama and M. Dokiya, *Hydrogen Energy Prog.*, **2** 569 (1981).

[30] T. Kameyama, M. Dokiya, M. Fujushige, H. Yokohama and K. Fukuda, *I&EC Fund.*, **20** 97 (1981).

[31] K. Itaya, S. Sugawara, K. Arai and S. Saito, *J. Chem. Eng. Japan*, **17** 514 (1984).

[32] R. Ash, R. M. Barrer and T. Foley, *J. Membrane Sci.*, **1** 355 (1976).

[33] R. W. Tock and K. Kammermeyer, *A.I.Ch.E. J.*, **15** 715 (1969).

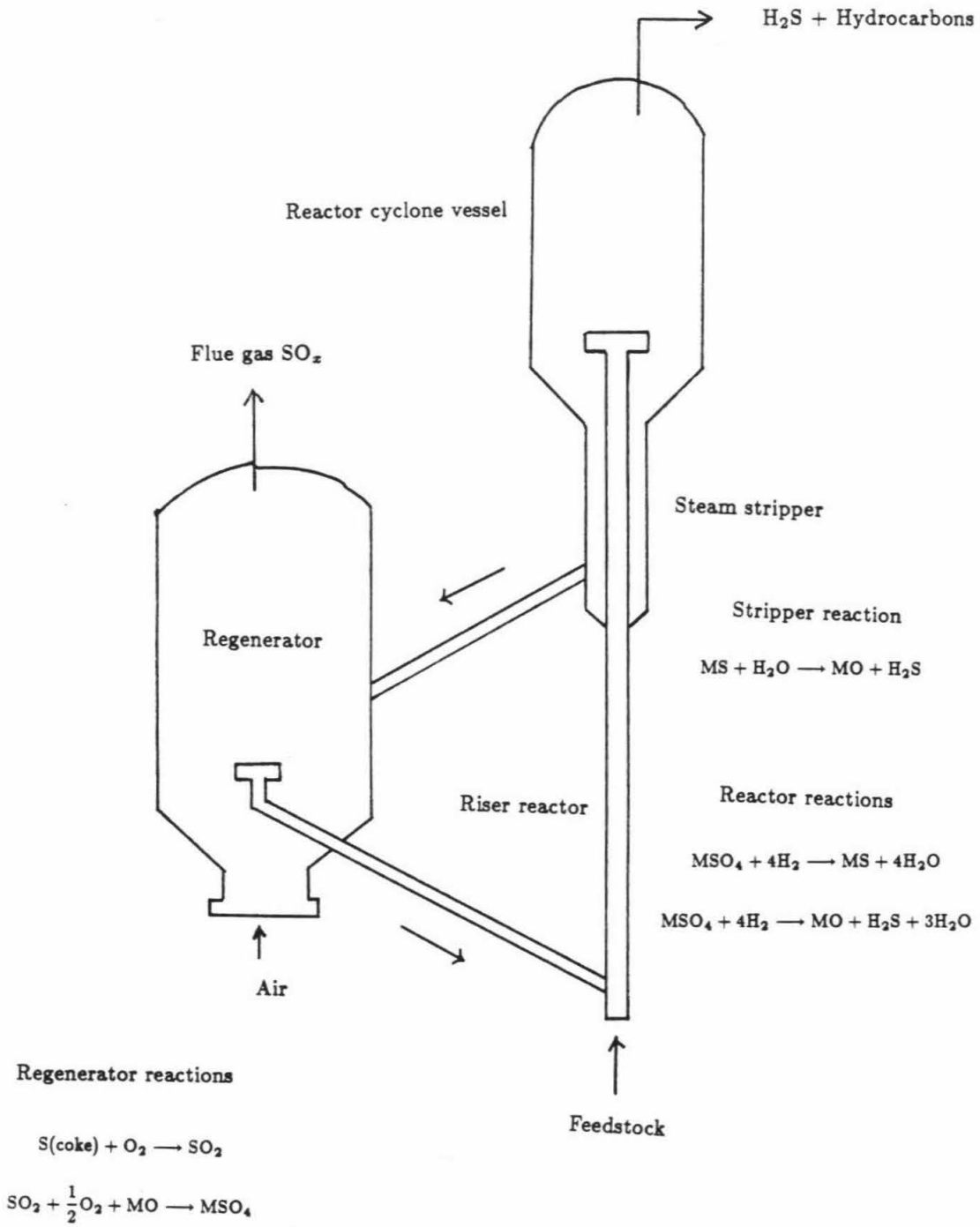

Figure 1. The mechanism for operation of a transfer catalyst in a typical FCC unit.

Table 1. H_2 separation by porous inorganic membranes.

Membrane material	Pore diameter (A°)	Gas mixture	Separation factor	Reference
Alumina	100-200	H_2/He	1.4	31
	100-200	H_2/N_2	4.1	31
	100-200	H_2/CO_2	5.0	31
	100-200	H_2/C_2H_6	4.1	31
	100-200	H_2/C_3H_8	5.0	31
Carbon		H_2/N_2	10-20	32
Glass	40	H_2/N_2	10-20	32
	40	H_2/N_2	2.5-3.6	33
	40	H_2/H_2S	1.9	30

CHAPTER II

Adsorption and Oxidative Adsorption of SO_2 on $\gamma - Al_2O_3$

ABSTRACT

The adsorption and oxidative adsorption of SO_2 on $\gamma - Al_2O_3$ have been investigated at temperatures of 500-700°C by Fourier transform infrared spectroscopy (FTIR) and thermogravimetric analysis (TGA). At temperatures above 500°C the adsorbed SO_2 species was characterized by an IR band at 1065 cm^{-1}. The equilibrium coverage and initial rate of adsorption decreased with temperature, suggesting a two-step adsorption. When $\gamma - Al_2O_3$ was contacted with a mixture of SO_2 and O_2, adsorption of SO_2 and oxidation of the adsorbed SO_2 to a surface sulfate characterized by broad IR bands at 1070 cm^{-1}, 1390 cm^{-1} took place. Sulfate formation was found to be reversible, but the reverse decomposition reaction took several hours even at 700°C. The results of a series of TGA experiments under different atmospheres ($SO_2 - O_2 - N_2$; $SO_2 - N_2$; $O_2 - N_2$; N_2) strongly suggest that surface SO_2 and surface sulfate involve the same active sites such that SO_2 adsorption is inhibited by already formed sulfate. The results also indicate a broad range of site strengths.

INTRODUCTION

Alumina, mostly in its γ form is used as a catalyst or sorbent for several sulfur removal and recovery processes. The most important of its catalytic applications involves the Claus reaction

$$2H_2S + SO_2 = 2H_2O + \frac{3}{2} S_2 \qquad (1)$$

used to convert H_2S removed from natural gas or refinery streams to elemental sulfur. The related reaction

$$2CO + SO_2 = 2CO_2 + \frac{1}{2} S_2 \qquad (2)$$

is also catalyzed by $\gamma - Al_2O_3$ with the catalytic activity greatly enhanced by the addition of iron or copper [1-3]. A similar reaction, the reduction of SO_2 with methane, has been commercialized [4].

Alumina has been investigated as a sorbent for *in situ* removal of SO_2 in combustion environments. In alkalized form, alumina was studied as a regenerable SO_2 sorbent in fluidized coal combustion [5-8]. In combination with a noble metal or a rare earth oxide component serving as an oxidation catalyst, $\gamma - Al_2O_3$ has been studied as a regenerable sorbent ("transfer catalyst") for SO_2 removal from fluid catalytic cracking regenerators. Several patents, *e.g.*, [9-11] and laboratory studies [12,13] have been published and the process is now commercial.

Much of the fundamental work on the $SO_2/\gamma - Al_2O_3$ system has been conducted at temperatures below 500°C with focus on the Claus reaction. The adsorption of SO_2 on $\gamma - Al_2O_3$ in the absence of oxygen was studied by IR spectroscopy from room temperature to 500°C [14-19]. Several surface

SO_2 species were identified, ranging in adsorption strength from physisorbed to strongly chemisorbed. In the most recent and detailed analysis, Datta *et al.* [19] identified five species: a species physically adsorbed on hydroxyl groups with bands at 1334 and 1148 cm^{-1}; a weakly chemisorbed species with bands at 1322 and 1140 cm^{-1}; two species chemisorbed on acidic (positively charged Al ions) sites with bands at 1255 and 1189 cm^{-1}; finally, one strongly chemisorbed species with a broad band about 1060 cm^{-1}. The last species is by far the most important at temperatures above 400°C and, essentially, the only one to be considered in connection to the desulfurization applications mentioned earlier. All other adspecies desorb readily below 400°C. The strongly chemisorbed species has the sulfite structure and is attached *via* the S atom [15,17,19] to an Al ion [17-19]. The nature of this adsorption was discussed in some detail in [19]. The strongly chemisorbed SO_2 reacts with H_2S at temperatures above 200°C [17,20], while the more weakly adsorbed species react at even lower temperatures [20]. In the aforementioned studies [15,17,19] it was found that increasing the calcination temperature of the sorbent increased the amount of the strongly chemisorbed species and shifted the band of that species to somewhat higher frequencies.

It has been known for some time that the presence of small amounts or even traces of oxygen in the feed of the Claus reactor caused gradual deactivation *via* aluminum sulfate formation [21,22]. The amount of accumulated sulfate over an extended period of catalyst use suggests the formation of the bulk aluminum sulfate rather than a surface compound. When $\gamma - Al_2O_3$ was exposed to SO_2 and O_2 at temperatures of 400°C or higher, an IR band at 1365 cm^{-1} appeared in addition to the band at 1060 cm^{-1}, which characterizes the strongly chemisorbed SO_2 [15,23]. Upon prolonged heating at 500°C (10

hours) the two bands intensified and shifted to 1100 and 1400 cm^{-1}. Thermal desorption studies showed that the bands at 1100 and 1400 cm^{-1} could not be removed until the sample was heated to 800°C. These two bands were attributed to an aluminum sulfate species, which could also be produced directly by chemisorption of SO_3. Below 400°C, oxygen had no effect on SO_2 chemisorption.

The adsorption of SO_2 on $\gamma - Al_2O_3$ in the presence of oxygen was studied recently thermogravimetrically [12] in connection with application to fluid catalytic cracking. This study showed that the amount of SO_2 chemisorbed in the presence of oxygen was about twice of that chemisorbed in the absence of oxygen and decreased as the temperature increased from 250 to 500°C. Further increase of the temperature from 500°C to 700°C caused an increase of the amount chemisorbed, opposite to what was observed in the absence of oxygen and consistent with a *kinetically limited* formation of a sulfate species.

In the aforementioned experimental studies [12,15,23] oxidative chemisorption of SO_2 was carried out on pure alumina. The process oriented studies [9-11,13], on the other hand, have used Al_2O_3 containing an oxidation catalyst such as platinum or a rare earth oxide in order to increase the rate of SO_2 removal. In the presence of the oxidation catalyst, SO_2 first oxidizes to gas-phase SO_3, which in turn reacts with alumina to form a sulfate. The mechanism of oxidative chemisorption in the absence of the oxidation catalyst has not been specifically investigated although one would expect that sulfate formation takes place by oxidation of surface SO_2 rather than by intermediate formation of gaseous SO_3.

In this paper we report our work on SO_2 adsorption and oxidative adsorp-

tion at temperatures of 500-700°C. Using transient IR and TGA experiments we have focused on the mechanism of sulfate formation and on the competitive coverage of alumina sites by SO_2 and surface sulfate.

EXPERIMENTAL

Materials

Gamma alumina (Al-1401-P) was obtained from Harshaw Chemical Corporation in the form of a powder with a particle size of approximately 60μ. This form of alumina is known to undergo considerable structural change upon thermal treatment. To assess the possible interference of this change with the planned high temperature adsorption experiments, preliminary measurements were made of BET surface area and SO_2 adsorption capacity after different calcination pretreatments. Calcination of each sample was carried out by passing air through a bed of alumina for one day at each temperature. The BET surface area and the SO_2 capacity at 200°C and SO_2 pressure of 50 Torr were measured by standard volumetric techniques. As shown in Figure 1 the specific surface area decreases with increasing calcination temperature while the SO_2 uptake goes through a maximum around 700°C. X-ray diffraction analysis of the sample calcined up to 700°C showed only the presence of $\gamma - Al_2O_3$ lines. When the calcination temperature exceeded 800°C, gradual change from $\gamma - Al_2O_3$ to $\delta - Al_2O_3$ was observed. Therefore, all samples used in the reaction experiments were calcined at 700°C. A mixture of SO_2 in N_2 was obtained from Matheson and was diluted with additional N_2 or air as required. All gases were passed through a water trap. The SO_2-N_2 mixture and the N_2 diluent were further purified by passing through an oxygen trap.

TGA

A Dupont 951 thermogravimetric analyzer interfaced with a micrcomputer was used to monitor the weight change of the sample during adsorption and desorption. Typically 20 mg of particles was placed on the quartz sample pan and pretreated in N_2 for 2 hours at 700°C. The total flow rate of the gases was 150 ml/min and the pressure was atmospheric. It was experimentally verified that under the conditions employed the reactions were free of external and internal mass transfer resistances.

FTIR

The alumina powder was ground to very fine particles and pressed at 10 MPa into self-supporting disks of approximately 15 mg/cm^2. Prior to each experiment the sample disk was evacuated at 700°C for 2 hours under pressure below 10^{-5} Torr. SO_2 was purified by freeze and thaw cycles and only the middle fraction was stored for use. In the kinetic experiments, SO_2 was admitted to the sample through an orifice and the system was adjusted to obtain the specified pressure.

The infrared spectra were scanned by a Mattson Sirius 100 FTIR operating in the transmission mode with a Globar source and a mercury-cadmium telluride detector operating at 77K. Typically, each spectrum was obtained by averaging 200 consecutive scans of 2 cm^{-1} resolution. In the kinetic experiments, 10 to 30 scans were used for each run. The spectra of adsorbed SO_2 and sulfate were obtained by a 1:1 subtraction of the spectrum of alumina before exposure to the gases from that after adsorption and reaction.

Two quartz infrared cells were used in the FTIR experiments. One is

similar to a Kiselev type cell [24] and was used to measure equilibrium adsorption isotherms and to examine the effects of heat treatment. With this cell the spectrum was always taken with evacuation at room temperature. The other cell shown in Figure 2 was used for the kinetic experiments. Placed in the middle section of the cell, the alumina wafer was heated by an external furnace and could be held at temperatures as high as 700°C for several hours. The total volume of the cell was relatively large, however, because of the cooling system protecting the NaCl window and O-rings in the window housing. At high temperatures, the heated sample emitted significant IR radiation, which had the effect of shifting the final adsorption band to lower wavenumbers. This effect was partially reduced by subtracting the spectrum of the heated sample obtained after masking the IR source of the instrument.

RESULTS AND DISCUSSION

1. Chemisorption of SO_2

a. TGA Results

The TGA was used to measure the amount of SO_2 adsorbed as a function of time under different temperatures and partial pressures of SO_2. Figure 3 shows the sample weight observed at different temperatures and 2200 ppm SO_2. At all temperatures, the sample weight increases very fast in the first few minutes and gradually approaches a constant value. The amount adsorbed decreases with temperature and, rather surprisingly, the initial rate of adsorption also decreases with temperature. The amounts of SO_2 adsorbed after 1 hour of exposure at different temperatures and concentrations of SO_2 are listed in Table 1. These results agree well with the data of Chang [15] who measured the adsorption

isotherm of SO_2 on $\gamma - Al_2O_3$ at temperatures up to 500°C using a volumetric method.

b. IR Results

As mentioned earlier, all alumina samples prior to FTIR experiments were calcined for two hours *in vacuo* at 700°C. The IR spectrum of the calcined alumina contained three bands, at 3790, 3730, and 3690 cm^{-1} due to surface hydroxyl groups. Upon adsorption of SO_2 at 500°C or higher the three hydroxyl bands were not affected, but two new bands appeared, a broad band at 1065 cm^{-1} and a shoulder at 1136 cm^{-1}. Figure 4 shows the spectra of alumina after exposure to 3 Torr of SO_2 for 30 minutes at 500°C and 700°C. In Figure 4 and in following figures only the region between 1000 and 1500 cm^{-1} is displayed.

In another experiment, successive doses of SO_2 were added to the IR cell at 500°C, the pressure was allowed to equilibrate and the peak intensity at 1065 cm^{-1} was recorded. This intensity versus pressure curve was compared with a weight versus pressure curve obtained in the TGA to relate the intensity with the amount of adsorbed SO_2. As shown in Figure 5 the relationship is linear and can serve to quantify the FTIR results. The correlation of Figure 5 was subsequently used to construct the adsorption isotherms shown in Figure 6 from the IR peak intensities. Isosteric heats of adsorption were calculated from the isotherms by utilizing the Clausius-Clapeyron equation. At coverage up to 3 mg/g the heat of adsorption was about 13 kcal/gmol.

During adsorption and desorption at 500°C and 700°C, the peak intensity at 1065 cm^{-1} was measured using the IR cell shown in Figure 2. The initial increase due to adsorption at 3 Torr of SO_2 was faster at 500°C, while the

decrease due to desorption under vacuum was faster at 700°C as shown in Figure 7. Considerable SO_2 remained on the surface after 15 minutes evacuation at 500°C. Upon heating this evacuated sample to 700°C for 1 hour, nearly all remaining SO_2 desorbed.

c. Discussion

Structure of Chemisorbed SO_2

In previous work [15,19] the bands at 1065 cm^{-1} and 1136 cm^{-1} were ascribed to symmetric (ν_s) and asymmetric (ν_a) S-O stretching vibrations of strongly bound SO_2. Since bands below 1000 cm^{-1} could not be observed owing to complete absorption by alumina, other forms of adsorbed SO_2 could not be excluded. However, the proportionality between the 1065 cm^{-1} band intensity and the SO_2 amount recorded with the TGA strongly suggest that the adsorbed SO_2 characterized by the band at 1065 cm^{-1} is the only surface species present.

Previous literature provides specific information about the structure of adsorbed SO_2. This species was proposed [15,19] to have the structure of sulfite on the basis of the similarity of its IR spectrum with that observed earlier in adsorption of SO_2 on MgO [25] and in unidentate sulfite complexes [26]. The bonding of SO_2 with the alumina surface could also be inferred from previous work concerning the bonding of SO_2 in a complex [27]. According to this report, SO_2 in a complex is O-bonded or S-bonded if $\nu_a - \nu_s$ is larger or smaller than 190 cm^{-1}, respectively. In our FTIR spectra, $\nu_a - \nu_s$ was always lower than 190cm^{-1} suggesting that the adsorbed SO_2 is bonded to the alumina through the sulfur atom. Adsorption in the form of a sulfite bound to the alumina *via* the

sulfur atom is also consistent with the observation [28] that sulfite coordination through sulfur would shift the S-O stretching band to higher frequencies than in the free sulfite ion (967, 933 cm^{-1}), whereas coordination through the oxygen would shift the same band to lower frequencies.

Kinetics and Mechanism of Adsorption

We first estimated the equilibrium surface coverage of SO_2 at different temperatures and pressures using the amount adsorbed, the BET surface area and the projected area for the SO_2 molecule, assuming close two-dimensional packing. The molecular area α was calculated by the equation of Emmett and Brunauer [29]:

$$\alpha = 1.09 \left[\frac{M}{N_0 \rho} \right]^{\frac{2}{3}} \quad (1)$$

where N_0 is Avogadro's number, M is molecular weight, and ρ is the density of the adsorbed molecules. Using in place of ρ the density of liquid SO_2 we estimated $\alpha = 0.1$ $m^2/\mu mole$ and with this value of α the coverage was found to be in the range 0.04 to 0.1 depending on the temperature and pressure of SO_2.

We next attempted to fit the transient adsorption-desorption curves of Figure 7 by Langmuir-Hinshelwood kinetics. For this purpose we used the early part of the desorption curves to estimate the desorption rate constants ($3x10^{-3}$ and 10^{-2} s^{-1} at 500 and 700°C) and the adsorption isotherm (Figure 6) to estimate the equilibrium constants (1.4 and 0.18 $Torr^{-1}$ at 500 and 700°C). With these equilibrium and desorption constants, the adsorption rate constants were calculated as $4.2x10^{-3}$ and $1.9x10^{-3}$ $(Torr\text{-}s)^{-1}$ at 500 and 700°C. These parameters provide a reasonable fit of the data in Figure 6 except for the tail of the

desorption curves, which cannot be fitted by first order kinetics. Furthermore, the estimated adsorption constants have the wrong temperature dependence, suggesting that simple Langmuir-Hinshelwood kinetics are not adequate. To explain the negative temperature coefficient of the initial rate of adsorption found both in the TGA and the FTIR experiments, one would need to postulate either very small activation energy for adsorption, or some other mechanism that involves multiple adsorbed species. The possibility of very low activation energy for adsorption is excluded by the low initial rates of adsorption observed experimentally. Thus we must turn to the possibility of stepwise adsorption involving a precursor species.

Stepwise adsorption of SO_2 is suggested by some previous experimental results. Chang [15] observed that when the Al_2O_3/SO_2 system was allowed to stand at room temperature for 2 hours, the intensity of the band at 1326 cm^{-1} declined while the intensity of the band at 1060 cm^{-1} increased. These changes suggest that species characterized by the band around 1330 cm^{-1} may be a precursor to the strongly chemisorbed SO_2 (band at 1065 cm^{-1}). The same results, however, can be explained by adsorption on weak (1330cm^{-1}) and strong(1065cm^{-1}) sites taking place in parallel in a batch system. Datta *et al.* [19] proposed a mechanism according to which SO_2 adsorbs on the basic sites of the alumina yielding a surface species with bands at 1322 and 1140 cm^{-1}. This weakly adsorbed species could then abstract an oxygen atom from the surface to form a strongly adsorbed species with bands at 1135 and 1065 cm^{-1} attached to the Al atoms in a unindentate fashion.

To examine the implications of stepwise adsorption, we considered the

simple sequence

$$SO_2(g) \underset{k_d^*}{\overset{\xi F_{SO_2}}{\rightleftharpoons}} SO_2^*(a) \underset{k_d}{\overset{k_a^*}{\rightleftharpoons}} SO_2(a) \qquad (2)$$

where ξ is the trapping probability of the incident molecule into the precursor state $SO_2^*(a)$, and F_{SO_2} is the incident flux of SO_2 molecules ($F_{SO_2} = \frac{P_{SO_2}}{\sqrt{2\pi MRT}}$). The rate constants $k_i = k_{i0} \exp[\frac{-E_i}{RT}]$ refer to chemisorption of the molecular precursor (i=a*), desorption of the precursor (i=d*), and desorption of the chemisorbed molecule (i=d). Assuming first order rate for all steps and eliminating the concentration of $SO_2^*(a)$ by the pseudo steady state approximation, we obtain the following expression for the initial rate of adsorption.

$$r_{a_0} = \frac{\xi F_{SO_2} k_a^*}{k_a^* + k_d^*} \qquad (3)$$

To be consistent with the experimental finding of decreasing rate of adsorption with increasing temperature, it is necessary that $E_d{}^* - E_a{}^* > 0$, i.e., the activation energy for desorption of the precursor be higher than the activation energy for conversion of the precursor to the final chemisorbed species. This situation is depicted in the schematic potential energy diagram of Figure 8 using the distance perpendicular to the surface as the reaction coordinate. At equilibrium the reaction sequence of Eq. 2 yields the adsorption isotherm

$$\frac{\theta_{SO_2}}{1 - \theta_{SO_2}} = \frac{\xi k_a^*}{k_d k_d^*} F_{SO_2} = K \qquad (4)$$

Expressing the equilibrium constant as $K = K_0 \exp[Q/RT]$ gives $Q = E_d^* + E_d - E_a^* = 13.4$ Kcal/mole.

2. Oxidative Chemisorption (SO_2, O_2)

a. IR Results and Discussion

(i) Formation of Surface Sulfate

Figure 9 shows the spectra from alumina that was exposed to a mixture of 7 Torr of SO_2 and 50 Torr of O_2 for 2 hours at 500 or 700°C and then evacuated for 30 minutes at the reaction temperature. The spectrum contains an intense band at 1390 cm^{-1} and a broad band at 1070 cm^{-1}. Similar bands were observed when SO_3 was adsorbed on $\gamma - Al_2O_3$ at room temperature [15], and when $\gamma - Al_2O_3$ was doped with $Al_2(SO_4)_3 \cdot 18H_2O$ [15,30] and heated above 400°C under vacuum. Therefore, the bands at 1390 cm^{-1} and 1070 cm^{-1} could be assigned to a sulfate compound. This sulfate is a surface species, since bulk $Al_2(SO_4)_3$ is unstable at temperatures above 600°C under the SO_2 and O_2 pressures employed in the reaction. The stability boundary between bulk $Al_2(SO_4)_3$ and $\gamma - Al_2O_3$ is shown in Figure 10.

Since the sulfate band at 1070 cm^{-1} is near the band of adsorbed SO_2 (1065 cm^{-1}), the intensity of the band at 1390 $cm^{-1}$was chosen to characterize the concentration of the sulfate species. Figure 11 shows the change of the intensity of the band at 1390 cm^{-1} during a reaction period and a subsequent evacuation period. Sulfate formation is about five times faster at 700°C than at 500°C. The change in the intensity of the band at 1390 cm^{-1} during evacuation shows that the surface sulfate is stable at 500°C and decomposes extremely slowly at 700°C. Only at 800°C the decomposition rate became significant with half time about 30 min.

In the next set of experiments we wished to determine whether or not sulfate is formed by direct oxidation of the chemisorbed SO_2. For this purpose an alumina sample, which had been exposed to 3 Torr of SO_2 at 700°C for 15 minutes, was evacuated for 10 minutes and then exposed to O_2 for 5 min-

utes while the temperature remained at 700°C. The spectra before and after exposure to oxygen are shown as curves a and b in Figure 12. Reaction with oxygen produces a new band at 1390 cm^{-1} and broadens the band at 1070 cm^{-1}, both characteristic of the surface sulfate. It is clear that the adsorbed SO_2 characterized by the band at 1065 cm^{-1} is oxidized to surface sulfate.

The oxidation experiments at 500°C yielded similar results as shown in Figures 12c and d. Since the amount of adsorbed SO_2 remaining on the surface before admission of O_2 was higher at 500°C, the amount of sulfate formed at that temperature was also higher. The reaction rate, however, was considerably lower.

(ii) Competition between chemisorbed SO_2 and sulfate for surface sites

In the next set of experiments, the alumina sample was exposed to a mixture of SO_2 (7 Torr) and O_2 (50 Torr) for a certain period, which we shall call the reaction period, and then was evacuated for 30 minutes. Curves a and b in Figure 13 show the spectra of the alumina sample at the end of a 5 minute reaction period at 500°C, and after evacuation, respectively. As in the experiments of Figure 9, the reaction produced bands at 1070 cm^{-1} and 1390 cm^{-1}. On evacuation, the band at 1390 cm^{-1} did not change but the band at 1070 cm^{-1} diminished, reaching the same peak height as the band at 1390 cm^{-1}. In view of the very low rate of sulfate decomposition (Figure 11), the decline in the 1070 cm^{-1} peak can be attributed to desorption of SO_2 that had adsorbed during the reaction period. When after reaction and evacuation the alumina sample was exposed to SO_2 (7 Torr) without oxygen, the peak at 1070 cm^{-1} increased nearly to the same level as before evacuation (Figure 13, curve c) confirming that after evacuation the sample possessed considerable capacity

for SO_2 adsorption.

Curves d and e show the spectra of the alumina sample after 2 hours reaction at 500°C (d) and subsequent evacuation (e). The decline of the peak at 1070 cm^{-1} upon evacuation is now very small, indicating negligible SO_2 adsorption capacity after two hours of reaction. Evidently, surface sulfate blocks sites that are active for SO_2 adsorption.

Similar results were obtained when reaction and evacuation were carried out at 700°C. Comparison of the spectra after 5 minutes of reaction and after subsequent evacuation showed that a small amount of SO_2 desorbed during the evacuation period. Sulfate decomposition during evacuation was very slow in agreement with the earlier results (Figure 11). Finally, the amount of SO_2 desorbed after evacuation following two hours of reaction was negligible.

b. TGA Results and Discussion

Figure 14 displays the weight of an alumina sample exposed to a series of flow sequences at 500°C or 700°C. Each sequence involved exposure to a stream of 1% SO_2 , 14% O_2 , balance N_2 ($SO_2/O_2/N_2$) for a period of 5, 10, or 70 minutes, followed by flow of either 1% SO_2 in N_2 (SO_2/N_2), 14% O_2 in N_2 (O_2/N_2), or pure N_2.

After 5 minutes of flow of $SO_2/O_2/N_2$ at 500°C, switching to O_2/N_2 or pure N_2 results in a loss of weight due to SO_2 desorption as established by the IR experiments. The weight loss in O_2/N_2 is somewhat lower due to slow oxidation of SO_2 occurring simultaneously with desorption. Switching to SO_2/N_2, on the other hand, increases the sample weight by virtue of SO_2 adsorption. When the initial flow of $SO_2/O_2/N_2$ lasts for 70 minutes, switching to flow of SO_2/N_2,

O_2/N_2, or pure N_2, does not cause any weight loss. This result is in agreement with the IR results of Figure 13, where extensive sulfation eliminated the SO_2 capacity of the surface. Two additional observations are worth making. First, the sulfate formation reaction at 500°C continues beyond 70 minutes under flow of $SO_2/O_2/N_2$, apparently implying that this reaction continues even after the SO_2 adsorption capacity has been eliminated. The second and related observation concerns the surface concentration of sulfate versus the equilibrium SO_2 capacity. At 1% SO_2 (7.6 Torr) the equilibrium surface concentration of SO_2 is 6.6 mg/g Al_2O_3, or about 0.1 mmol/g Al_2O_3. After 70 minutes of sulfation, the weight gain is 16 mg/g Al_2O_3, or 0.2 mmol/g Al_2O_3. Thus part of the surface sulfate is formed on sites that would not be occupied by SO_2 under equilibrium conditions.

We now turn to the flow sequences at 700°C. The weight gain under flow of $SO_2/O_2/N_2$ is about three times higher than the gain obtained at 500°C, due to faster sulfate formation, and despite lower SO_2 adsorption. After 5 minutes flow of $SO_2/O_2/N_2$, switching to O_2/N_2 or pure N_2 results in weight loss similar to that observed at 500°C. On the other hand, switching to SO_2/N_2 causes some weight increase, due to SO_2 adsorption.

After 70 minutes flow of $SO_2/O_2/N_2$, the rate of weight increase becomes very low and the surface species seem to be near equilibrium. Upon subsequent change of the flow to O_2/N_2 or pure N_2, the weight decreases similar to the previous run (after 5 minutes of $SO_2/O_2/N_2$ flow). However, unlike that previous run, switching to SO_2/N_2 also causes a weight decrease, indicating that sulfate decomposition more than compensates any concurrent SO_2 adsorption. The large coverage of surface sulfate generated during 70 minutes of exposure

to $SO_2/O_2/N_2$ has evidently eliminated the capacity for SO_2 adsorption as observed earlier in the IR experiments (Figure 13).

In attempting to relate the SO_2 adsorption capacity with the sulfate already on the surface we are faced with an apparent contradiction. The alumina surface after 5 minutes of $SO_2/O_2/N_2$ flow at 700°C with surface coverage of 25 mg/g has higher capacity for SO_2 adsorption than after 70 minutes of $SO_2/O_2/N_2$ flow at 500°C when the coverage is only 16 mg/g. This observation will be explained below in terms of site heterogeneity with respect to SO_2 adsorption and sulfate formation.

Similar experiments were carried out at 800°C. Although alumina undergoes a slow phase transformation and loss of surface area at 800°C, these should not greatly change the material within the two hours of the TGA experiment. Figure 15 compares experiments at 700 and 800°C where 70 minutes flow of $SO_2/O_2/N_2$ was succeeded by flow of pure N_2. There is little difference in the rate of sulfation between the two temperatures. However, the rate of the reverse decomposition is considerably faster at 800°C resulting in lower equilibrium coverage.

Figure 16 shows the weight gain at 500°C under 0.7% of SO_2 and different mole fractions of oxygen. The initial reaction rate is nearly the same as the initial adsorption rate suggesting that adsorption of SO_2 is the first step in sulfate formation followed by oxidation of the adsorbed SO_2. At 700°C and O_2 mole fraction above 1%, the initial reaction rate is nearly independent of O_2 concentration.

The results presented above are consistent with the hypothesis that adsorbed SO_2 is oxidized to surface sulfate, which remains at the original SO_2

adsorption site. There are strong indications that there is a broad range of site strengths. For a qualitative argument we may divide the SO_2 adsorption sites into two groups, strong sites and weak sites. The surface density of the weak sites is roughly $2x10^{17}cm^{-2}$ but the equilibrium coverage of SO_2 on these sites is too small to make a substantial contribution to the observed SO_2 coverage. Most of the SO_2 adsorption capacity is due to the strong sites.

Adsorbed SO_2 reacts with oxygen to form surface sulfate with a faster rate rate on the strong sites. SO_2 adsorbed on weak sites oxidizes very slowly at 500°C but quite rapidly at 700°C. These qualitative observations can be summarized in the reaction sequence

$$SO_2(g) \underset{k_1'}{\overset{k_1}{\rightleftharpoons}} SO_2^*(1)$$

$$SO_2^*(1) + \frac{1}{2}\, O_2 \underset{k_3'}{\overset{k_3}{\rightleftharpoons}} SO_3^*(1)$$

$$SO_2(g) \underset{k_2'}{\overset{k_2}{\rightleftharpoons}} SO_2^*(2)$$

$$SO_2^*(2) + \frac{1}{2}O_2 \underset{k_4'}{\overset{k_4}{\rightleftharpoons}} SO_3^*(2)$$

where (1) and (2) denote strong and weak sites while SO_2^*, SO_3^* denote adsorbed SO_2 and surface sulfate. The various rate constants are in the order $k_1/k_1' >> k_2/k_2'$. At 500°C $k_3 >> k_4$ but at 700°C k_3 and k_4 are comparable ($E_4 > E_3$). Finally, $k_3' << k_4'$.

The above scheme explains the previously noted anomalous effect of surface sulfate on SO_2 adsorption. We may assume that a site occupied by surface sulfate is unavailable for SO_2 adsorption. Now at 500°C, after 70 minutes of exposure to $SO_2/O_2/N_2$, all strong sites and a certain fraction of the weak sites are covered by sulfate. As a result, there is little capacity for SO_2 adsorption

in view of the low equilibrium coverage of the weak sites. In contrast, after 5 minutes flow of $SO_2/O_2/N_2$ at 700°C, the coverage by sulfate is higher than before, but more evenly distributed among strong and weak sites. A certain fraction of sites in both categories remains free, and the strong sites that are free provide the observed capacity for SO_2 adsorption.

c. Interaction of Surface Sulfate with Hydroxyl Group and Water

FTIR experiments were carried out to examine the role of surface hydroxyl group on alumina. Alumina disk was evacuated for 2 hours at 700°C and spectrum was scanned. Then SO_2 and O_2 were admitted to the sample and the spectra were scanned 2 hours after the reaction starts. As shown in Figure 16, there still was a considerable amount of surface hydroxyl group before the reaction but during the reaction the intensity of these hydroxyl bands was reduced. After 2 hour reaction and subsequent evacuation the intensity of hydroxyl bands was not restored to the original position. When only SO_2 was admitted at 700°C very little change in the intensities of the bands of OH group was observed. The irreversible reduction in intensity of OH group by the reaction means the removal of OH group during the reaction, and water may be produced by the reaction. Previously, Andersson *et al.* reported that the amount of SOx adsorption in a dry atmosphere is larger than that in a humid atmosphere [12]. From our observation it can be explained that if water vapor exists in the gas phase, water formation by OH group is not plausible, and the reactants that would drive OH group away and form sulfate on the surface in a dry atmosphere could not remove OH group.

At room temperature it is known that H_2O added to the sulfated alumina causes a chemical transformation and new bands are observed at the expense of the bands at 1400 and 1070cm^{-1} [23]. The species formed after water addition

at room temperature for 1 day was characterized by FTIR and laser Raman spectroscopy and the results were shown in Figures 18 and 19. Depending on the concentration of water, shifts of the bands to a lower wave number were observed, and after a long time of exposure to H_2O only one band was found by IR spectroscopy near 1180cm^{-1}. Raman spectrum, however, clearly shows the existence of inorganic sulfate, which was characterized by the band at 981cm^{-1}. Desorption of water by heating and evacuation of the sample which had been exposed to water vapor causes restoration of surface sulfate bands. The chemical transformation at room temperature can be written as

$$\text{sulfate(I)} + H_2O \rightleftharpoons \text{sulfate(II)}$$

where sulfate(I) is the product of the reaction under dry conditions and sulfate(II) is the species formed under humid conditions. Saur *et al.* proposed the structure of both sulfates [23].

CONCLUSIONS

Based on this study, we present the following conclusions : (1) Gamma-alumina has a broad distribution of site strengths, but above 500°C most of SO_2 adsorption capacity drives from the strong sites. (2) Adsorbed SO_2 is oxidized to surface sulfate which remains at the original SO_2 adsorption site. (3) The rate of oxidation of adsorbed SO_2 decreases with decreasing site strengths, but the weaker sites constitute the major fraction of the surface sulfate capacity.

REFERENCES

[1] S.E. Khalafalla, E.F. Foerster and L.A. Hass, *I&EC Prod. Res. Develop.*, **10**, 133 (1971).

[2] S.E. Khalafalla and L.A. Hass, *J. Catal.*, **24**, 115 (1972).

[3] R. Querido and W.L. Short, *I&EC Process Des. Develop.*, **12**, 10 (1973).

[4] W.D. Hunter,Jr., J.C. Fedoruk, A.W. Michener and J.E. Harris, "Sulfur Removal and Recovery," *Adv. Chem. Ser. No. 139,* ACS, p. 23 (1975).

[5] D. Bienstock, J.H. Field and J.G. Myers, Bureau of Mines Inv. No. 5735 (1961).

[6] J.W. Town, J.I. Paige and J.H. Russell, *Chem. Eng. Progress Symp. Series*, Vol. 66, No. 105 (1970) 261.

[7] M.D. Schlesinger and E.G. Illig, *Chem. Eng. Progress Symp. Series*, Vol. 67, No. 115 (1971) 46.

[8] G.R. Gavalas, S. Edelstein, M. Flytzani-Stephanopoulos and T.A. Weston, *A.I.Ch.E.J.*, **33**, 258 (1987).

[9] W.A. Blanton, Jr. and R.L. Flanders, U. S. Patent 4,071,436 (1978).

[10] I.A. Vasalos, U. S. Patent 4,153,534 (1979).

[11] J.S. Yoo and J.A. Jaecker, U. S. Patent 4,495,305 (1985).

[12] S. Andersson, R. Pompe and N-G. Vannerberg, *Appl. Catal.*, **16**, 49 (1985).

[13] A.A. Bhattacharyya, G.M. Woltermann, J.S. Yoo, J.A. Karch and W.E. Cormier, *I&EC Research*, **27**, 1356 (1988).

[14] A.V. Deo, I.G. Dalla Lana and H.W. Habgood, *J. Catal.*, **21**, 270 (1971).

[15] C.C. Chang, *J. Catal.*, **53**, 374 (1978).

[16] R. Fiedorow, I.G. Dalla Lana and S.E. Wanke, *J. Phys. Chem.*, **82**, 2474

(1978).

[17] H.G. Karge, I.G. Dalla Lana, S.T. de Suarez and Y. Zhang, *Proc.* 8th International Congress on Catalysis, Berlin, Vol.III, 453 (1984).

[18] H.G. Karge and I.G. Dalla Lana, *J. Phys. Chem.*, **88**, 1538 (1984).

[19] A. Datta, R.G. Cavell, R.W. Tower and Z.M. George, *J. Phys. Chem.*, **89**, 443 (1985).

[20] A. Datta and R.G. Cavell, *J. Phys. Chem.*, **89**, 454 (1985).

[21] Z.M. George, *Canad. J. Chem. Eng.*, **56**, 711 (1978).

[22] K.P. Goodboy, J.C. Downing and H.L. Fleming, *Oil and Gas J.*, Nov. 89 (1985).

[23] O. Saur, O.S. Bensitel, A.B. Mohammed Saad, J.C. Lavalley, C.P. Tripp and B.A. Morrow, *J. Catal.*, **99**, 104 (1986).

[24] H.G. Karge, *Z. Phys. Chem.* (Wiesbaden), **76**, 133 (1971).

[25] R.A. Schoonheydt and J.H. Lunsford, *J. Catal.*, **26**, 261 (1972).

[26] K. Nakamoto, "Infrared Spectra of Inorganic and Coordination Compounds, " 5th ed., Wiley, New York (1985).

[27] D.M. Byler and D.F. Shriver, *Inorg. Chem.*, **15**, 32 (1976).

[28] F.A. Cotton and R. Francis, *J. Am. Chem. Soc.*, **82**, 2986 (1960).

[29] P.H. Emmett and S. Brunauer, *J. Am. Chem. Soc.*, **59**, 1553 (1937).

[30] J. Preud'homme, J. Lamotte, A. Janin and J.C. Lavalley, *Bullt. Soc. Chim. France.*, **I**-433 (1981).

Table 1. Equilibrium adsorbed SO_2 [mg/g-alumina] at different temperatures and mol fraction of SO_2 (atmospheric total pressure).

T, °C	mole% of SO_2 0.22	0.66	1.10
500	5.0	6.2	6.6
600	3.5	5.2	5.8
700	2.0	3.8	4.7

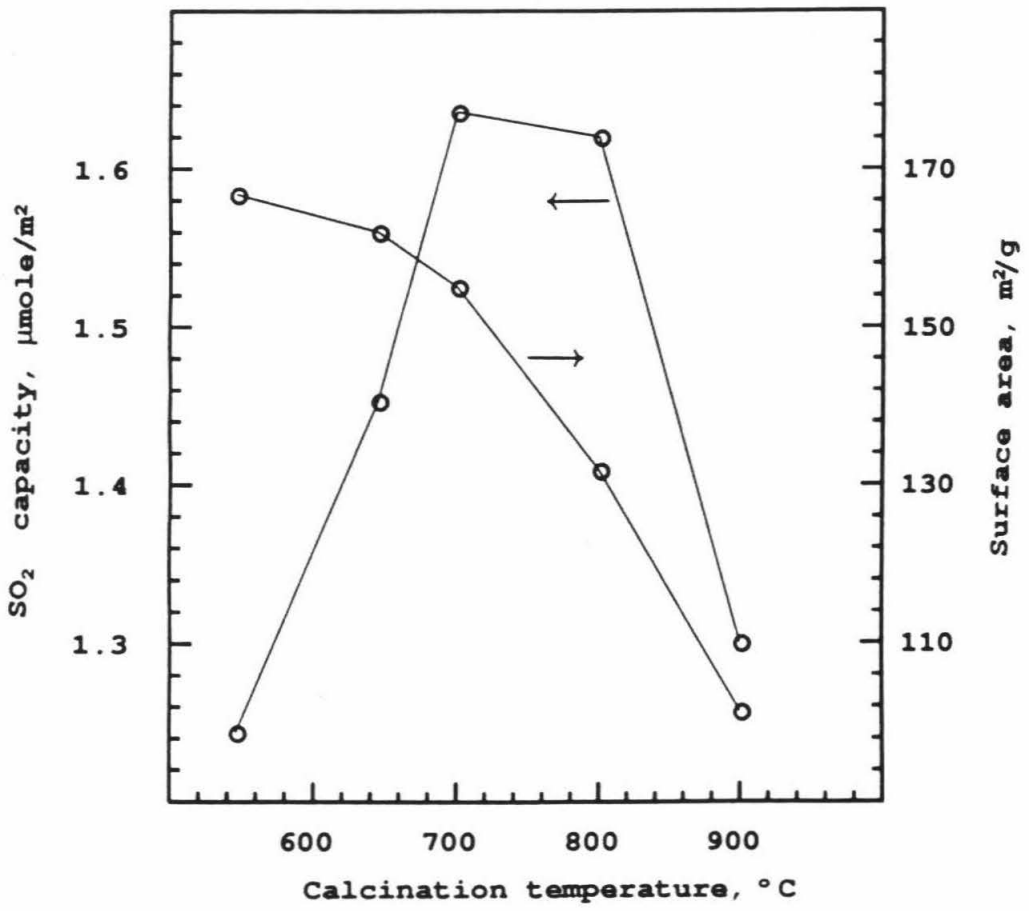

Figure 1. Specific surface area and SO_2 adsorption capacity of alumina at 200°C, P_{SO_2} = 50 Torr as functions of calcination temperature.

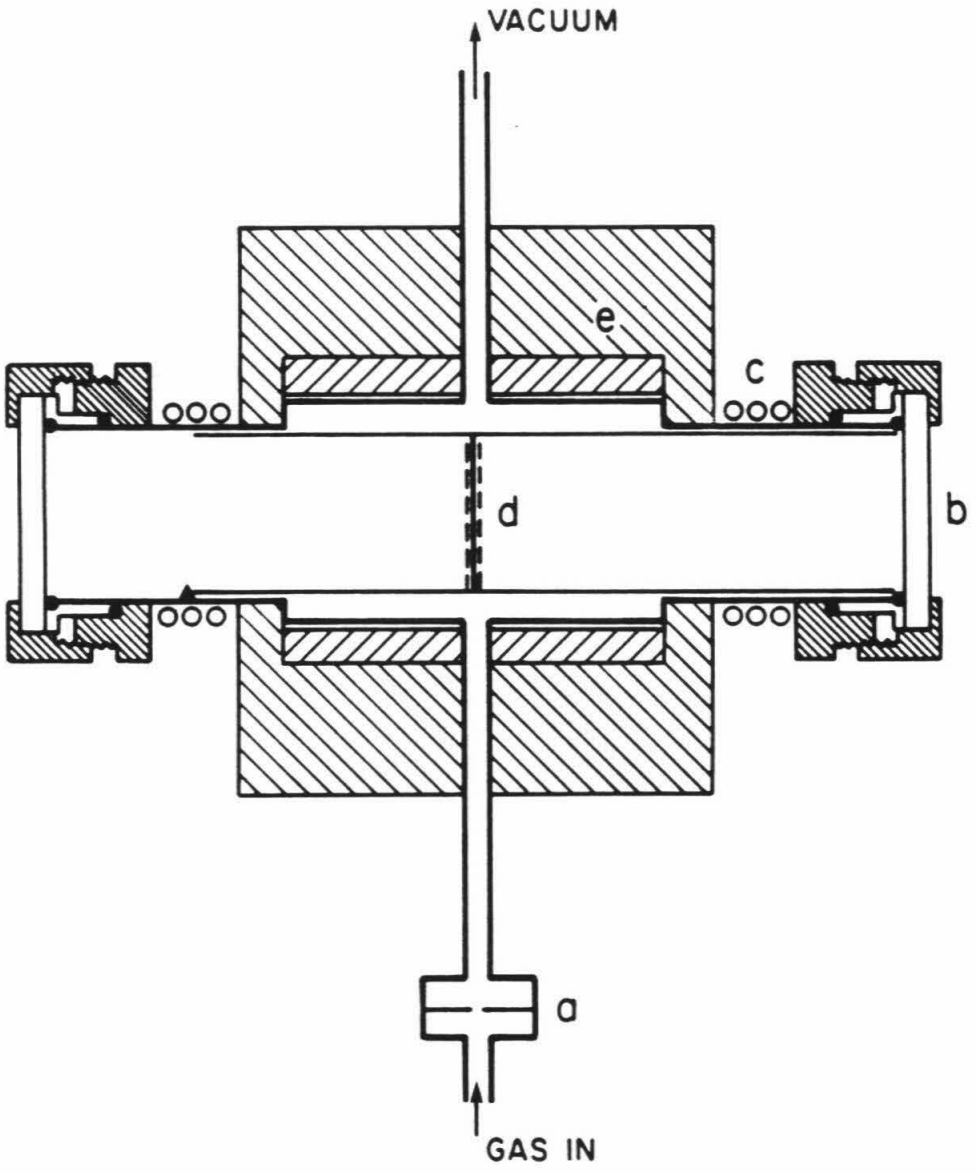

Figure 2. Infrared cell for high temperature kinetic experiments.

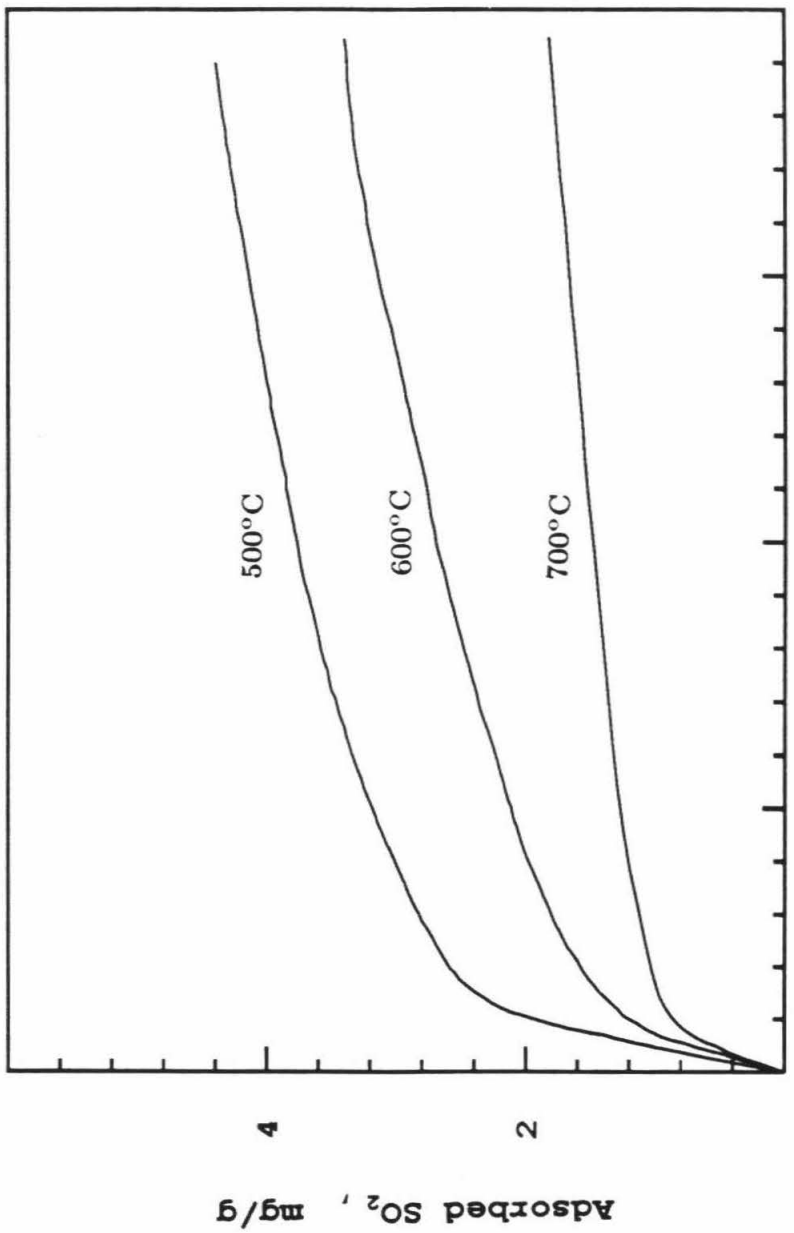

Figure 3. Adsorption of SO_2 versus time under 0.22% SO_2 and different temperatures (total pressure 1 atm).

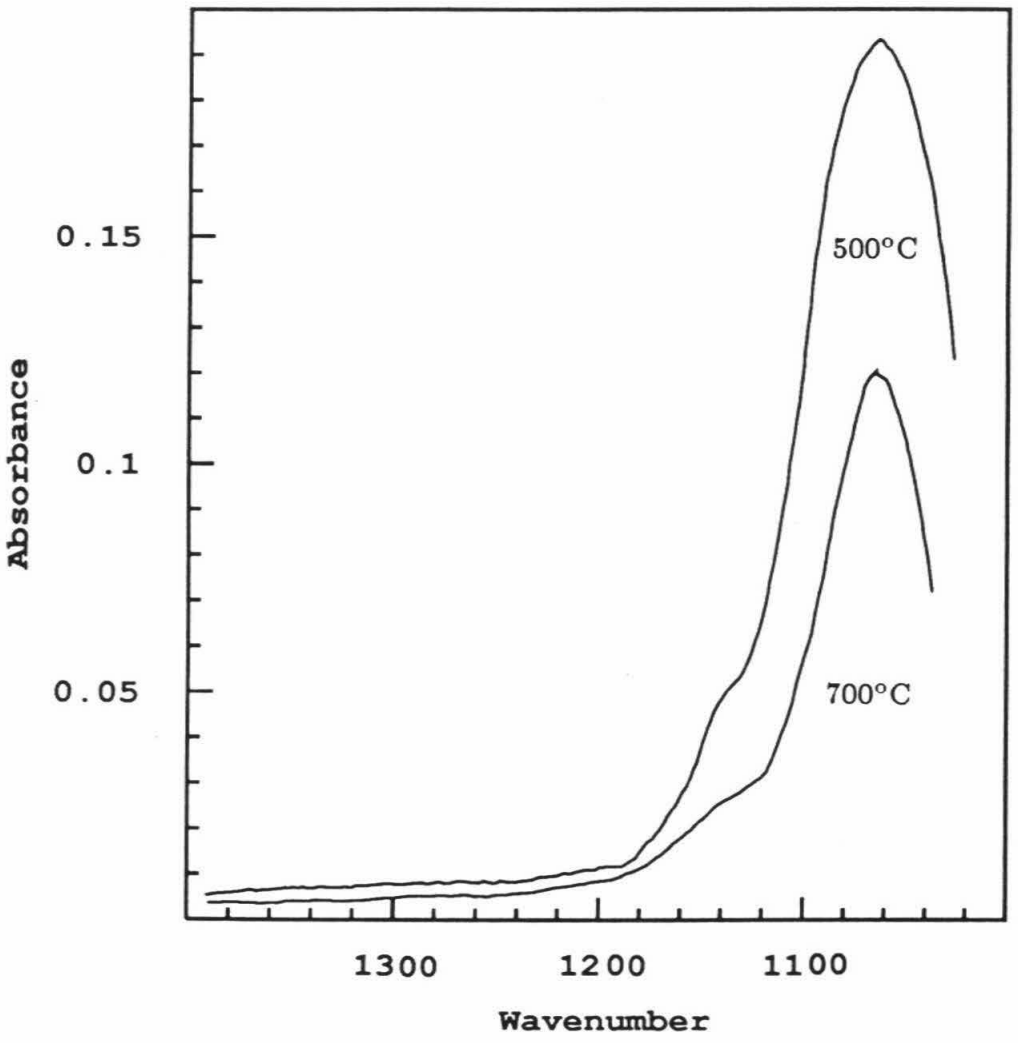

Figure 4. Infrared spectra of SO_2 chemisorbed under P_{SO_2}= 3 Torr for 30 minutes.

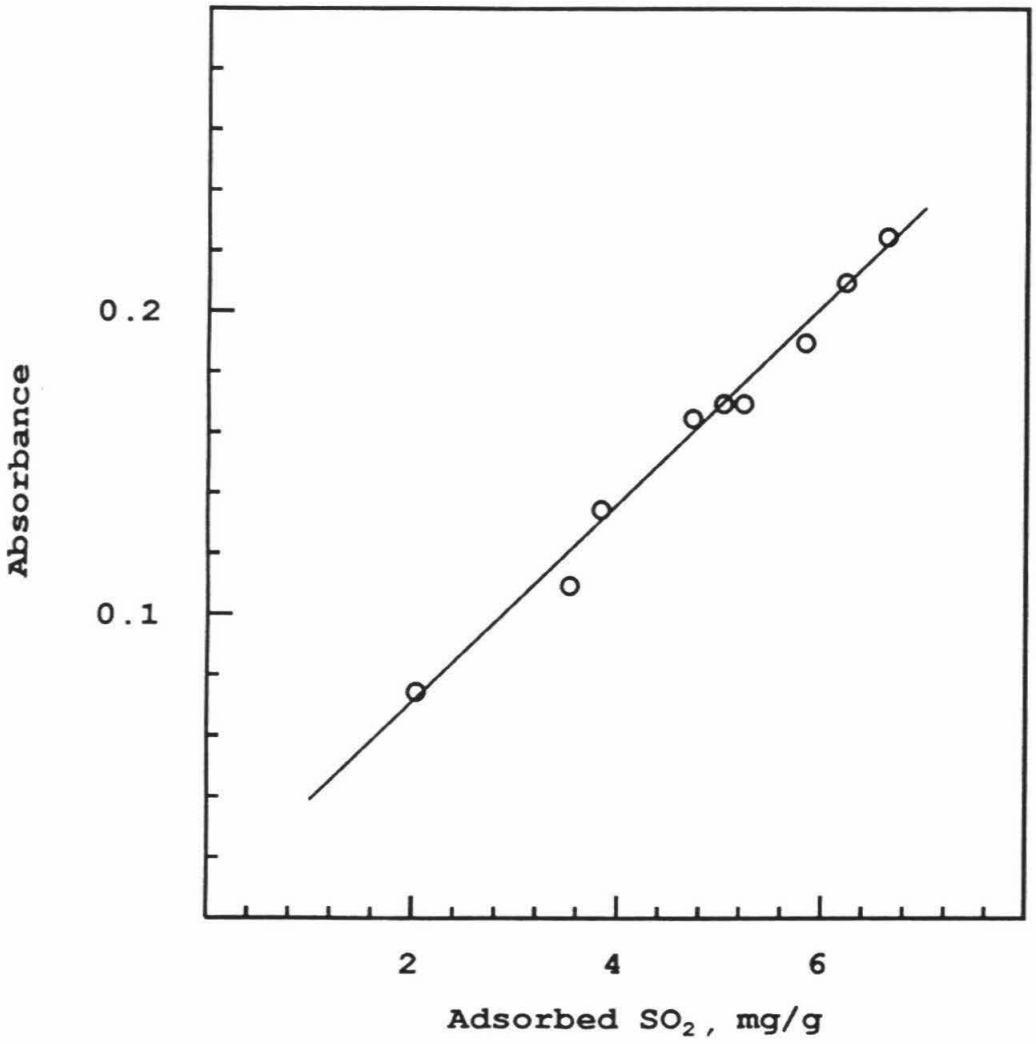

Figure 5. Absorbance at 1065cm^{-1} vs. adsorbed SO_2 determined in the TGA.

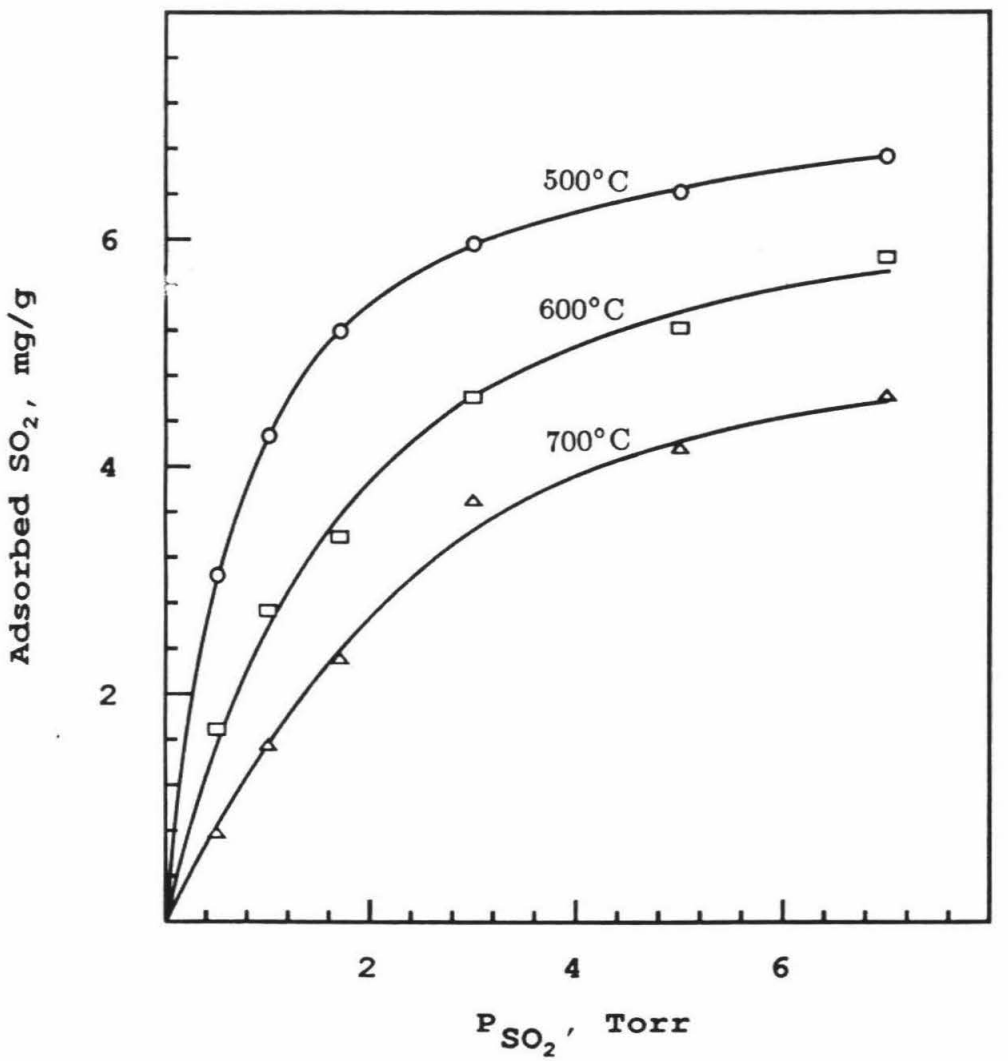

Figure 6. SO_2 adsorption isotherms

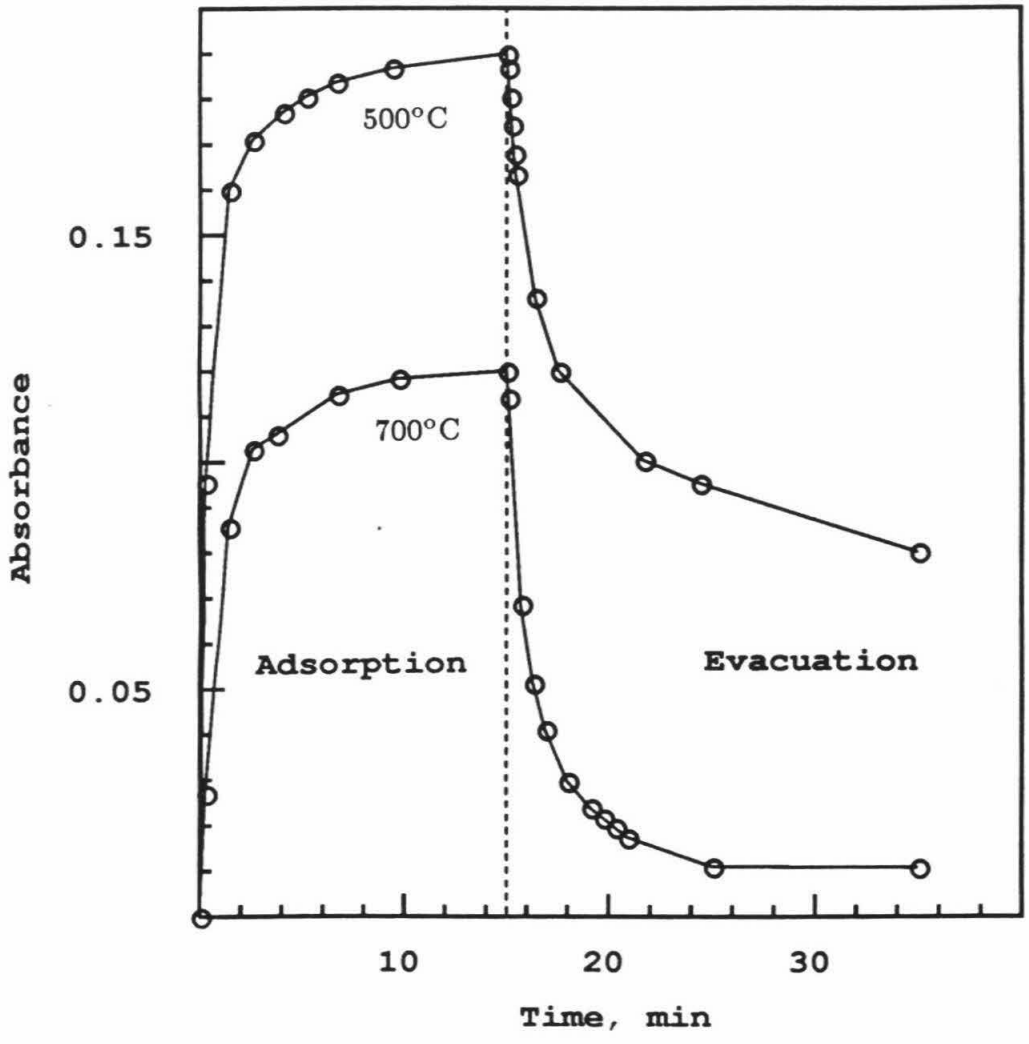

Figure 7. IR absorbance at 1065cm^{-1} during exposure to P_{SO_2}= 3 Torr (t < 15 minutes) and subsequent evacuation (t > 15 minutes).

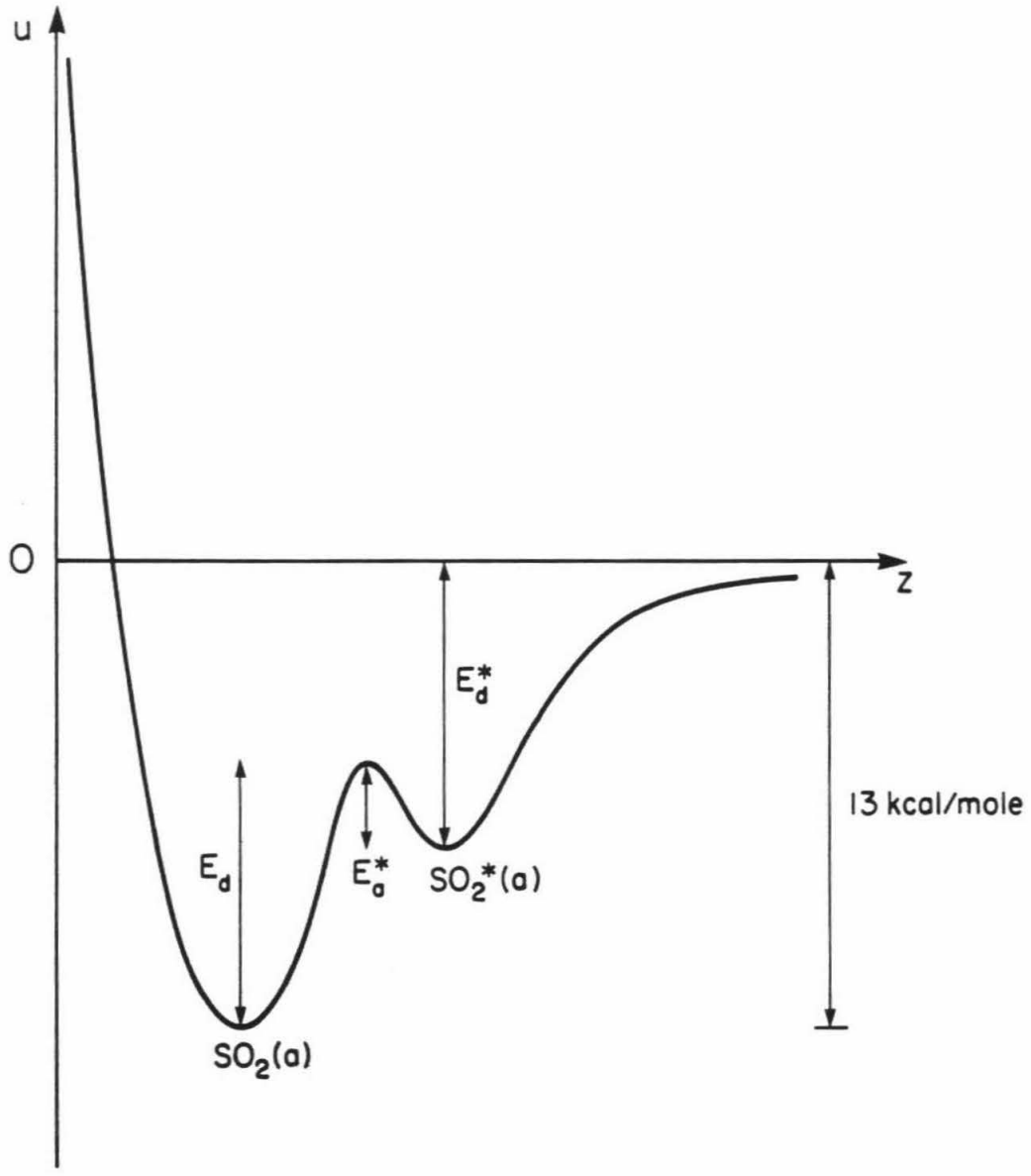

Figure 8. Schematic of potential energy diagram for two-step adsorption of SO_2.

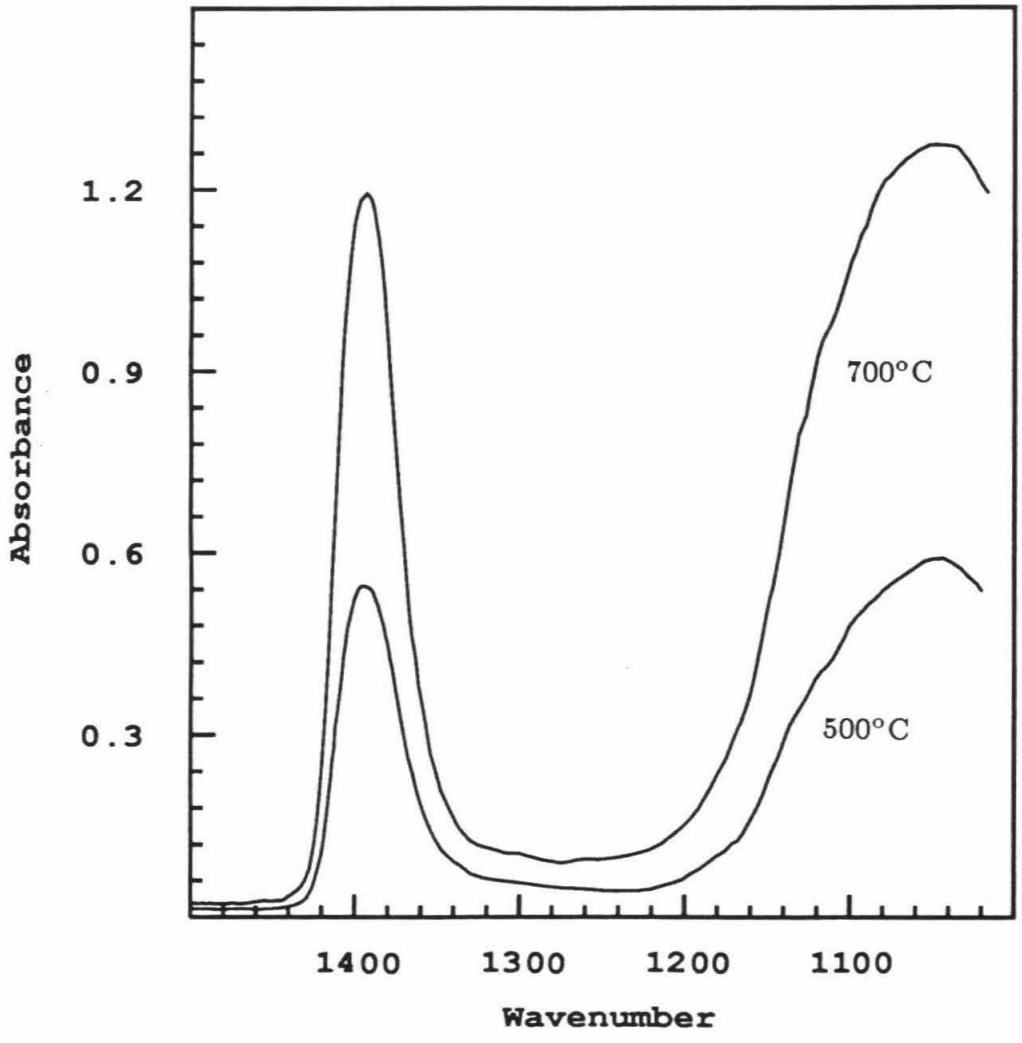

Figure 9. Infrared spectra of alumina after exposure to P_{SO_2}= 7 Torr and P_{O_2}= 50 Torr for 2 hours.

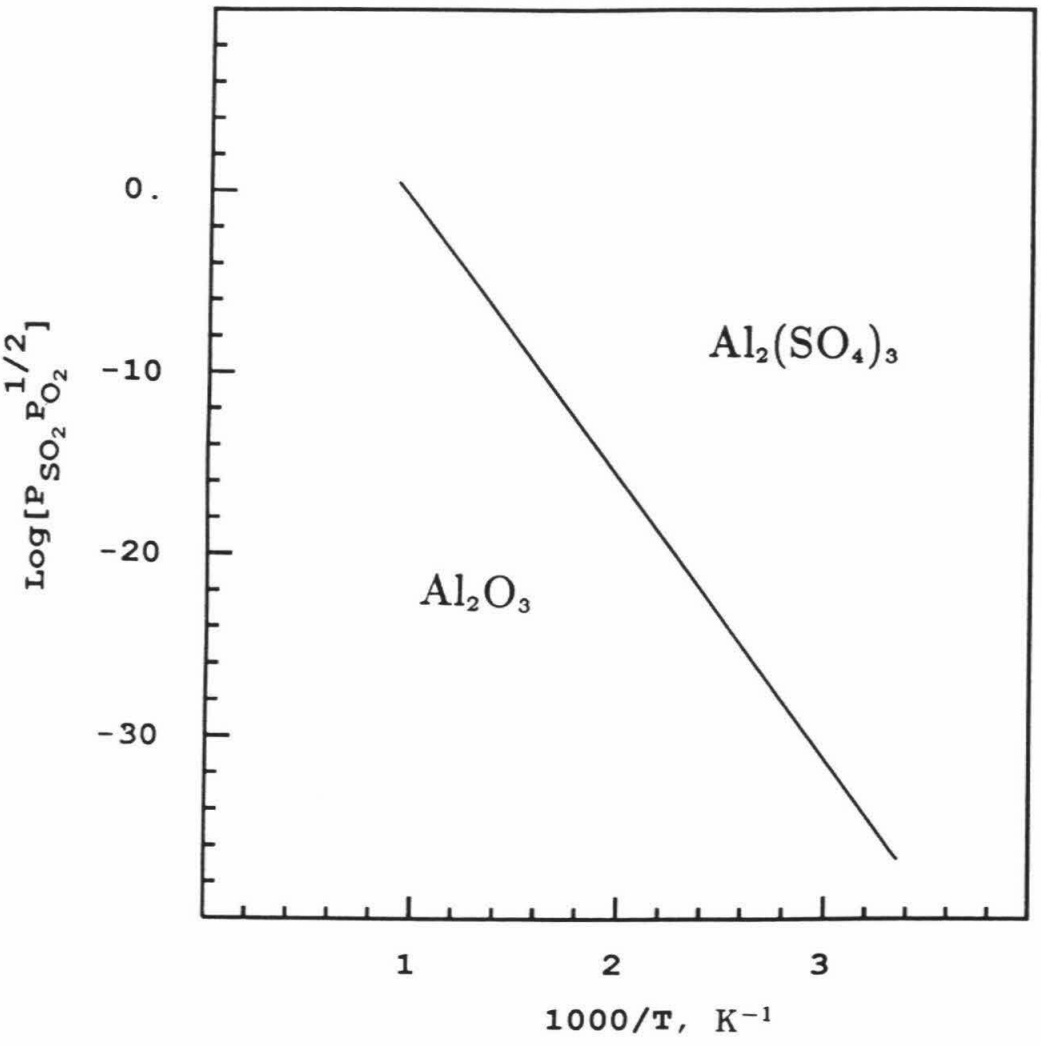

Figure 10. Stability diagram of aluminum sulfate - γ -alumina. Pressures are given in atm.

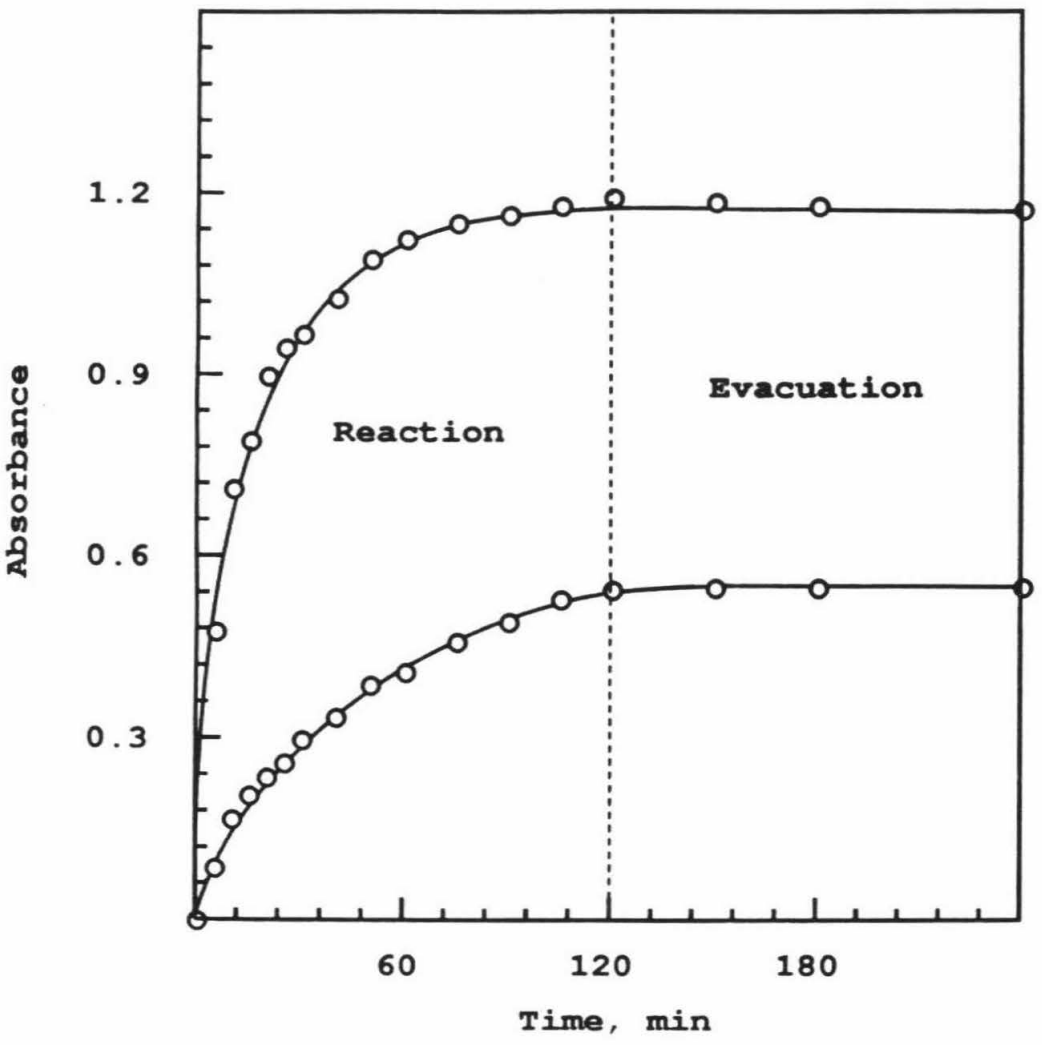

Figure 11. IR absorbance at 1390cm^{-1} during exposure to P_{SO_2}= 7 Torr and P_{O_2}= 50 Torr for 2 hours followed by evacuation.

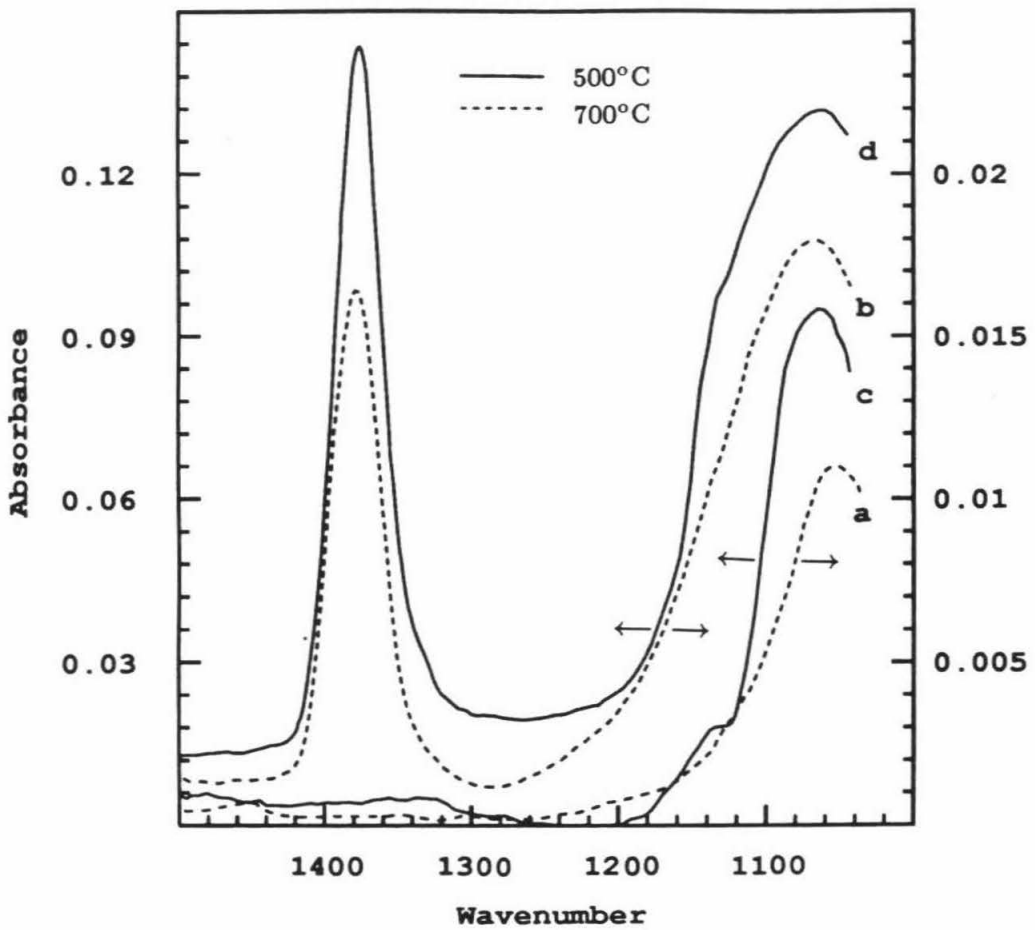

Figure 12. Infrared spectra of alumina after exposure to P_{SO_2}= 3 Torr for 15 minutes and (a) before and (b) after exposure to O_2 for 10 minutes at 700°C; (c) before and (d) after exposure to O_2 for 30 minutes at 500°C.

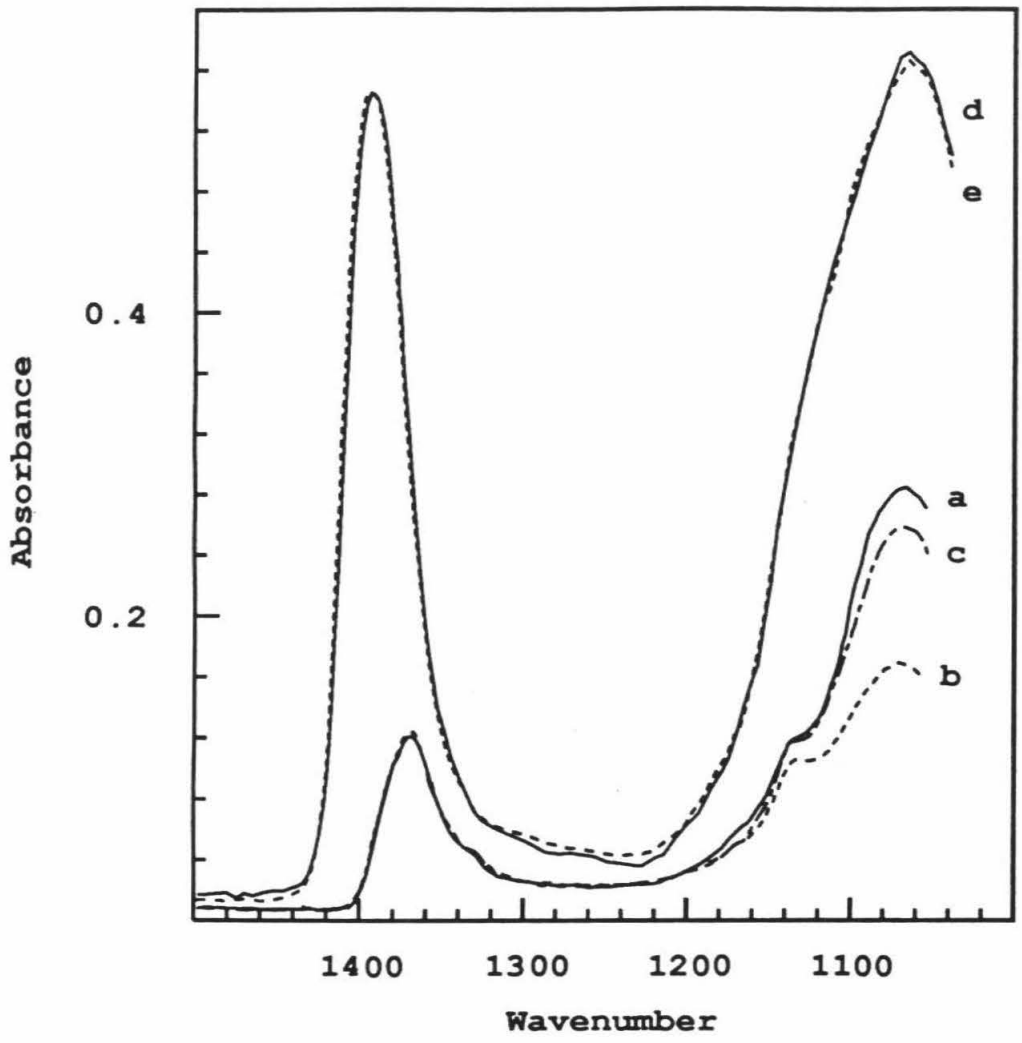

Figure 13. Infrared spectra of alumina after exposure to P_{SO_2}= 7 Torr and P_{O_2}= 50 Torr : (a) after 5 minutes reaction at 500°C and (b) subsequent evacuation for 30 minutes ; (c)after exposure to P_{SO_2}= 7 Torr for 5 minutes at 500°C; (d) after 2 hour reaction at 500°C and (e) subsequent evacuation for 30 minutes.

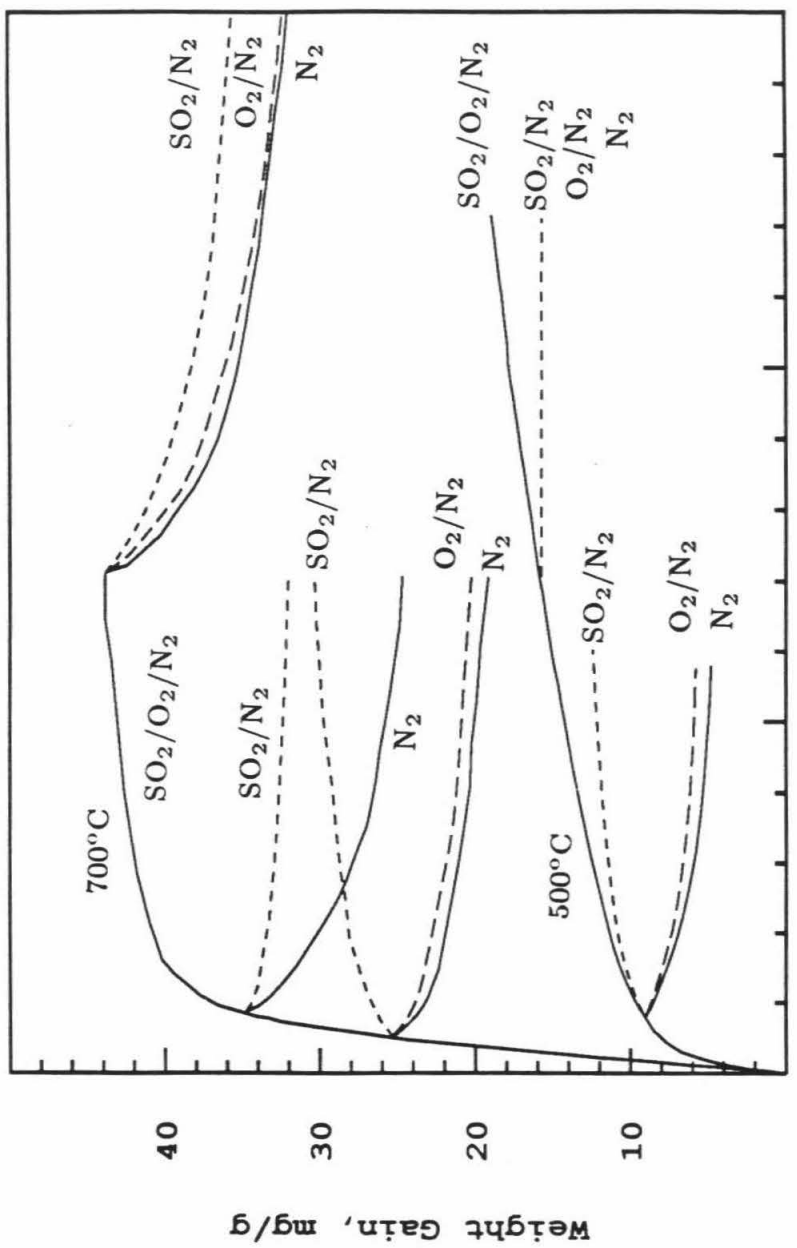

Figure 14. Weight gain in the TGA under different gas composition sequences.

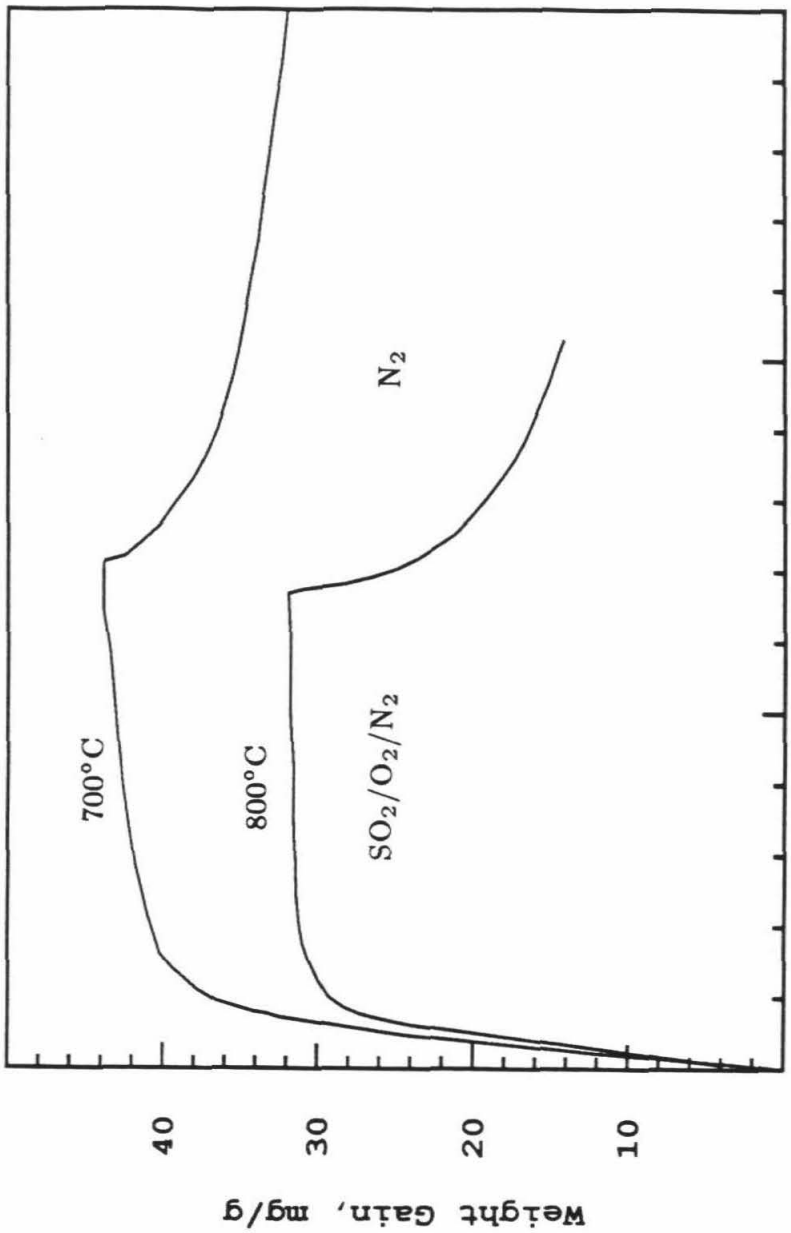

Figure 15. Weight gain in the TGA under exposure to 1% SO_2, 14% O_2 followed by purge with N_2 (total pressure 1 atm).

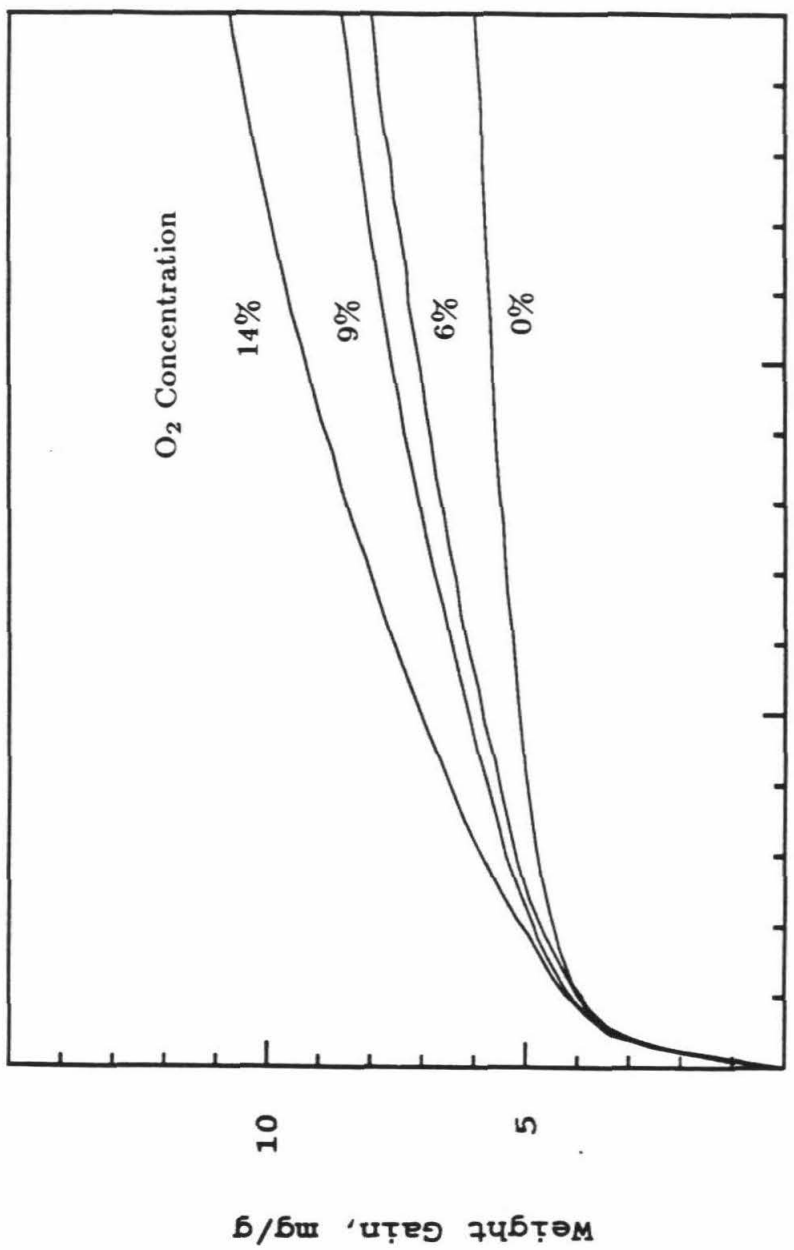

Figure 16. Weight gain in the TGA under exposure to a gas containing 0.7% SO_2 and different amounts of oxygen (total pressure 1atm).

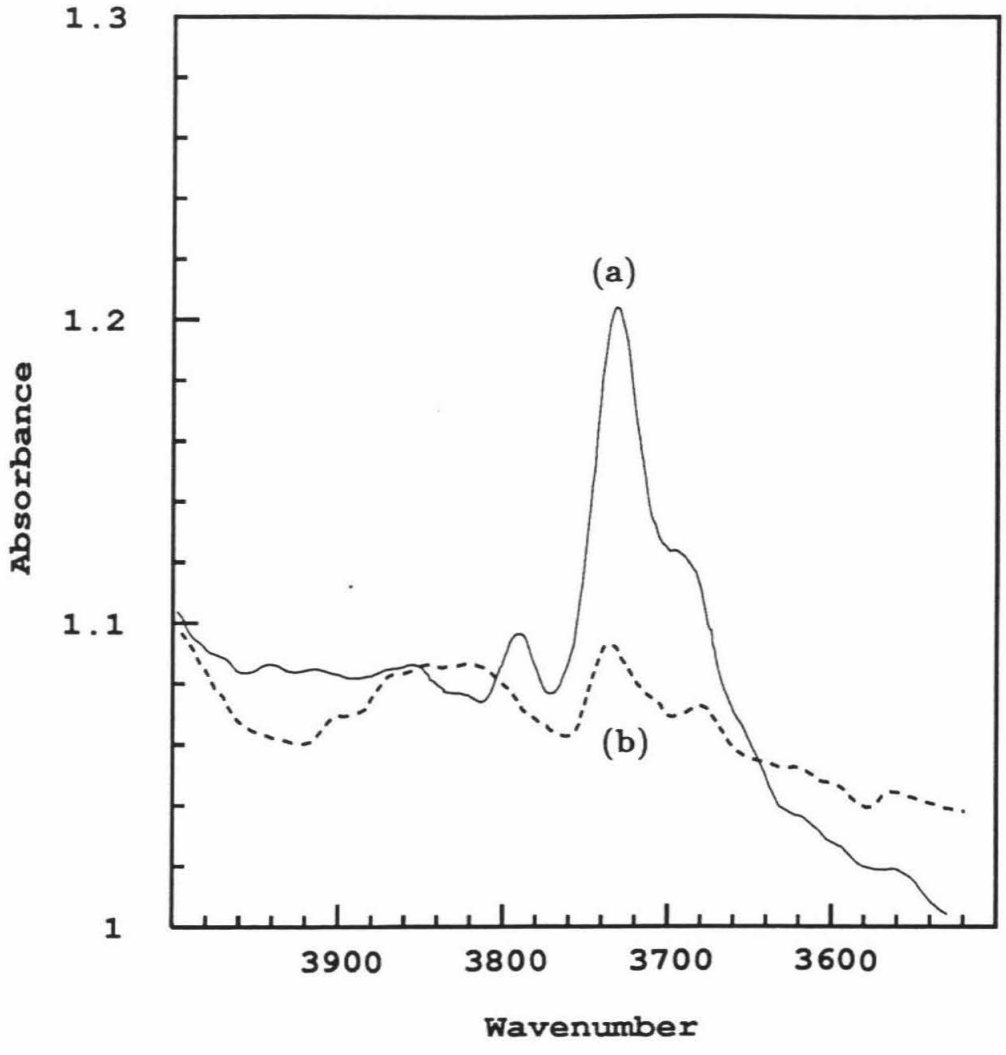

Figure 17. Infrared spectra of surface hydroxyl on alumina : (a) before and (b) after the oxidative adsorption of SO_2.

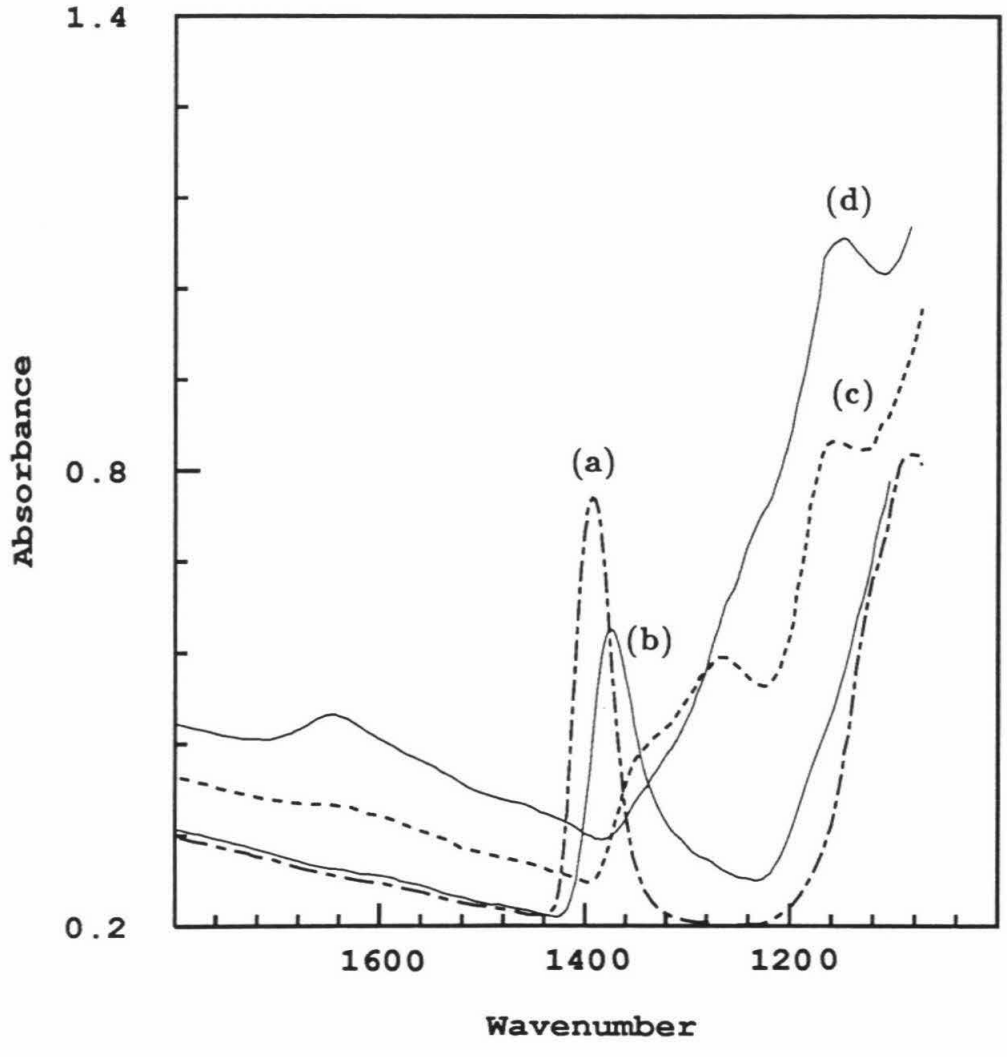

Figure 18. Infrared spectra of alumina : (a) after the oxidative adsorption of SO_2 ; (b),(c),(d) subsequent gradual addition of water vapor at room temperature.

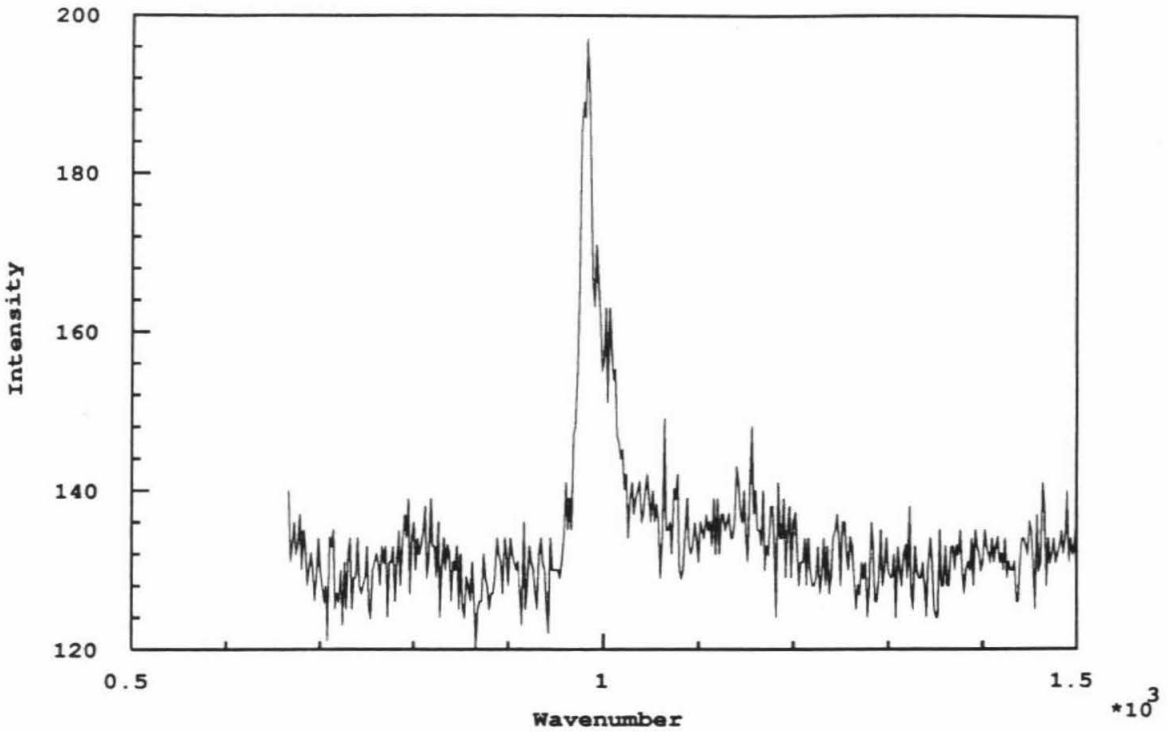

Figure 19. Raman spectrum of alumina after the oxidative adsorption of SO_2 and subsequent addition of water vapor at room temperature.

CHAPTER III

Reductive Desorption of SO_2 on γ -Al_2O_3

ABSTRACT

The desorption of SO_2 from $\gamma - Al_2O_3$ and the reductive desorption of oxidatively adsorbed SO_2 on $\gamma - Al_2O_3$ have been investigated by microreactor experiments and thermogravimetric analysis (TGA). Temperature-programmed desorption (TPD) of adsorbed SO_2 showed one broad desorption peak. Temperature-programmed reduction (TPR) experiments showed that SO_2 was desorbed without significant reaction with H_2, when the H_2 concentration was low, while a considerable amount of adsorbed SO_2 was reduced to elemental sulfur and H_2S when 100% H_2 was used. It was strongly chemisorbed SO_2 that was reduced to sulfur during the reduction. Isothermal reduction experiments of oxidatively adsorbed SO_2 reveal that the rate of reduction is very slow below 550°C even with 100% H_2. The main reduction product was SO_2. A small amount of H_2S was produced at a high temperature, probably from the reaction of elemental sulfur and H_2. TPR experiments of oxidatively adsorbed SO_2 showed that H_2S arose from a stable form of surface sulfate.

INTRODUCTION

The interactions of SO_2 with γ-alumina at high temperatures are relevant to *in situ* SO_2 removal from fluid catalytic cracking (FCC) regenerators, fluidized coal combustion furnaces and other high temperature desulfurization applications. An attractive scheme for in situ SO_2 removal involves a two-step cycle of oxidative adsorption of SO_2 and reductive regeneration of a "sulfated" catalyst. Alumina-based catalysts have been used as a sulfur oxide (SO_x) "transfer" catalyst to reduce SO_x emissions from FCC units. During the burning of coke the transfer catalyst captures sulfur oxide in the regenerator and releases sulfur as hydrogen sulfide in the reactor or in the stripper. Several patents [1-3] and laboratory studies [4-7] have been published and the process is now commercial. The SO_x transfer catalyst can be either incorporated within the cracking catalyst particles or can be added in the form of a powder along with the cracking catalyst.

When alumina was incorporated within the cracking catalyst, SO_2 removal increased with increasing alumina content [6] suggesting the important role of alumina in capturing sulfur oxides. Alumina, in combination with a suitable oxidation promoter (*e.g.*, Pt) is by far the most common SO_x transfer catalyst. In the presence of the oxidation catalyst, SO_2 oxidizes to SO_3, which then reacts with alumina to form a surface sulfate. The surface sulfate is believed to be reduced in the FCC reactor to release H_2S.

$$Al_2(SO_4)_3 + 12H_2 \rightleftharpoons Al_2O_3 + 3H_2S + 9H_2O$$

The details of adsorption, oxidative adsorption of SO_2 and reductive regeneration of alumina would be valuable in designing the catalyst for SO_2 removal and process configuration.

A number of studies have been reported on the interactions of SO_2 with alumina in connection with Claus catalysis, especially at low temperatures (below 500°C). Adsorption of SO_2 on $\gamma - Al_2O_3$ has been investigated by infrared (IR) spectroscopy from room temperature to 500°C [8-13]. Several surface SO_2 species were identified ranging in adsorption strength from physisorbed to strongly chemisorbed. The strongly chemisorbed species characterized by the IR band at $1060cm^{-1}$ was by far the most important at temperatures above 400°C and, essentially, the only one to be considered in connection with the desulfurization applications. The strongly chemisorbed SO_2 reacts with H_2S at temperatures above 200°C [11,14], while the more weakly adsorbed species react at even lower temperatures [14].

When $\gamma - Al_2O_3$ was exposed to SO_2 and O_2 at temperature above 400°C or higher, surface sulfate characterized by the IR bands near 1100 and $1400cm^{-1}$ was produced [9,15]. Andersson *et al.* [4] studied oxidative adsorption of SO_2 on alumina. At 500°C surface sulfate was not decomposed while at 700°C part of the adsorbed sulfate decomposed. Based on the decomposition results, two types of chemisorbed sulfate species were suggested. We have recently reported adsorption and oxidative adsorption of SO_2 on γ-alumina at high temperatures [16]. Adsorbed SO_2 was oxidized to surface sulfate, which remained at the original SO_2 adsorption sites. There was a broad range of site strength on the surface of alumina.

The reduction of the surface sulfate formed on alumina have been investigated in the aforementioned study [4]. The reduction of sulfate with 1% H_2 at 500°C was very slow while propane and H_2S slowly reacted with surface species. The work with CeO_2 in $\gamma - Al_2O_3$ showed that the sulfate reduced easily at

650°C with H_2 [5]. Khalafalla and Hass investigated the steady state reduction of SO_2 with CO on alumina [17]. Alumina provided adsorption sites for SO_2 and adsorbed SO_2 reacted with CO to produce CO_2 and elemental sulfur at 450-600°C. In the presence of metallic components the activity of the catalyst was enhanced.

Herein we report our work on the reductive desorption of SO_2 on $\gamma - Al_2O_3$ undertaken with the hope of identifying the mechanism of the reduction.

EXPERIMENTAL

Materials

Gamma alumina (Al-1401-P) was obtained from Harshaw Chemical Corporation in the form of a powder with particle size approximately 60μ. The structural change of this material upon thermal treatment has been addressed before [9]. A mixture of SO_2 in N_2 was obtained from Matheson and was diluted with additional N_2 or air as required. All gases were passed through a water trap. The SO_2-N_2 mixture and the N_2 diluent were further purified by passing through an oxygen trap.

TGA

A Dupont 951 thermogravimetric analyzer interfaced with a micrcomputer was used to measure the weight change of the sample during adsorption and desorption. Typically 20 mg of particles was placed on a quartz sample pan and pretreated in N_2 for 2 hours at 700°C. The total flow rate of the gases was 150 ml/min and the pressure was atmospheric. It was experimentally verified that

under the conditions employed the reactions were free of external and internal mass transfer resistances.

Microreactor

A quartz microreactor was used for isothermal and temperature programmed reduction. Usually 50mg of the alumina sample were placed in the middle of the reactor by quartz frit and quartz wool and thermally treated at 700°C for 2 hours in N_2. Then the temperature of the system was adjusted to the desired level and adsorption and reduction experiments were carried out. The temperature of the bed was monitored with a thermocouple inserted inside a quartz well imbedded in the sample. The microreactor was furnished with a temperature programmer, allowing linear temperature increase or isothermal operation. Gaseous products were analyzed using a quadrupole mass spectrometer (Dycor M200) with multiple peak scanning. The temperature-programmed experiments were performed using a heating rate of 60°C/min.

Procedure

TPD and TPR of adsorbed SO_2 were carried out using the TGA and the microreactor system. SO_2 was first adsorbed at temperatures between 300 and 500°C by passing 1% SO_2 in N_2 through the alumina bed for 10 minutes. Then the system was flushed with N_2 for 10 minutes while the temperature decreased to the desired level. For temperature-programmed experiments the temperature of the system increased at a rate 60°C/min up to 800°C and the desorbed gases were monitored by mass spectrometer. For the reduction of the oxidatively adsorbed SO_2, the oxidation reaction was first carried out at 500-700°C with 1% SO_2 and 14% O_2 in N_2. Then the temperature of the system was adjusted and the reduction was carried out using H_2.

RESULTS and DISCUSSION

(a) TPD and TPR of adsorbed SO_2

Figure 1 shows TPD of adsorbed SO_2 when N_2 was used as a carrier gas. One broad peak was found with peak maximum around 340°C. The TPR using 5% H_2 in N_2 as a carrier is similar to the TPD spectra as shown in Figure 2. But small amounts of H_2S were produced above 700°C. When 100% H_2 was used for TPR the main reduction product was still SO_2, but considerable amounts of H_2S were produced at high temperatures as shown in Figure 3. Quantitative analysis of gases released from TPD and TPR were carried out by integrating the spectra. The amount of SO_2 produced from TPD and TPR with 5% H_2 is about 9.3 μmol/50mg Al_2O_3. The amounts of gases produced from TPR with 100% H_2 were 7.7 μmolSO_2 and 1.5 μmolH_2S / 50 mg Al_2O_3. Total moles of sulfur produced were about the same (9.3 μmol). The results reflect constant SO_2 coverage before each reaction. SO_2 desorbed without significant reaction with 5% H_2 below 700°C (Figs. 1 and 2) while there was a reaction to produce H_2S in TPR with 100% H_2.

TPR of SO_2 adsorbed at 400 and 500°C using 100% H_2 are shown in Figures 4 and 5, respectively. Comparison of the amount of SO_2 and H_2S released during TPR shows that the amount of SO_2 desorbed from the surface decreases as the adsorption temperature increases. The amount of H_2S produced was not significantly affected by the adsorption temperature variation. The results suggest that there may be two types of adsorbed SO_2: one weakly adsorbed species is easily desorbed and the other strongly adsorbed species is reduced to H_2S. The amount of the weakly adsorbed SO_2 decreases as the adsorption temperature increases.

The formation of H_2S during the reduction could be written by the following reaction.

$$SO_2(*) \xrightarrow{H_2} H_2S + H_2O \qquad (1)$$

where * denotes the adsorption sites. There is a possibility that the above reaction is taking place *via* sulfur, which is produced during the reduction.

$$SO_2(*) \xrightarrow{H_2} S(*) \xrightarrow{H_2} H_2S \qquad (2)$$

Figure 6 shows TPR results in the TGA system. SO_2 was adsorbed at 400°C for 15 minutes. TPR experiments started from 300°C with simultaneous measurement of both weight change and exit gas composition. SO_2 was first released and then a very small amount of H_2S was produced. The decrease in sample weight in the first few minutes was due only to the desorption of SO_2 since the total moles of SO_2 produced were equal to the decrease in weight. But the decrease in sample weight after the SO_2 release was much larger than the total moles of H_2S released. The discrepancy between the moles of H_2S and the decrease in weight was calculated and shown in Figure 6 in a broken line. The species attributed to this curve is sulfur since it is not detectable in our experimental system because of a cooling trap placed in the exit gas stream. The peak maxima of H_2S and sulfur were nearly the same, suggesting that H_2 reacted with sulfur to produce H_2S. The amount of H_2S released from the TGA system was, however, much smaller than the amount from the microreactor (Figure 4) although the adsorption conditions were the same (400°C and 15 minutes adsorption). The results can be explained by the fact that the readsorption of sulfur could have occurred in the microreactor system and readsorbed sulfur could react with H_2 to form H_2S with the help

of alumina as a catalyst. The readsorption is negligible in the TGA system and sulfur can be released without significant reaction with H_2.

The results from TPR of adsorbed SO_2 can be summarized in the following reduction mechanism.

$$SO_2(*) \longrightarrow SO_2(g) \qquad (3)$$

$$\downarrow H_2$$

$$S(*) \xrightarrow{H_2} H_2S(g) \qquad (4)$$

$$\downarrow \qquad (5)$$

$$S_2(g)$$

When SO_2 adsorbed on the weak sites on alumina reaction (3) is dominant. When SO_2 adsorbed on the strong sites, reactions (4) and (5) will take place. Reaction (4) can be catalyzed by alumina.

(b) Reduction of Oxidatively Adsorbed SO_2,

Figure 7 displays the weight of an alumina sample in a TGA system during reduction with 100% H_2. At temperatures above 650°C, the reduction was very fast and was completed in 10 minutes. Below 550°C, the reduction rate is very slow. At 500°C the rate of reduction is about 0.6mg/g-min. As shown in Figure 7, the reduction was incomplete below 600°C. Figure 8 shows the change of the sample weight and the composition of exit gases during the isothermal reduction at 550°C for 17 minutes, followed by temperature-programmed reduction with 100% H_2. After 17 minutes of reduction at 550°C, the sample weight changed very slowly. The main reduction product was SO_2 up to this stage of the

reaction. TPR experiment after this stage further decreased the sample weight and showed evolution of both SO_2 and H_2S.

Figures 9 and 10 display the reduction results using 100% H_2 at 600°C and 5% H_2 at 700°C in the microreactor system. As soon as H_2 was introduced, SO_2 started to evolve, followed by smaller amounts of H_2S. TPR after 10 minutes reduction at 600°C showed the production of mainly H_2S.

The results from TPR of the samples that were exposed to SO_2-O_2 mixture at different temperatures, were shown in Figure 11. The evolution of SO_2 with peak maximum at 600°C followed by formation of H_2S with peak maximum at 650°C were observed. The effect of surface concentration on TPR spectra was examined by varying the adsorption time at 500°C. Figure 12 displays the evolution of SO_2 and H_2S at various stages of the oxidative chemisorption. Most reduction products was H_2S at the beginning of the reaction. As the adsorption time became longer, the amount of SO_2 formed during TPR became larger. The maximum temperature of SO_2 desorption shifted to higher temperatures as the concentration of surface sulfate increased. The amount of H_2S evolved, however, was more or less constant at various adsorption steps. Figure 13 shows TPR of oxidatively adsorbed SO_2 with 5% H_2 in N_2. Similar to TPR with 100% H_2 SO_2 desorption followed by H_2S production was observed but at higher temperatures. SO_2 desorbed with peak maximum at 680°C, and H_2S released with peak maximum at 750°C.

The isothermal reduction with H_2 at temperatures above 600°C occurred in two stages, the first characterized by SO_2 release, the second by H_2S release, as shown in Figures 9 and 10. The amount of H_2S produced was very little when compared to the amount of SO_2. The most probable source of H_2S may be from

the reaction of H_2 and sulfur produced during the reduction reaction similar to the reduction of adsorbed SO_2. As shown in Figure 12 the sulfate adsorbed at 500°C reacted with H_2 to form both SO_2 and H_2S during the TPR. We know from previous adsorption results [16] that at 500°C the adsorbed SO_2 reacted slowly with O_2 to form a surface sulfate. At the beginning of the reaction the strongly adsorbed SO_2 was involved in the oxidation reaction. The results of Figure 9 suggest that the sulfate formed on the strong sites reduced mainly to H_2S. Increasing the surface concentration of the sulfate caused an increase in the amount of SO_2 released. The amount of H_2S released was more or less constant (4.2 μmol/g Al_2O_3) suggesting that H_2S derived from only one form of the sulfate, probably the one formed on the strong sites. As the reaction times increased, the SO_2 adsorbed on weak sites also formed surface sulfate, which upon reduction produced SO_2.

To summarize the reduction results we propose the following mechanism for the reduction of surface sulfate.

$$SO_2(*) \longrightarrow SO_2(g) \qquad (7)$$

$$SO_3^*(a) \xrightarrow{H_2} S(*) \xrightarrow{H_2} H_2S(g) \qquad (8)$$

$$\downarrow \qquad (9)$$

$$S_2(g)$$

where (*) denotes adsorption sites while S(*), SO_2(*) and SO_3(*) denote adsorbed sulfur, adsorbed SO_2, and surface sulfate. When the sulfate is formed on the strong sites, reaction (8) or (9) is preferable while reaction (7) will take

place when the sulfate is formed on the weak sites. At temperatures below 600°C, the reduction of the surface sulfate is incomplete because the reactions are slow. Reaction (7) is relatively faster than reaction (8) or (9) from the reduction results at 550°C (Fig. 8). Since only SO_2 was released at the beginning of reduction, the TGA results of Figure 7 were analyzed to obtain activation energy of reduction reaction (7) assuming that the SO_2 desorption step is very fast. Analysis of initial reaction rates at various temperatures gave an activation energy of 40.3 kcal/mole for the reduction of sulfates to adsorbed SO_2.

CONCLUSIONS

Reductive desorption of SO_2 has been studied using a microreactor and a TGA system. TPD of adsorbed SO_2 showed one broad peak while TPR with 100% H_2 showed SO_2 desorption followed by H_2S production. The H_2S arose from the reaction of adsorbed sulfur and H_2. The SO_2 adsorbed on the strong sites was reduced to sulfur while the SO_2 adsorbed on the weak sites desorbed without reaction with H_2. The strongly adsorbed species was dominant at high temperatures. When oxidatively chemisorbed SO_2 was reduced in H_2, SO_2 desorption followed by H_2S formation was observed at high temperatures. The amount of H_2S produced was very small compared to that of SO_2. H_2S was formed from the sulfate adsorbed on strong sites on alumina. Below 600°C, the reduction reaction was very slow, producing mainly SO_2.

REFERENCES

[1] W.A. Blanton, Jr. and R.L. Flanders, U.S. Patents 4 071 436 (1978).

[2] I.A. Vasalos, U.S. Patents 4,153 534 (1978).

[3] J.S. YOO and J.A. Jaecker, , U.S. Patents 4,495 305 (1985).

[4] S. Andersson, R. Pompe, and N-G. Vannerberg, *Appl. Catal*, **16**, 49 (1985).

[5] A.A. Bhattacharya, G.M. Woltermann, J.S. Yoo, J.A. Karch, and W.E. Cormier, *I&EC Research*, **27**, 1356 (1988).

[6] E.H. Hirschberg and R.J. Bertolacini, *ACS Symposium Series* **375**, 114 (1988).

[7] L. Rheaume and R.E. Ritter, *ACS Symposium Series* **375**, 146 (1988).

[8] A.V. Deo, I.G. Dalla Lana, and H.W. Habgood, *J. Catal.*, **21**, 270 (1971).

[9] C.C. Chang, *J. Catal.*, **53**, 374 (1978).

[10] R. Fiedorow, I.G. Dalla Lana, and S.E. Wanke, *J. Pys. Chem.*, **82**, 2474 (1978).

[11] H.G. Karge, I.G. Dalla Lana, S.T. de Suarez, and Y. Zhang, *Proc.* 8th International Congress on Catalysis, Berlin, Vol.III, 453 (1984).

[12] H.G. Karge, I.G. Dalla Lana, *J. Pys. Chem.*, **88**, 1538 (1984).

[13] A. Datta, R.G. Cavell, R.W. Tower, and Z.M. George, *J. Pys. Chem.*, **89**, 443 (1985).

[14] A. Datta, R.G. Cavell, *J. Pys. Chem.*, **89**, 454 (1985).

[15] O. Saur, O.S. Bensitel, A.B. Mohammed Saad, J.C. Lavalley, C.P. Tripp,

and B.A. Morrow, *J. Catal.*, **99**, 104 (1986).

[16] S.W. Nam and G.R. Gavalas *Appl. Catal.* accepted for publication (1989).

[17] S.E. Khalafalla and L.A. Hass, *J. Catal.*, **24**, 115 (1972).

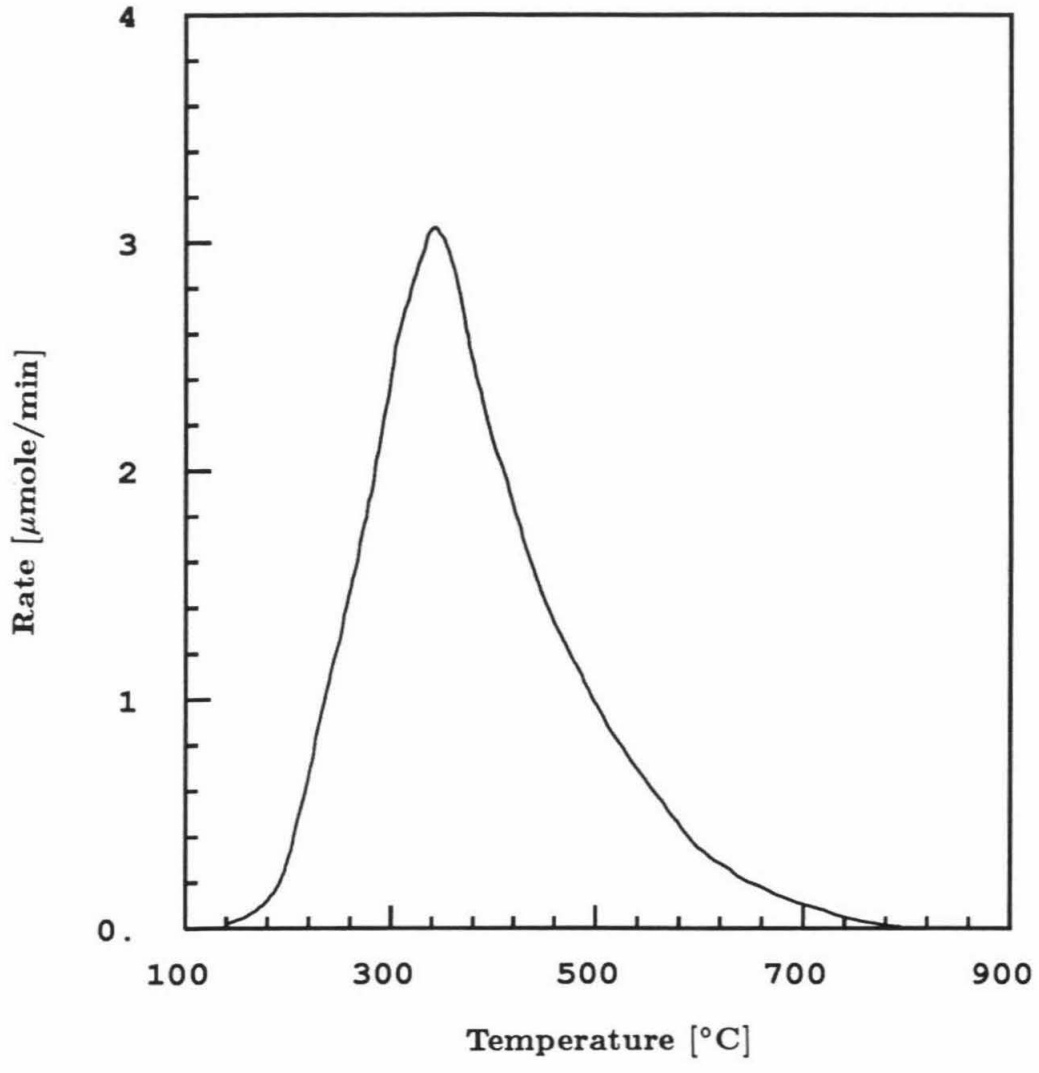

Figure 1. TPD of SO_2 adsorbed at 300°C on alumina (50mg).

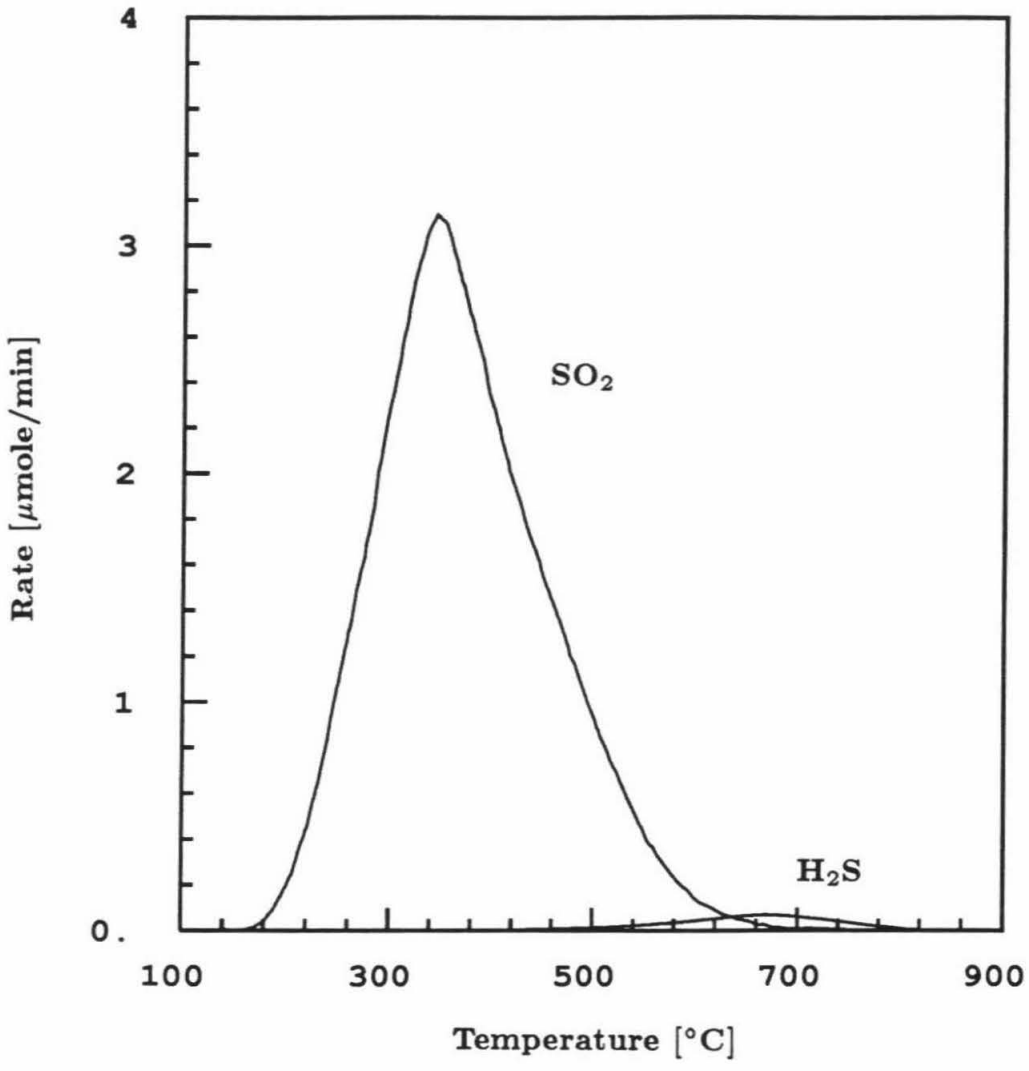

Figure 2. TPR of SO_2 adsorbed at 300°C on alumina (50mg) using 5% H_2 in N_2 as a carrier.

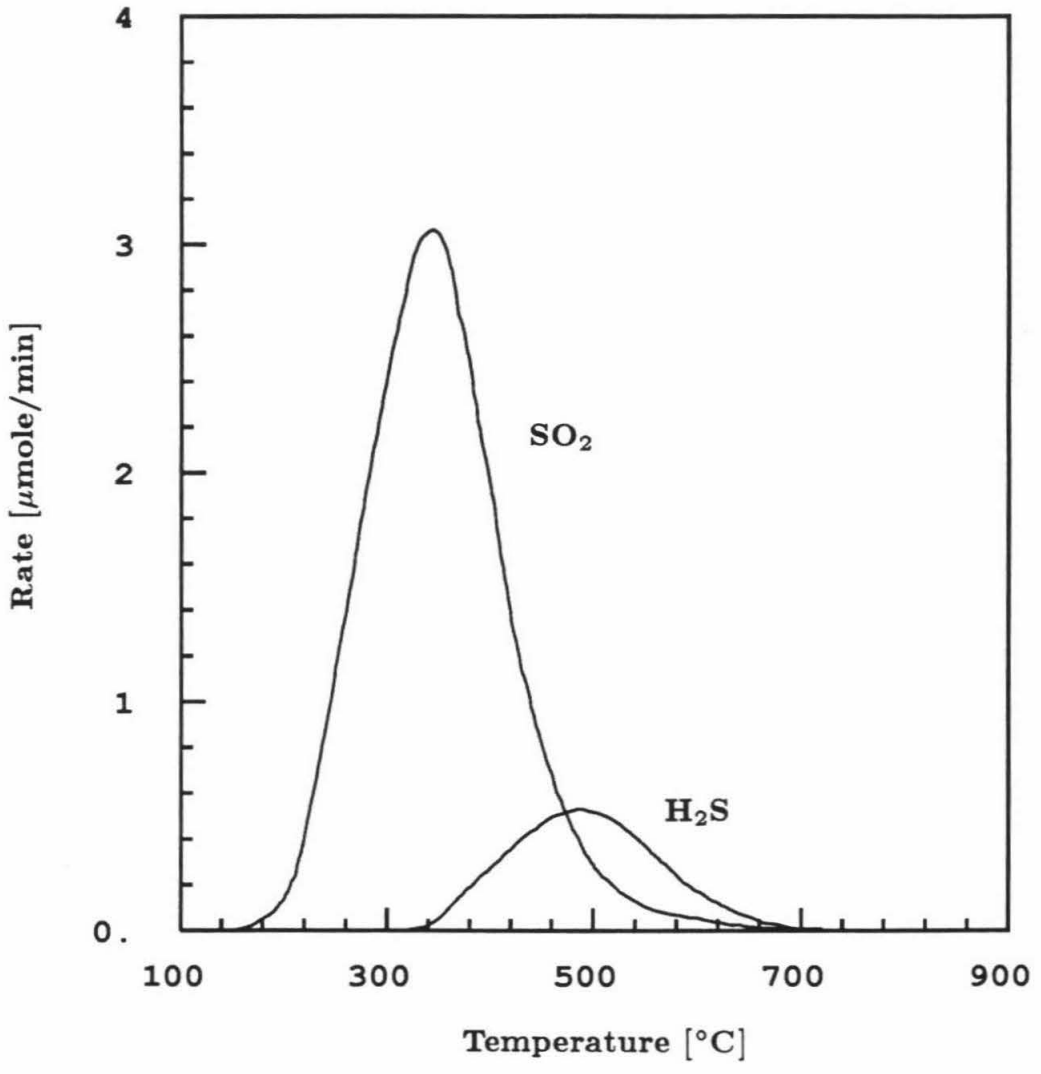

Figure 3. TPR of SO_2 adsorbed at 300°C on alumina (50mg) using 100% H_2 in N_2 as a carrier.

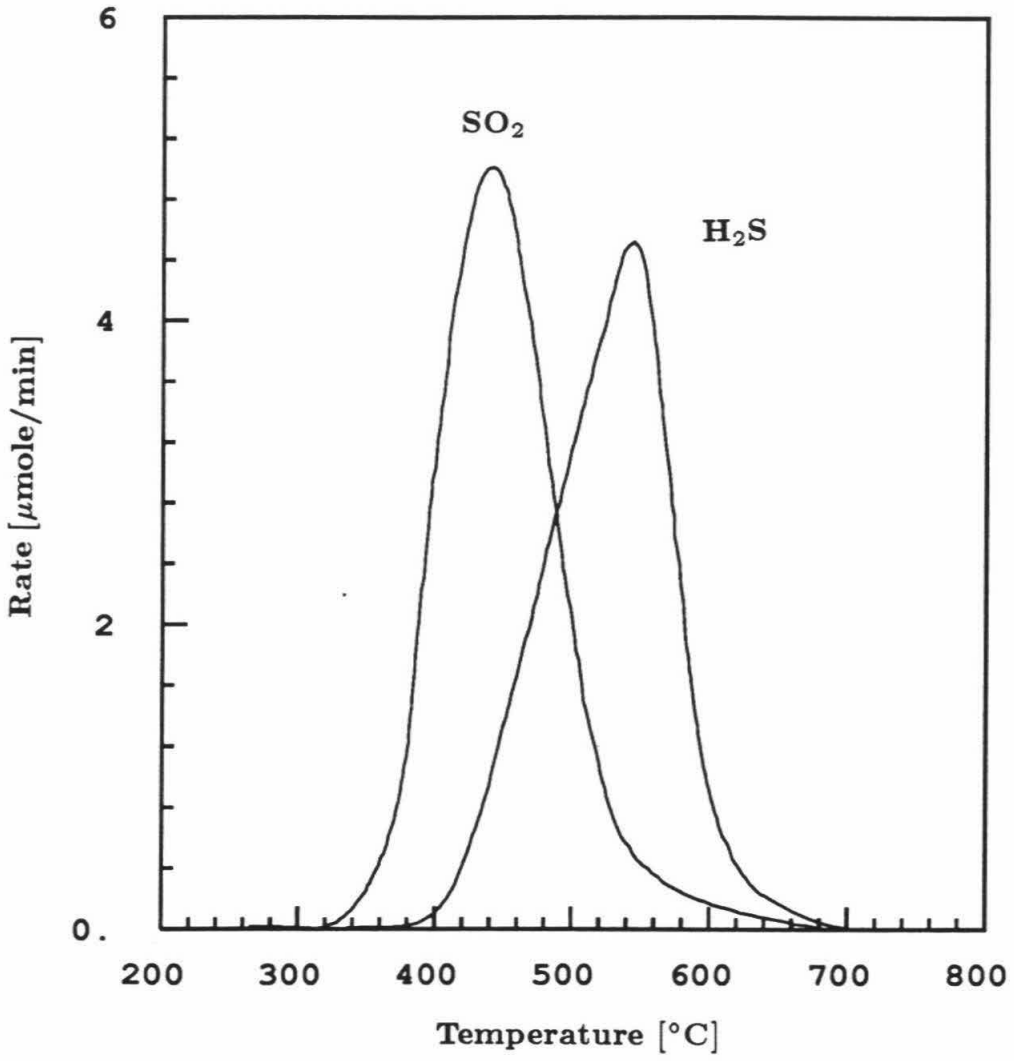

Figure 4. TPR of SO_2 adsorbed at 400°C on alumina (100mg) using 100% H_2 in N_2 as a carrier.

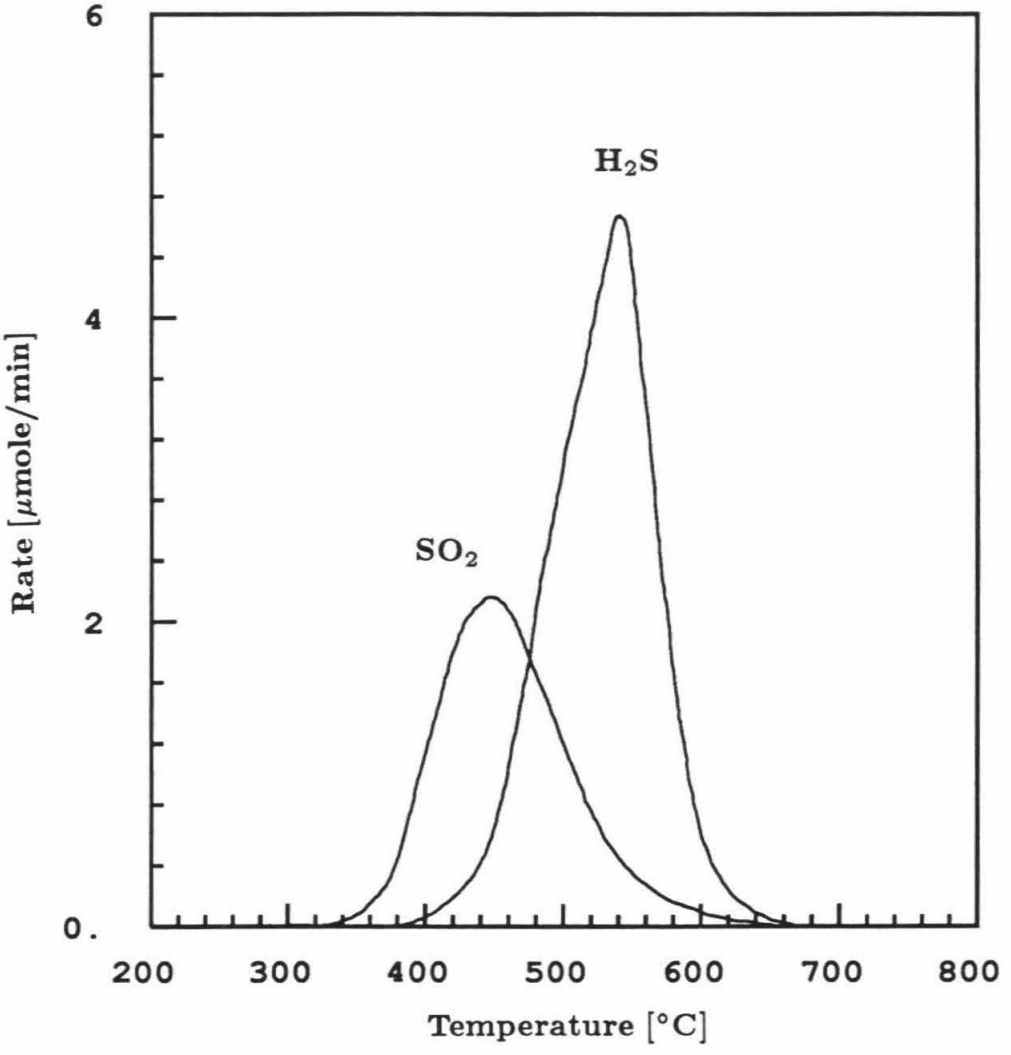

Figure 5. TPR of SO_2 adsorbed at 500°C on alumina (100mg) using 100% H_2 in N_2 as a carrier.

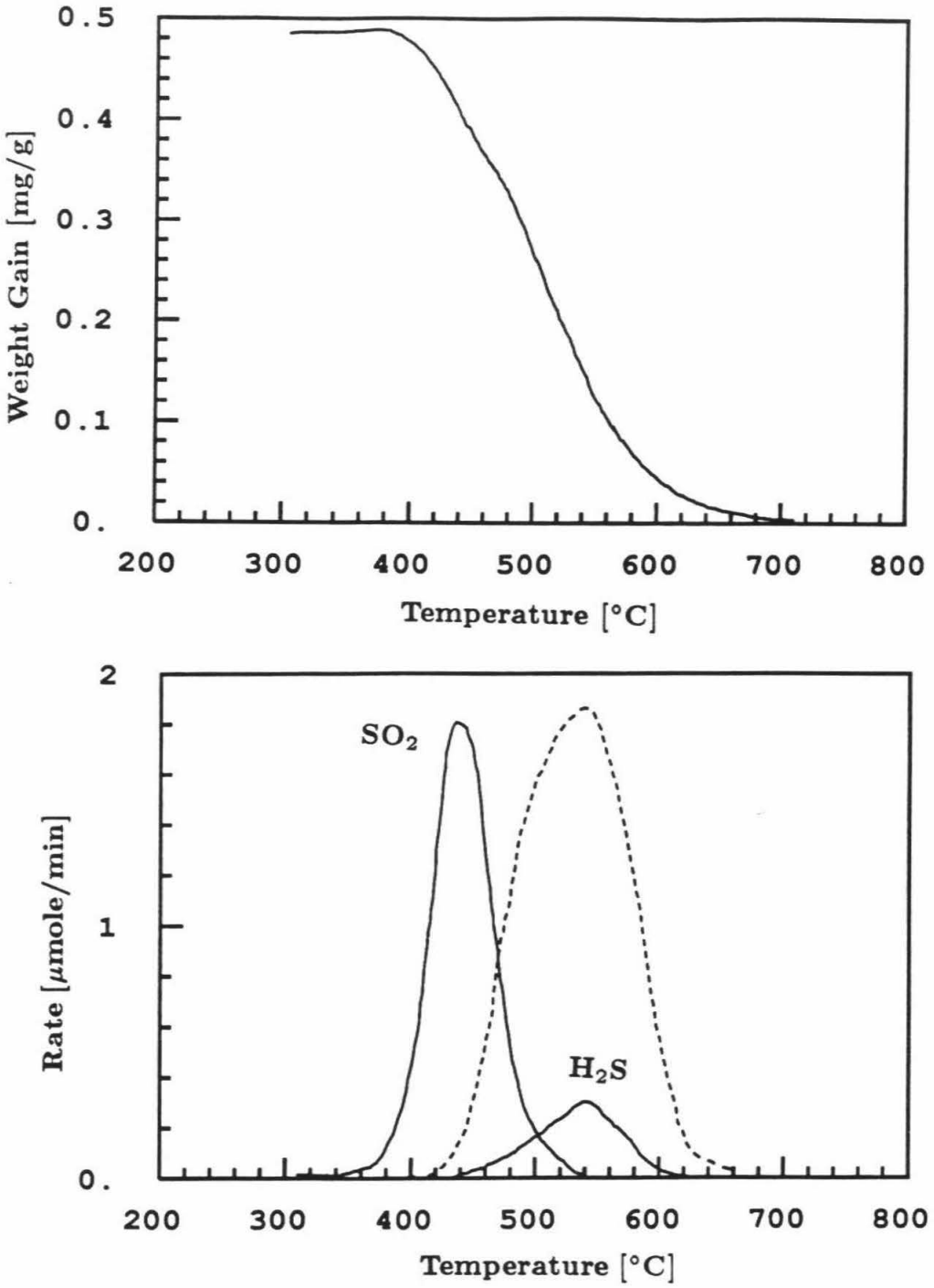

Figure 6. Weight of adsorbed SO_2 and composition of exit gases during TPR.

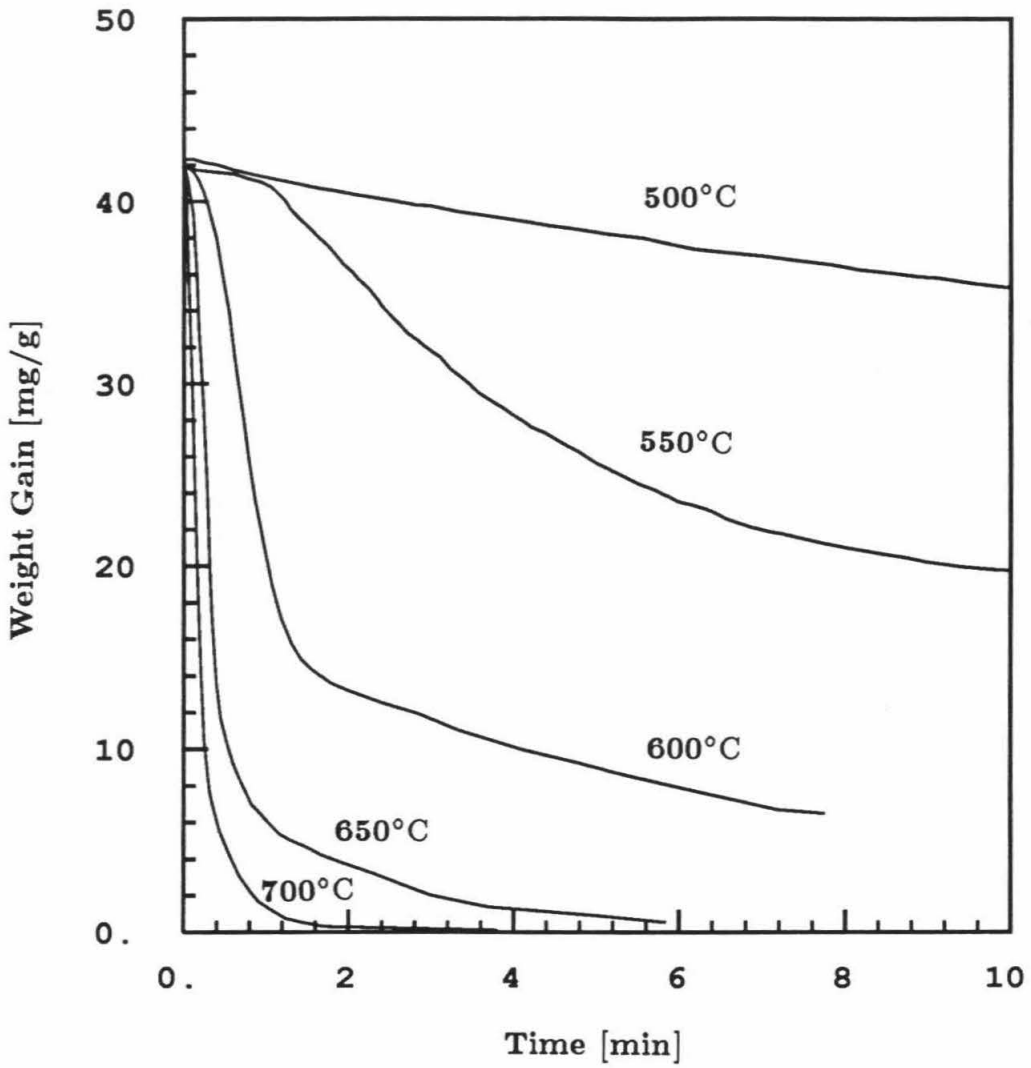

Figure 7. Weight of adsorbed species during the isothermal reduction of surface sulfate at different temperatures.

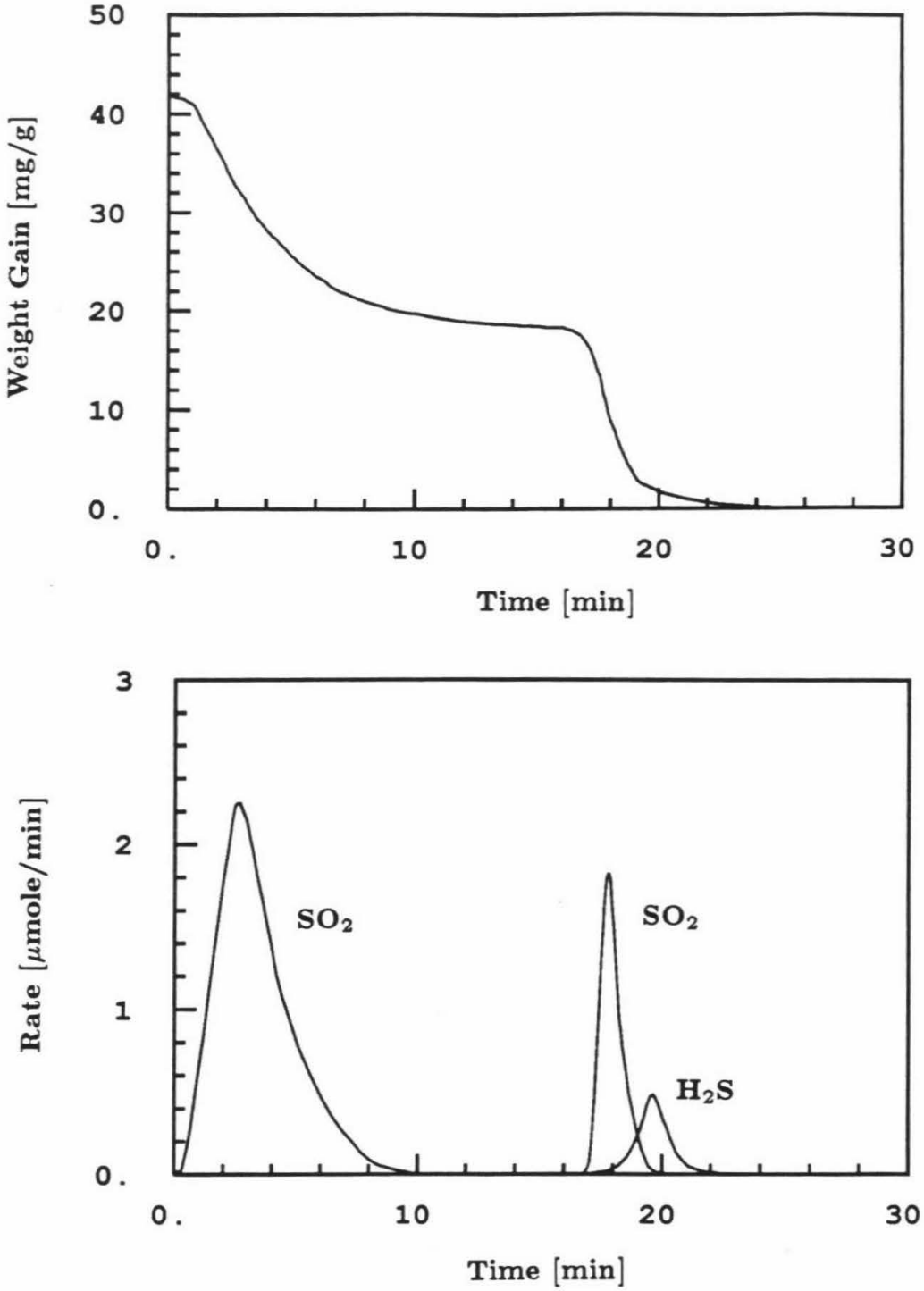

Figure 8. Weight of adsorbed species and composition of exit gases during the isothermal reduction for 17 minutes at 550°C followed by TPR.

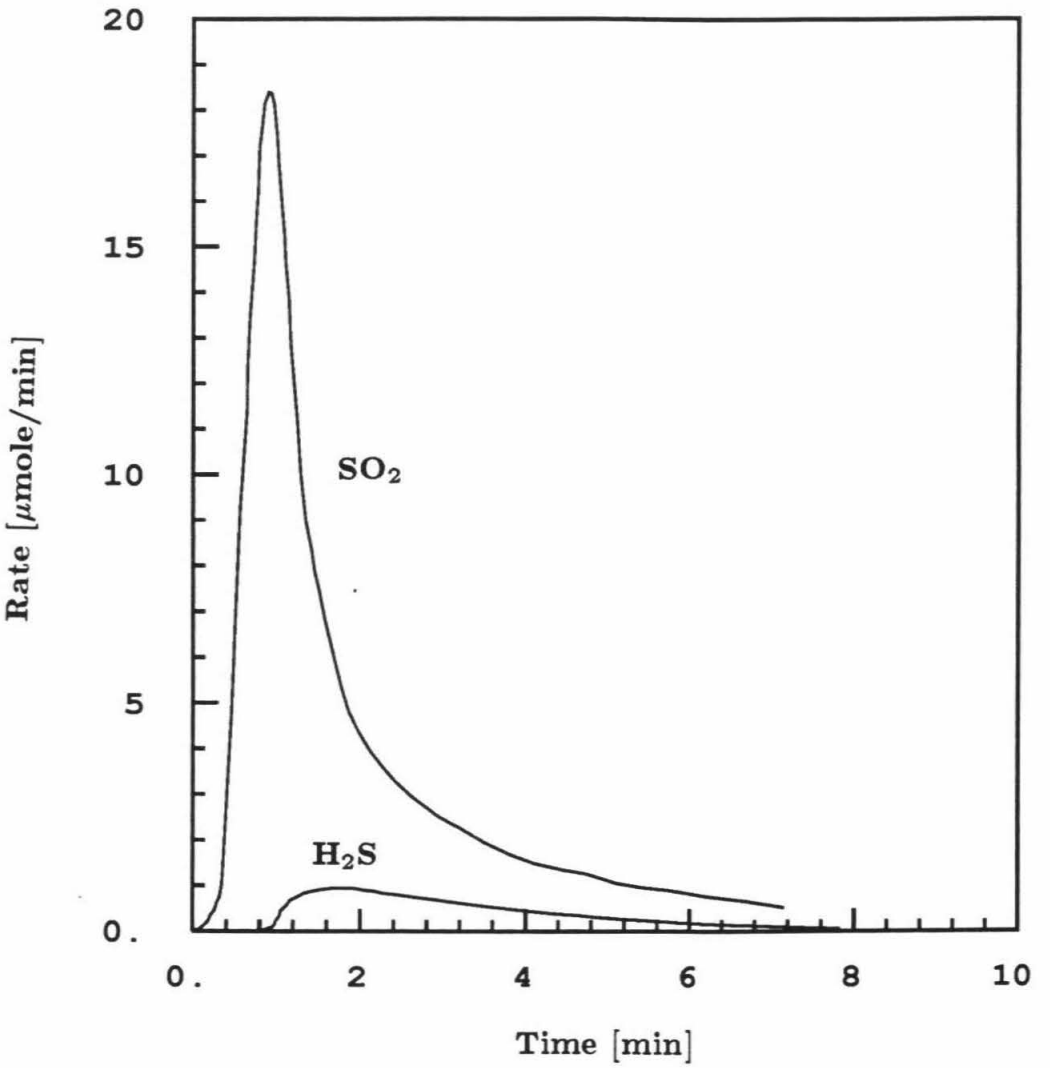

Figure 9. Isothermal reduction of surface sulfate at 600°C using 100% H_2.

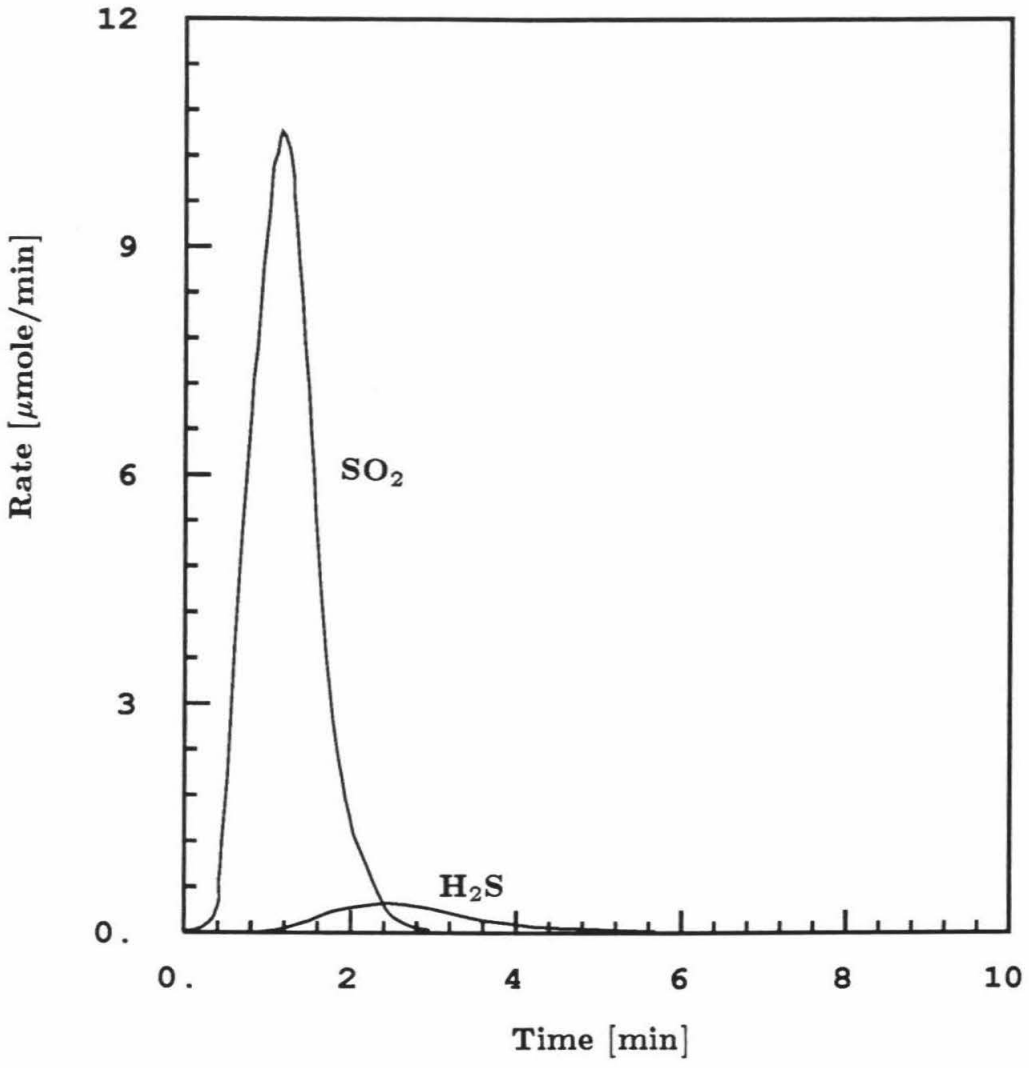

Figure 10. Isothermal reduction of surface sulfate at 700°C using 5% H_2 in N_2.

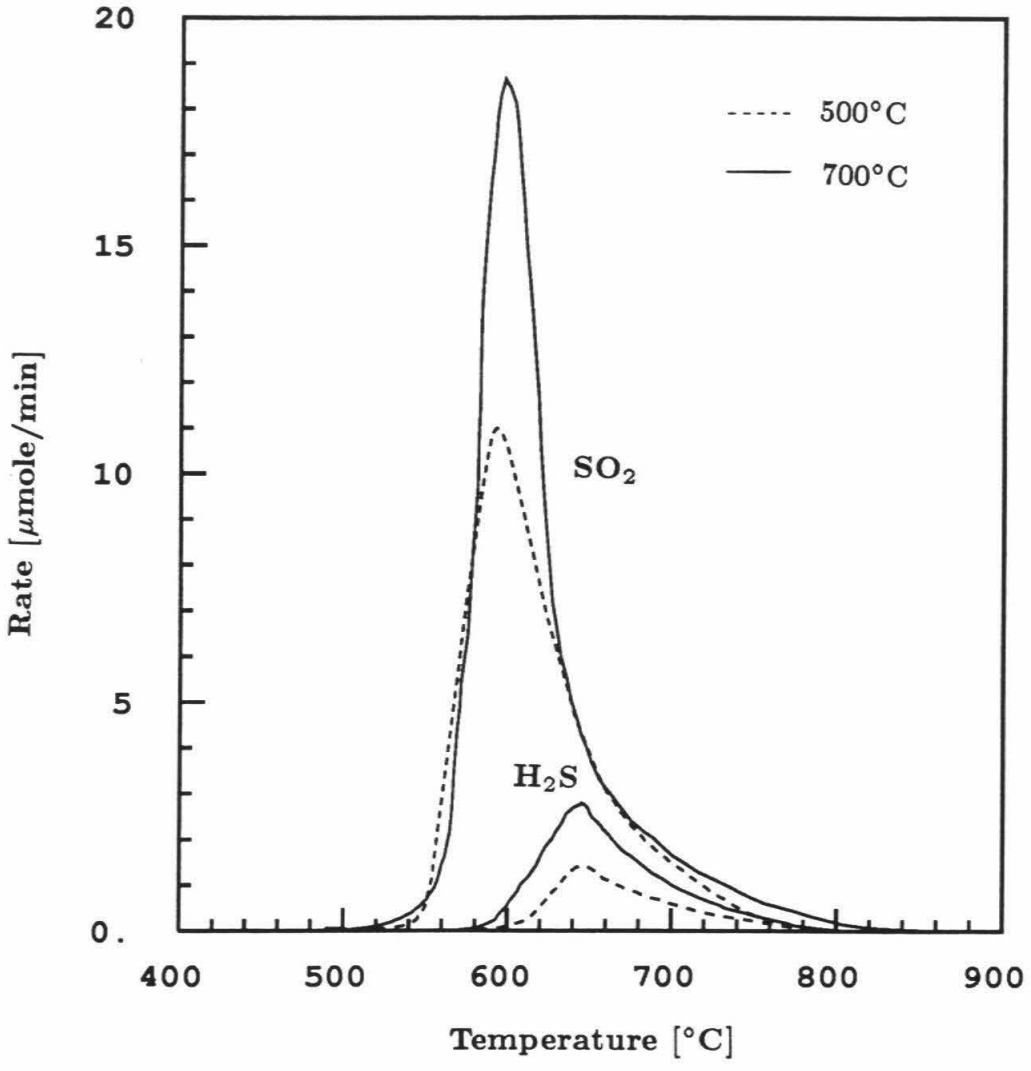

Figure 11. TPR of surface sulfate adsorbed at 500°C and 700°C using 100% H_2.

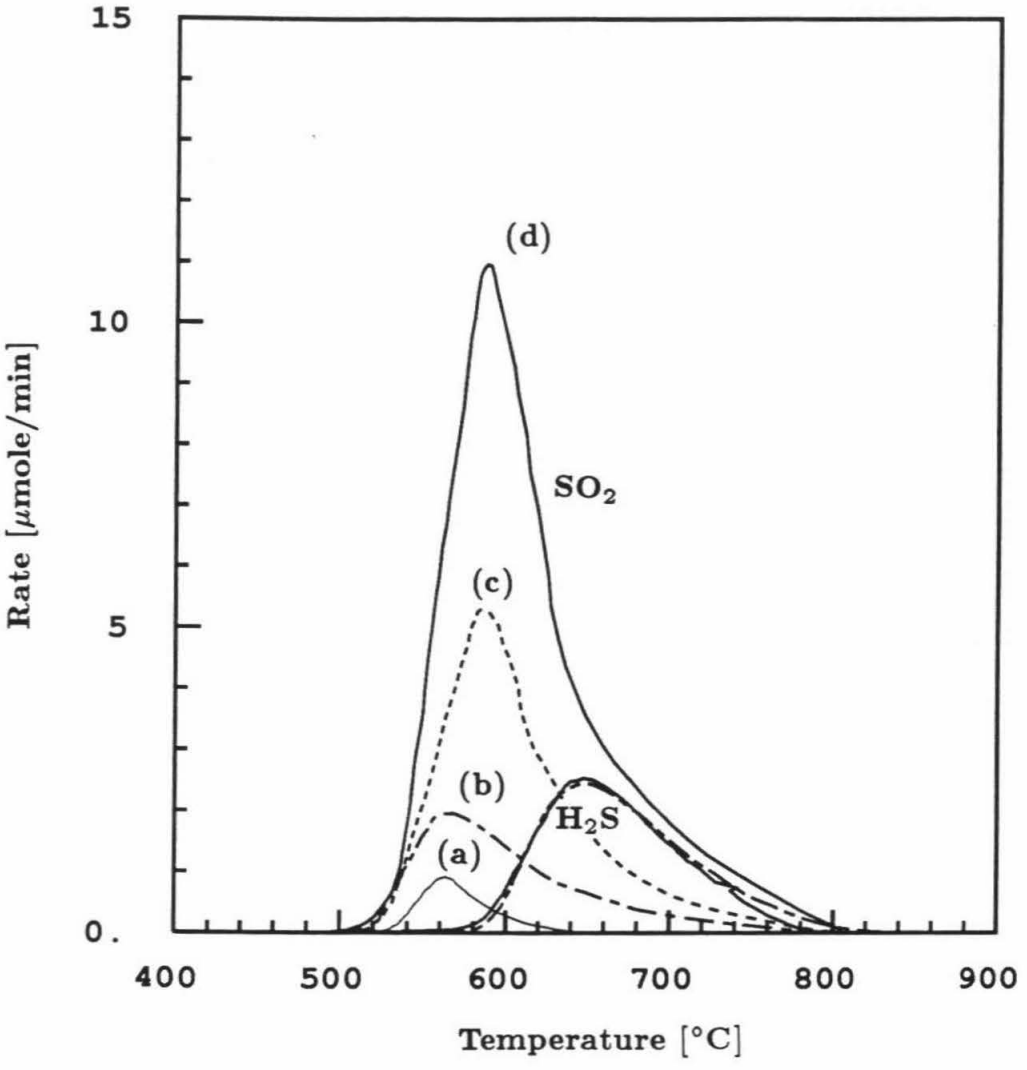

Figure 12. TPR of surface sulfate adsorbed at 500°C using 100% H_2. Adsorption time; (a) 5 min; (b) 15 min; (c) 30 min; (d) 60 min.

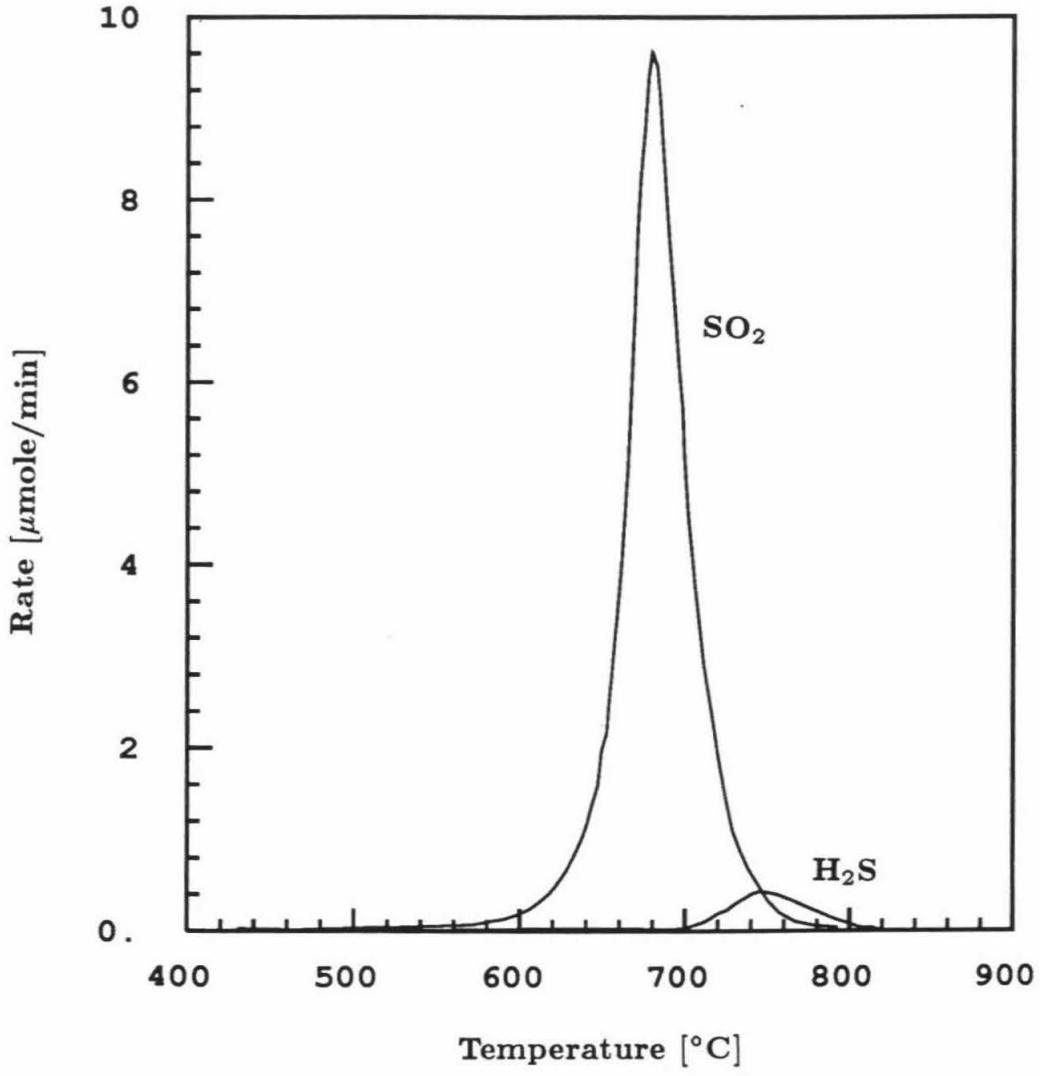

Figure 13. TPR of surface sulfate adsorbed at 700°C using 5% H_2 in N_2.

CHAPTER IV

Deposition and Stability of H_2-Permselective SiO_2 Films

1. DEPOSITION OF H_2–PERMSELECTIVE SiO_2 FILMS

ABSTRACT

Films of amorphous SiO_2 were deposited within the walls of porous Vycor tubes by SiH_4 oxidation in an opposing reactants geometry : SiH_4 was passed inside the tube while O_2 was passed outside the tube. The two reactants diffused opposite to each other and reacted within a narrow front inside the tube wall to form a thin SiO_2 film. Once the pores were plugged the reactants could not reach each other and the reaction stopped. At 450°C and 0.1 and 0.33 atm of SiH_4 and O_2, the reaction was complete within 15 minutes. The thickness of the SiO_2 film was estimated to be about 0.1μm. Measurements of H_2 and N_2 permeation rates showed that the SiO_2 film was highly selective to H_2 permeation. The H_2:N_2 flux at 450°C varied between 2000-3000. Thermal annealing at 600°C reduced somewhat that selectivity. Thermal annealing in the presence of H_2O vapor decreased further the flux of hydrogen and increased the flux of nitrogen. Permeation of hydrogen is believed to occur through an activated diffusion mechanism. Applications of such H_2-permeable films to membrane reactors for equilibrium-limited reactions are discussed.

INTRODUCTION

Recent advances in ceramic materials processing have stimulated renewed efforts to develop ceramic membranes for gas separations. Such membranes would be suitable for separations at high temperatures where the well-established organic polymer membranes cannot function. For example, the commercially available hollow fiber membranes are limited to temperatures below 100°C, but membranes made out of SiO_2 can operate at 600°C or higher.

Both porous (microporous) and nonporous inorganic membranes have been considered for gas separations. Japanese investigators have studied the separation of gases by porous glass membranes with pore size 30-50 Å [1-6]. Membranes with similar pore sizes were made by depositing a coating of microporous $\gamma - Al_2O_3$ on macroporous $\alpha - Al_2O_3$ and are available commercially as filters for liquid purification. Kameyama *et al.* describe the application of microporous (30-50 Å) glass membranes and $\gamma - Al_2O_3$ membranes to the catalytic decomposition of H_2S with simultaneous H_2 separation.

Governed by Knudsen diffusion, the separation selectivity of microporous membranes is insufficient for membrane reactors and other demanding applications. Only activated diffusion through nonporous or ultramicroporous materials can provide higher selectivities.

At present only a few inorganic materials with selective permeation properties are known. Some metals are highly selective for hydrogen permeation [7]. The best known of these metals, palladium, has been studied in connection with hydrogen separation in certain dehydrogenation reactions [8,9]. Zirconium is also selectively permeable to hydrogen and has been studied as a material for hydrogen and deuterium removal from fusion blanket fluids [10]. Certain oxides

like ZrO_2 and Bi_2O_3 are good conductors of oxygen ions and can be used for electrochemical separation of oxygen.

Besides metals, silica glass is known to be highly selective to hydrogen permeation [11-13]. For example, at 500°C the permeation rate of hydrogen is more than four orders of magnitude higher than that of O_2. This selectivity towards hydrogen is due to the small openings in the glass network being permeable only by hydrogen. The permeation is activated and increases rapidly with temperature. In this project we focus on the synthesis and properties of SiO_2 films with a principal goal of the separation of hydrogen at high temperatures. To the best of our knowledge, nonporous silica glass has not been previously investigated from the standpoint of gas separation.

One potential application of hydrogen-permeable ceramic membranes is the so-called "membrane reactor" proposed for improving conversion of equilibrium-limited reactions. This concept can be illustrated with the catalytic dissociation of hydrogen sulfide. As shown in Figure 1.1, the membrane reactor consists of a tube packed with the catalyst, housed in a nonpermeable shell (in a commercial reactor many catalyst-carrying tubes will be assembled within the reactor shell). The wall of the catalyst-carrying tube is permeable to hydrogen only by virtue of a thin nonporous layer of SiO_2. Produced by the reaction

$$H_2S = H_2 + \frac{1}{2} S_2$$

hydrogen diffuses across the tube wall and is pumped away from the annulus. Elemental sulfur flowing out of the inside tube is condensed and stored while any residual H_2 and H_2S remaining after condensation of the sulfur is recycled to the reactor.

In a conventional reactor operating at 600°C and 1 atm, the equilibrium H_2S conversion is only 2%, explaining why catalytic dissociation is not now a viable process. In a hydrogen-permeable membrane reactor operating at 600°C with inside pressure 1 atm and annulus hydrogen pressure 0.01 atm, the equilibrium conversion is 15%. This application of ceramic membrane reactors could in time displace the well established but complicated Claus process.

Selective hydrogen removal could be used to increase the conversion of other reactions such as dehydrogenation of cyclohexane to benzene [14]. and the water gas shift reaction. In the latter process a CO-rich stream generated from steam reforming of natural gas or naphtha (or gasification of coal) reacts with steam to produce hydrogen for use in ammonia synthesis or other hydrogenation reactions. Starting with a 2:1 mixture of H_2O and CO at 10 atm and 500°C, the equilibrium conversion of CO is 73.4% in a conventional reactor and 92.7% in a membrane reactor with the annulus operating at 1 atm.

We have outlined a few potential uses of ceramic gas separation membranes. Many other uses will undoubtedly be proposed if suitable membranes become available. Practical application of these membranes, however, will not be economical unless they can be made to have adequate permeation rates as well as good selectivity, requirements that are tantamount to small thickness and absence of cracks and pinholes. In addition, the membranes will have to be mechanically strong in order to be integrated into practical equipment.

Similar to polymeric membranes, ceramic membranes can be made to have mechanical strength and high permeability by applying a thin film of the selective material on a thick porous support, usually in tubular form. For this purpose one can exploit the rather extensive technology of film deposition. Both

liquid phase and gas phase techniques are widely used to deposit thin films in making optical and electronic devices. Among liquid phase techniques, the sol-gel technique in combination with dip-coating has been used extensively to deposit thin films of SiO_2 and other oxides on glass substrates [15,16]. This deposition technique may not work well with porous substrates because of the difficulty of controlling the imbibition of the alkoxide solution within the porous solid. Chemical vapor deposition (CVD) and various other gas-phase techniques have also been used widely for film synthesis. Gas phase techniques have many advantages, including the ability to produce films of controllable and uniform thickness, and are also applicable to porous substrates [17].

In this paper we report the deposition of hydrogen permselective films of SiO_2 *within* the wall of porous support tubes. Film deposition within the solid matrix prevents the formation of large pinholes and protects the deposited film from loss of adhesion or other mechanical damage. Film deposition was carried out by the oxidation of silane in the opposing reactants geometry. This geometry had been previously employed by Westinghouse researchers [18] and more recently by Carolan and Michaels [19] to deposit stabilized zirconia films on porous support tubes.

EXPERIMENTAL

Materials

Gas mixtures 10% SiH_4 in N_2, pure O_2 and pure N_2 were supplied by Matheson. Porous Vycor tubes 7 mm OD, 4.8 mm ID, 30.5 cm length, 0.3 porosity and 40Å mean pore diameter were supplied by Corning Glass. The tubes were sintered at the two ends to generate nonporous segments for connecting with fittings to the gas lines.

Film Deposition Equipment and Procedure

Film deposition was carried out using the well-known oxidation of silane

$$SiH_4 + (1+\alpha)O_2 = SiO_2 + 2(1-\alpha)H_2 + 2\alpha H_2O \quad \alpha << 1$$

Two reaction geometries were tested. The first geometry was chosen to carry out standard low pressure chemical vapor deposition. The porous support tube was placed in a cylindrical quartz shell maintained at a base pressure of 8-22 mTorr. Streams of SiH_4-N_2 and O_2-N_2 were introduced at one end of the shell while the other end was connected to a vacuum pump. The partial pressures of SiH_4 and O_2 were typically 100 and 200 mTorr respectively and the total pressure was 2 Torr. A heating element placed inside the support tube heated the entire tube length to temperatures of 250-350°C. The two ends of the support tube were sealed to prevent reactant penetration to the inside of the porous tube, other than by Knudsen diffusion through the tube wall. The deposition time varied between 15 and 85 minutes.

The second reaction geometry was implemented by the simple reactor shown in Figure 1.2. The porous support tube and a cylindrical quartz tube (1.2 cm ID) form a concentric system connected to various gas lines and placed within a clam-shell furnace. With SiH_4 flowing within the tube and O_2 flowing in the annulus, the two reactants diffuse opposite to each other and react in a narrow front—the film deposition front—within the porous wall. Because of this characteristic geometry, this deposition technique will be called the "opposing reactants" technique. The pressure at both sides of the tube wall was atmospheric and the flow rates were 30 and 45 cm^3(STP)/min for SiH_4–N_2 and O_2–N_2 respectively. A typical film deposition experiment was started by heating the system to the deposition temperature, usually 450°C, for two hours

under nitrogen flow, and then simultaneously switching on the flow of the two reactant streams. A few tubes were subjected to two or more deposition periods separated by heat treatment periods.

Heat Treatment

The tubes bearing the deposited SiO_2 film were subjected to various heat treatments. One treatment involved heating under a nitrogen flow at 450°C or 600°C for a period extending from a few hours to one day. In another treatment, the tube was cooled to ambient temperature and exposed to laboratory air for a few days or weeks. Subsequently, the tube was heated under nitrogen at 600°C. Upon exposure to laboratory air the tube adsorbed water, which turned out to have a strong effect on the subsequent thermal annealing of the film.

Permeability Measurements

The rates of hydrogen and nitrogen permeation through tubes subjected to various treatments were measured in the concentric system used for the deposition experiments (Figure 1.2). Hydrogen or nitrogen was passed through the inside tube usually at 207 kPa pressure while the system was maintained at the desired temperature. The rate of gas permeation to the annular space was measured by a bubble flow meter. The lowest flow rate that could be detected by that meter was 0.1 cm^3/min. For nitrogen the permeation rate was often below that limit. To measure lower permeation rates, the annular space was evacuated and connected through a capillary to a quadrupole mass spectrometer kept under vacuum by a turbomolecular pump. A calibration curve established between permeation rate to the annular space (measured by the bubble flow

meter) and mass intensity signal was extrapolated to low signals to measure the very low flowrates of nitrogen. In a few experiments, a mixture of 5% H_2 in N_2 was admitted in the porous tube and the mass intensity ratio for H_2 and N_2 yielded the relative permeability of the tube to the two gases.

Scanning Electron Microscopy

Scanning electron microscopy of tubes carrying the deposited SiO_2 film was carried out by a *CamScan* scanning electron microscope operating at 20 kV with resolution of 50Å. Samples sectioned from various parts of the tube were cast in epoxy, polished, and gold coated for examination. In an effort to measure the film thickness, the tube was impregnated with copper nitrate and the cross-section was examined by a *JEOL Superprobe* 733 electron microprobe by wavelength dispersive spectroscopy. Distribution of copper was measured every 1 μ in the radial direction of the tube.

RESULTS AND DISCUSSION

One-Sided Film Deposition

Films deposited on the outside surface of the support tubes using one-sided silane oxidation were found to be quite porous. SEM of sectioned tubes showed these films to be 1-4 μm thick and to consist of extensively fused particles about 0.5 μm in diameter. This particulate structure indicated particle formation and growth in the gas phase accompanied by deposition and further heterogeneous growth and fusing on the tube surface. Measurement of nitrogen permeation showed equal rates for a tube carrying the SiO_2 film as for the bare tube.

An effort was made to eliminate film porosity by sintering. A tube was sintered for several hours at temperatures starting at 600°C, gradually increasing

to 800°C and staying at that temperature for two hours. Gas permeation measurements following sintering showed that porosity had not been eliminated. Sintering at temperatures above 800°C was not attempted because it would have reduced or eliminated the porosity of the Vycor tube as well as that of the film.

The properties of the films produced by one-sided reaction could have been improved by lowering the pressure of the reactant gases in order to eliminate homogeneous reaction and nucleation of SiO_2. However, at that time we started testing the opposing reactants technique and because of quick success with that technique, we totally abandoned the one-sided low pressure SiO_2 deposition.

Opposing Reactants Film Deposition

As mentioned in the experimental section, the two reactant streams are introduced at atmospheric pressure at opposite sides of the support tube wall as shown in Figure 1.2. In the first series of experiments we varied the temperature of deposition. At 350°C we found that the oxidation reaction was so slow that one hour's deposition did not measurably change the tube permeability. Evidently at such low temperature, deposition was very slow and did not constrict significantly the pores of the support tube. The next deposition experiment was carried out at 500°C. After one hour's reaction, the tube became completely impermeable to hydrogen as well as nitrogen, and a brown deposit accumulated at the inside tube surface, indicating pyrolysis of silane with formation of elemental silicon. Since pyrolysis can take place over a substantial fraction of the tube wall (from the inside surface to the point of oxygen penetration), the product, silicon, eventually formed an impermeable layer.

Having narrowed down the range of temperatures, we chose an intermedi-

ate temperature, 450°C, for the remaining experiments. Table 1.1 shows the progress of pore plugging by SiO_2 deposition at 450°C in terms of the decline of the permeation rate of nitrogen. Pore plugging is rapid, becoming complete after about ten minutes.

Table 1.2 shows the permeation rates of H_2 and N_2 through a tube subjected to various treatments. Immediately after deposition at 450°C, the film was permeable to H_2 only. Upon heating at 600°C the flux of hydrogen declined somewhat while the flux of nitrogen remained negligible. After exposure to ambient (moist) air for two weeks and subsequent heating at 600°C, the flux of hydrogen declined further while a measurable flux of nitrogen appeared for the first time, evidently due to densification and shrinkage intensified by the presence of water vapor. Additional exposure to moist air and heating did not cause any further change of permeation rates. The densification of SiO_2 by heat treatment in the presence of water vapor has been documented in previous studies of film deposition for electronic and optical devices [20].

A second SiO_2 deposition at 450°C was carried out to plug the microporosity that developed due to heating at 600°C in the presence of moisture. Figure 1.3 shows the fluxes of hydrogen and nitrogen versus temperature for the tube after the second SiO_2 deposition. At 25°C, the flux of both gases is at the ratio of the respective Knudsen diffusion coefficients, evidently due to a small residual porosity. With increasing temperature the flux of nitrogen decreases in accordance to Knudsen diffusion. In contrast, the flux of hydrogen increases due to the increasing contribution of activated diffusion. At 600°C the ratio of the H_2:N_2 fluxes is 300:1.

Further experiments were carried out to study the progress of pore plug-

ging during deposition and the effect of subsequent thermal annealing at the same temperature, 450°C. A tube was subjected to a sequence of five minute depositions (450°C, 5% SiH_4 in N_2, 15% O_2 in N_2), each followed by a two-hour period during which the permeation rates of H_2 and N_2 were measured at the same temperature, 450°C. The results are shown in Table 1.3. The first row gives the rates for the untreated tube, where the rate ratio 3.68 is close to 3.74, the ratio of Knudsen diffusivities. After five or six reaction periods, the nitrogen permeation rate declined to zero while the permeation rate of hydrogen reached a stable value, which is about one third that of the untreated tube. The hydrogen to nitrogen ratio reached a value above 3,000. After the sixth deposition the tube was heat treated for one-day and two-day periods at 450°C without appreciable change in the rate of hydrogen permeation. The rate of nitrogen permeation increased slightly such that the rate ratio stabilized to a value near 2000.

The permeation rates listed in Tables 1.1–3 are determined by two resistances in series, that of the SiO_2 film, and that of the porous tube. To compare the relative permeability of the film material alone we have calculated and listed in the last two columns of Table 1.3 the fluxes that would occur in the absence of the resistance of the porous tube. The corrected fluxes were computed as outlined in the subsection on activation energy.

The thickness of the SiO_2 films deposited by the opposing reactants technique could not be measured directly. SEM of polished cross sections at 5000 magnification also did not identify the location of the film. Evidently the similarity of film and substrate materials did not provide sufficient contrast, or polishing smeared any existing contrast. Another idea that was tried was to

impregnate the tube with a solution of copper nitrate. After drying, cutting, and polishing, we traced the cross section by an electron microprobe. The expectation was that the salt solution could penetrate everywhere except the film region. Again, the analysis did not reveal any region that had not been penetrated by the salt. Either polishing smeared the salt profile, or the film thickness was substantially smaller than the electron beam diameter of 1 μm.

The location of the SiO_2 film within the tube wall can be estimated if the reaction stoichiometry is known. Assuming a fast 1:1 reaction with products SiO_2 and H_2 (neglecting the small amount of H_2O product) we obtain the simple relation

$$\frac{\ln\left(\frac{r_o}{r_f}\right)}{\ln\left(\frac{r_f}{r_i}\right)} = \frac{P_{O_2} D_{K,O_2}}{P_{SiH_4} D_{K,SiH_4}}$$

where r_i, r_o, r_f are the inner, outer and film radii, P_{O_2}, D_{K,O_2} and P_{SiH_4}, D_{K,SiH_4} are the partial pressure and Knudsen diffusivities of O_2 and SiH_4. For the reactant pressures used in the experiments described in Table 1.1–3, the film location was calculated as $r_f = 2.6$mm ($r_i = 2.4$mm, $r_o = 3.5$mm).

Estimation of Film Thickness

We first note that the film consists of patches of deposited SiO_2 within an underlying structure of Vycor glass (>96% SiO_2). The geometry is quite complicated, but the film region can be assumed to be a slab of uniform thickness. We shall further assume that the Vycor matrix and the deposited SiO_2 have the same permeability, an assumption that plausible for the films that have been subjected to densification. We consequently consider the film described in Table 1.2 before the second SiO_2 deposition. Furthermore, we neglect the resistance to permeation by the porous tube itself. At 450°C the flux of hydrogen is 3.6×10^{-2}cm^3 (STP) /cm^2 atm min. This can be corrected for the Knudsen

flux through the small residual microporosity as follows

$$Q'_{H_2} = Q_{H_2} - \left(\frac{28}{2}\right)^{1/2} Q_{N_2}$$

The corrected flux is $Q'_{H_2} = 2.5\text{x}10^{-2}\text{cm}^3$ (STP) /cm^2 atm min. The permeability of nonporous Vycor at that temperature is

$2.4\text{x}10^{-7}\text{cm}^3$(STP)/cm atm min [21]. Using these values we estimate the film thickness to be about 0.1μm.

Estimation of Activation Energy

Permeation of hydrogen is believed to occur through a solution-diffusion mechanism. The mechanism involves the steps of adsorption at the high pressure side, solution of the gas within the bulk of the solid, diffusion to the low pressure surface, and desorption from that surface. Reaction of hydrogen with oxygen groups in the solid may also play some role in the transport.

The results of Figure 1.3 can be used to estimate an activation energy for hydrogen permeation. For that purpose the flux must be adjusted for the effect of the resistance by the porous tube itself as well as for the small microporosity present in the film.

The gas flux can be written as the ratio of the pressure difference, ΔP, and a suitable resistance, R, :

$$Q = \frac{\Delta P}{R}$$

The resistance is the sum of the resistance of the film, R_f, and the resistance of the bare tube, R_t, in view of the negligible volume occupied by the film. We then have

$$\frac{1}{Q} = \frac{R_t + R_f}{\Delta P} = \frac{R_t}{\Delta P} + \frac{R_f}{\Delta P} = \frac{1}{Q_t} + \frac{1}{Q_f}$$

where Q_t and Q_f are the gas fluxes possessed by the bare tube and by the film in the absence of the support tube. Since the flux through the bare support tube is known, we can calculate the hypothetical flux Q_f through a bare film. The flux of nitrogen needs no comparable correction, for the resistance of the film far outweighs the resistance of the porous tube. Thus, we may define the corrected flux of hydrogen as

$$Q'_{f,H_2} = Q_{f,H_2} - \left(\frac{28}{2}\right)^{1/2} Q_{N_2}$$

An Arrhenius plot of the corrected hydrogen flux above 200°C was fitted very well by a straight line yielding an activation energy of 34.7 KJ/mol. This is similar to the activation energy 37.7 KJ/mol reported by [22] for fused quartz.

CONCLUSIONS

Thin films of SiO_2 were deposited within the wall of porous support tubes using the SiH_4–O_2 reaction in an opposing reactants geometry. Although in this initial study we did not examine systematically the effect of reaction conditions, we expect that film thickness decreases with increasing temperature and reactant concentrations. For the conditions of our experiments the film thickness was estimated to be about 0.1 μm.

The SiO_2 material deposited at 450°C is stable upon further heat treatment at 450°C but undergoes densification upon heat treatment at 600°C. This densification is intensified by the presence of water vapor. The SiO_2 deposited at 450°C is selectively permeable to hydrogen with the permeability ratio of hydrogen to nitrogen at 450°C being about 2000. Densification by heating at 600°C, especially in the presence of water vapor, reduces the permeability

and the selectivity of the film. The reduction of selectivity is due to shrinkage creating a small microporous volume permeable by Knudsen flow.

Deposition of thin SiO_2 films within the wall of porous tubes can be used to make ceramic membranes for very selective hydrogen separation at high temperatures. Such membranes can be used to improve the conversion of equilibrium-limited reactions such as hydrogen sulfide decomposition. The opposing reactants technique could be applicable to the deposition of other oxides materials by gas phase or liquid phase reactions.

REFERENCES

[1] T. Kameyama, M. Dokiya, H. Yokokawa and K. Fukuda, *Ind. Eng. Chem. Fundam.* **20**, 97 (1981).

[2] Y. Shindo, T. Hakuta, H. Yoshitome and H. Inouye, *J. Chem. Eng. Japan* **16**, 120 (1983).

[3] Y. Shindo, T. Hakuta, H. Yoshitome and H. Inouye, *J. Chem. Eng. Japan* **17**, 650 (1984).

[4] Y. Shindo, T. Hakuta, H. Yoshitome and H. Inouye, *J. Chem. Eng. Japan* **18**, 485 (1985).

[5] K. Haraya, Y. Shindo, T. Hakuda and H. Yoshitome, *J. Chem. Eng. Japan* **19**, 186 (1986).

[6] K. Haraya, Y. Shindo, T. Hakuda and H. Yoshitome, *J. Chem. Eng. Japan* **19**, 461 (1986).

[7] W. G. Perkins, *J. Vac. Sci. Technol.* **10**, 543 (1973).

[8] H. Nagamoto and H. Inouye, *Chem. Eng. Commun.* **34**, 315 (1985).

[9] N. Itoh, *A.I.Ch.E. J.* **33**, 1576 (1987).

[10] C. Hsu and R. E. Buxbaum, Palladium-coated zirconium membranes for oxidative extraction. *Preprint Annual AIChE Meeting*, New York (1987).

[11] V. O. Altemose, *J. Appl. Phys.* **32**, 1309 (1961).

[12] V. O. Altemose, Permeation of gases in glass. *Seventh Symposium on the Art of Glassblowing*, The American Scientific Glassblowers Society, Wilmington, Del. (1962).

[13] D. C. Boyd and D. A. Thompson, Glass., Encyclopedia of Chemical Tech-

nology Vol. 11, pp 807-881 (1981).

[14] O. Shinju, M. Misonou and Y. Oneda, *Bull. Chem. Soc. Japan* **55**, 2760 (1982).

[15] S. M. Lee, Film deposition techniques., Encyclopedia of Chemical Technology Vol. 10, pp 246-283 (1980).

[16] S. Sakka, *Treatise on Material and Technology* **22**, 129 (1982).

[17] J. M. Blocher, *Thin. Solid Films* **77**, 51 (1981).

[18] A. O. Isenberg, *Solid State Ionics* **3**, 431 (1981).

[19] M. F. Carolan and J. N. Michaels, *Solid State Ionics* **25**, 207 (1988).

[20] W. A. Pliskin, *J. Vac. Sci. Technol.* **14**, 1064 (1977).

[21] C. C. Leiby, Jr. and C. L. Chen, *J. Appl. Phys* **31**, 268 (1960).

[22] R. W. Lee, *J. Chem. Phy.* **38**, 448 (1963).

Table 1.1. Progressive pore plugging during film deposition at 450°C with reactants 10% SiH_4 in N_2 and 33% O_2 in N_2.

Deposition Time (min)	Q_{N_2} [cm^3(STP)/cm^2 atm min] at 450°C,ΔP = 30 psi
0	1.75×10^{-1}
6	1.17×10^{-2}
11	5.33×10^{-5}
16	0.

Table 1.2 Effect of heat treatment and exposure to humid air on the permeation of H_2 and N_2 through SiO_2 films deposited at 450°C with reactants 10% SiH_4 in N_2 and 33% O_2 in N_2.

Treatment	Permeation rate [cm^3 (STP) /cm^2 atm min] $Q_{H_2}x10^3$	$Q_{N_2}x10^3$
Immediately after deposition	196	0
After 1 h at 600°C	135	0
After 17 hr at 600°C	75	0
After 2 week ambient and 1 day at 600°C	42	2.9
After 3 month ambient and 1 day at 600°C	36	2.8
After second SiO_2 deposition at 450°C	19	0.17

Table 1.3. Evolution of hydrogen and nitrogen permeation rates after successive five minute depositions at 450°C, with reactants 5% SiH_4 in N_2 and 15% O_2 in N_2.

Numbers of Depositions	Gas Flux [cm^3 (STP) / cm^2 atm min] H_2	N_2	Flux Ratio	Corrected Flux [cm^3 (STP) / cm^2 atm min] H_2	N_2
0	0.637	1.73×10^{-1}	3.68		
1	0.542	7.82×10^{-2}	6.93	3.65	1.43×10^{-1}
2	0.440	5.51×10^{-2}	7.99	1.42	8.09×10^{-2}
3	0.353	3.01×10^{-2}	11.7	0.792	3.64×10^{-2}
4	0.221	3.07×10^{-3}	72.0	0.338	3.13×10^{-3}
5	0.196	4.82×10^{-4}	407	0.284	4.84×10^{-4}
6	0.182	5.50×10^{-5}	3310	0.255	5.50×10^{-5}

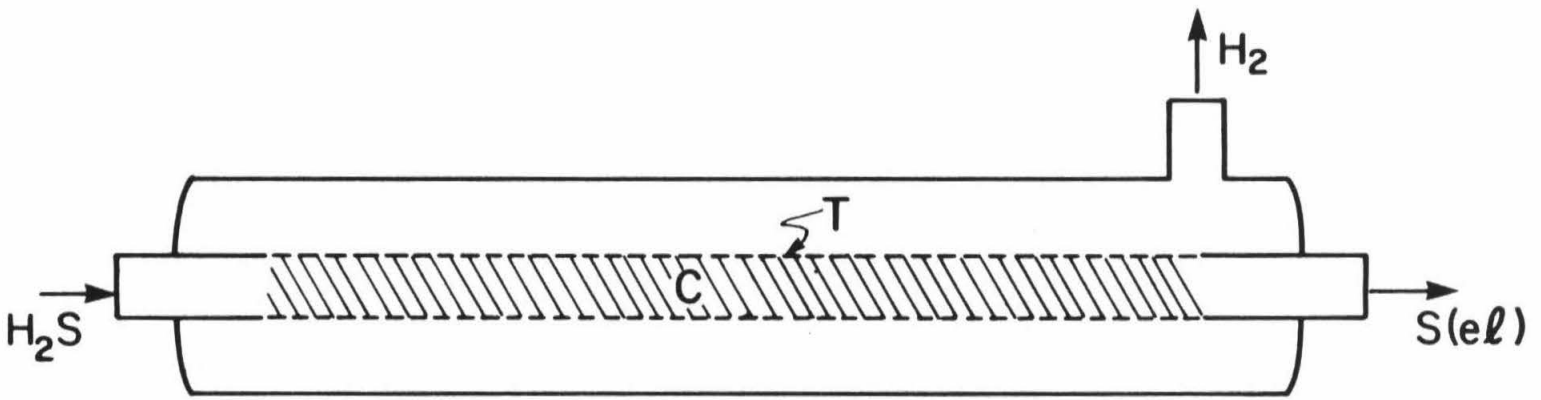

Figure 1.1 Schematics of a membrane reactor for H_2S conversion to elemental sulfur and hydrogen. T : hydrogen permeable tube ; C : catalyst bed

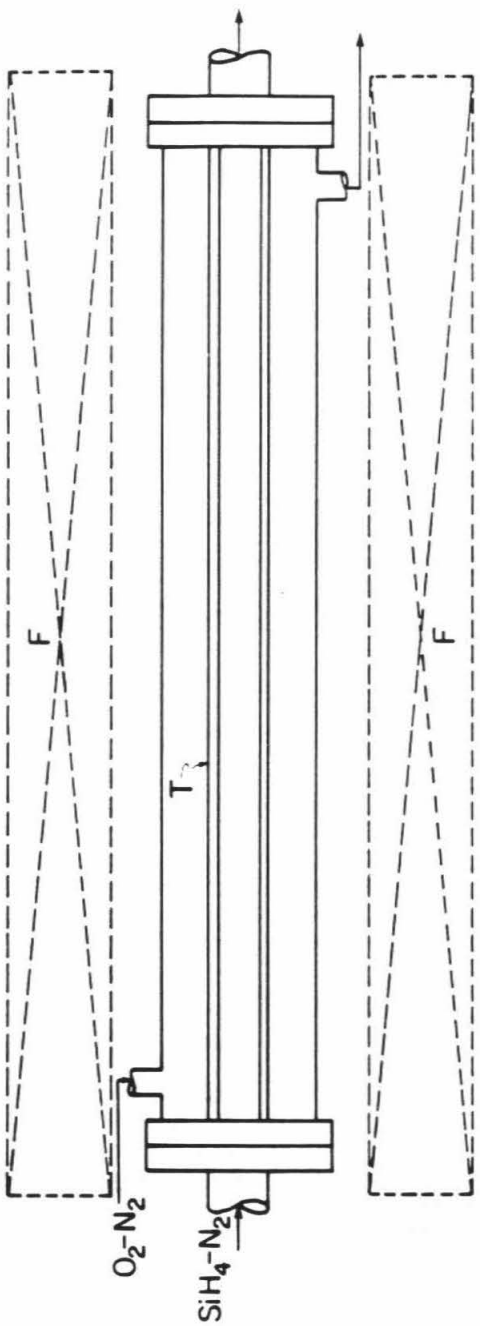

Figure 1.2 Apparatus for film deposition by the opposing reactants technique. T : porous Vycor tube ; F : furnace

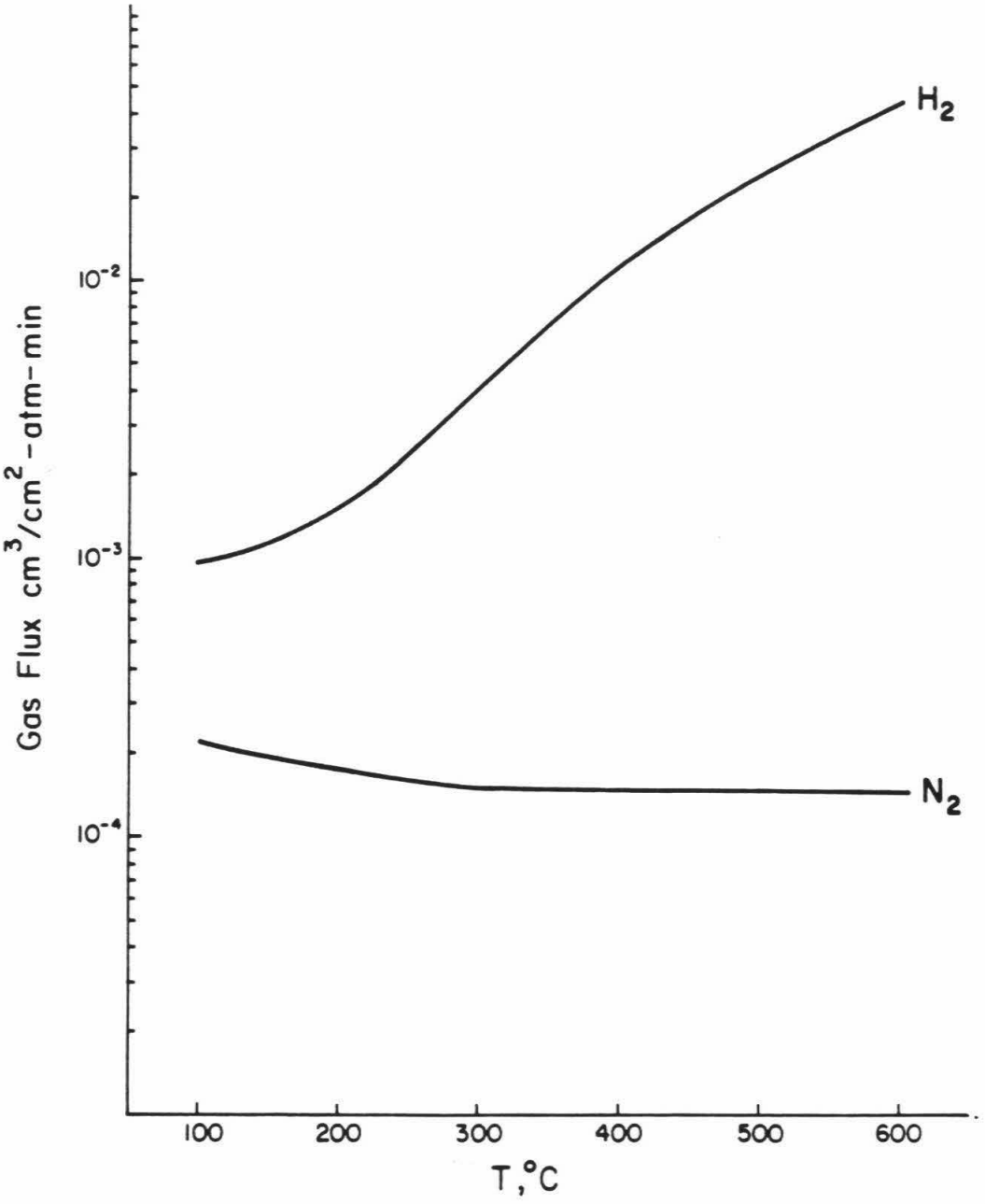

Figure 1.3 Hydrogen and nitrogen fluxes through a porous Vycor tube carrying a SiO_2 film deposited by the opposing reactants technique.

2. STABILITY OF H_2-PERMSELECTIVE SiO_2 FILMS FORMED BY CHEMICAL VAPOR DEPOSITION

ABSTRACT

Thin SiO_2 films were heat treated in different gas mixtures to determine their stability in functioning as high-temperature hydrogen permselective membranes. The films were formed within the walls of porous Vycor tubes by SiH_4 oxidation in an opposing reactants geometry. Film deposition was carried out at 450 °C in the presence and absence of water vapor. Immediately after formation, the films were highly selective to hydrogen permeation having a H_2:N_2 permeability ratio of about 3000 : 1. The films were subsequently heat-treated at 450 - 700°C in dry N_2, dry O_2, N_2-H_2O, and O_2-H_2O mixtures. The permeation rates of H_2 and N_2 changed depending on the original conditions of film formation as well as on the heat treatment. Heating in dry N_2 slowly reduced the permeation rates of both H_2 and N_2. Heating in a N_2-H_2O atmosphere led to a steeper decline of H_2 permeability. But the permeation rate of N_2 increased or decreased according to whether the film deposition had been carried out in the absence or presence of H_2O vapor, respectively. Thermal treatment in O_2 caused rapid decline of the permeation rates of H_2 and N_2 in films that were deposited under dry conditions. The decline was moderate in films deposited under wet conditions.

INTRODUCTION

Hydrogen permselective ceramic membranes can be used in membrane-reactor configurations to improve the yield of certain equilibrium-limited catalytic reactions such as hydrogen sulfide decomposition and water gas shift reaction. Such a combination of catalysis and gas separation requires a membrane with high selectivity, adequate permeation rate, and mechanical, thermal, and chemical stability. Amorphous silicon dioxide in nonporous form has very high selectivity but low permeability for hydrogen. Its application to membrane separations consequently hinges on the ability to produce it in the form of a very thin film free of cracks or pinholes and applied on a porous support material to achieve mechanical stability.

We have recently deposited films of amorphous SiO_2 within the walls of porous Vycor tubes by SiH_4 oxidation in an opposing reactant geometry [1] : SiH_4 was passed inside the tube while O_2 was passed outside the tube. The two reactants diffused opposite to each other and reacted within a narrow front inside the tube wall to form a thin SiO_2 film. Measurements of H_2 and N_2 permeation rates showed that the SiO_2 film was highly selective to H_2 permeation. The H_2:N_2 flux varied between 2000-3000 while the hydrogen permeation coefficient was on the order of 0.2 cm^3 [STP] $/cm^2 - atm - min.$

Silicon dioxide formed by chemical vapor deposition is known to undergo densification upon prolonged exposure to high temperatures [2,3]. This densification is intensified in the presence of water vapor to such an extent that heating in steam at 450°C for 10 hours decreased the film thickness by 7.9% from the as-deposited value [4]. In our previous experiments we found that thermal treatment in the presence of water vapor caused significant changes in

the film properties [1]. In particular we observed a decrease in the hydrogen permeation coefficient and selectivity of the membrane.

In membrane reactor operation, the extent of property degradation would depend on the gaseous environment (reactants, products) and the temperature. For example, in hydrogen sulfide decomposition the membrane will be subjected to temperatures 600°C or higher, while in the water-gas shift reaction the membrane will be exposed to water vapor but at substantially lower temperatures. The purpose of this paper was to report some results on the effect of thermal treatment at different temperatures and gaseous atmospheres. Some limited results are also reported on the effect of water vapor during film deposition on the subsequent film stability to thermal treatment.

EXPERIMENTAL

Film Deposition

Films of SiO_2 were deposited within the walls of porous Vycor tubes by SiH_4 oxidation in the opposing reactant geometry described elsewhere [1]. The dry deposition was carried out at 450 and 440°C with 0.05 atm of SiH_4 in N_2 and 0.15 atm of O_2 in N_2. The humid deposition was carried out at the same temperatures with 0.05 atm of SiH_4 in N_2, and 0.04 atm of H_2O and 0.15 atm of O_2 in N_2. The moist gases were prepared by passing the oxygen nitrogen stream through a glass vessel filled with water and maintained at 30°C. The deposition reactions were carried out for 30 to 60 minutes until the rates of N_2 permeation decreased to about 10^{-5} cm^3 [STP] $/cm^2 - atm - min$.

Heat Treatment

The tubes bearing the deposited SiO_2 films were subjected to various heat treatments. The ambient gases used were dry N_2, 4% H_2O in N_2 (wet N_2), dry O_2, and 4% H_2O in O_2 (wet O_2). One treatment involved heating of the film deposited under dry conditions at 450°C with dry N_2, wet N_2, and dry O_2. In another treatment, the tubes were successively heated in different gaseous environments for 1 day at 440, 600, and 700°C.

Permeability Measurements

The rates of hydrogen and nitrogen permeation through the tubes during the reaction and during various treatments were measured in the concentric system used for the deposition experiments. Hydrogen or nitrogen was passed through the inside of the tube usually at 310 kPa pressure while the system was maintained at 440 or 450°C. The rate of gas permeation to the annular space was measured by a bubble flow meter when the gas flux was high. To measure lower permeation rates, the annular space was evacuated and connected to a Baratron pressure gauge interfaced with a microcomputer. After the annular volume was isolated from the evacuation system, the initial pressure increase gave the permeation rate, with the use of a calibration curve. The permeation coefficient (cm^3 [STP] $/cm^2 - atm - min$) was defined as the flux of gas through the inner surface area of the tube when the pressure difference was 1 atm.

RESULTS AND DISCUSSION

Effects of water during film deposition

The evolution of hydrogen and nitrogen permeation rates after successive 5-minute reaction intervals is shown in Figure 2.1. Before deposition, the

H_2:N_2 flux ratio was close to 3.7, the ratio of Knudsen diffusivities. During SiO_2 deposition the permeation rates of both gases decreased. In 30 minutes the H_2 permeation rate declined from 0.7 to 0.2cm^3 [STP] /cm^2−atm−min whereas the N_2 permeation rate decreased from 0.2 to $10^{-5}cm^3$ [STP] /cm^2−atm−min. With water vapor present during the reaction, the permeation rate of N_2 declined further. Comparing two films when they have the same value of H_2 permeation rate, the N_2 permeation rate through the film deposited in the presence of water is lower than the rate through the film deposited under dry conditions (Fig. 2.2). The somewhat higher H_2 selectivity of the film prepared in the presence of water vapor may be due to the formation of a denser but more uniform film.

Thermal treatment

The first series of densification experiments was carried out at 450°C under dry N_2 and wet N_2 (4% H_2O in N_2) on a film that had been deposited under dry conditions. The permeation rates of H_2, N_2, and He during a 5-day treatment period are presented in Figure 2.3. The permeability plots demonstrate that treatment with wet N_2 causes a pronounced change in the permeation rates. Thermal treatment in wet N_2 for 1 day decreases the H_2 flux by 55% and the decrease becomes 68% after five days. The permeation rate decreases rapidly during the first day of treatment and then decreases more slowly. When the heat treatment is carried out in dry N_2, the H_2 flux decreased by only 1% or 9% after one day and five days respectively. The flux of N_2 also changed with thermal treatment. In dry N_2, the flux of N_2 decreased by 32% in 5 days while in treatment with wet N_2, the N_2 flux decreased by 83% in the same period. The permeation rate of He did not change very much upon thermal treatment.

Treatment for 5 days in dry N_2 and wet N_2 caused 5% and 25% declines in the He permeation rate.

The second series of thermal treatment experiments was carried out under dry N_2, wet N_2, dry O_2, or wet O_2 using films deposited under dry or wet conditions. The temperature was stepwise increased from 440°C to 600°C to 700°C with 1 day heating at each temperature. The gas flux generally decreased with each treatment and the rate of this decrease depended on both ambient conditions and film type.

For a film that had been deposited under dry conditions, treatment with dry N_2 at 440°C caused a small change in permeation rates as mentioned earlier. But treatment with dry N_2 at 600°C significantly decreased the H_2 flux and further heating at 700°C reduced this flux further as shown in Figure 2.4. The flux of N_2 also decreased slowly under heating in dry N_2. The decline of the H_2 and N_2 permeabilities reflects the densification of the SiO_2films. In the case of H_2, densification raises the activation energy of permeation as shown in the Arrhenius plot of Figure 2.5. The activation energies estimated for films treated in dry N_2 at 440, 600, and 700°C were 6.2, 22, and 30 kJ/mole, respectively.

Heat treatment in wet N_2 at 440°C of films deposited under dry conditions decreased the H_2 flux and increased the N_2 flux, as mentioned earlier. Further heating at 600 and 700°C with wet N_2 reduced the H_2 flux and increased the N_2 flux further. But once the film was subjected to densification at 440°C, the change of the gas flux upon further heating was relatively small. Heat treatment in dry O_2 significantly decreased the permeation rates of both H_2 and N_2, although the decrease was more pronounced for N_2. These decreases are rapid

in the first 6 hours at 440°C and then become very slow. Further heating under O_2 at 600°C caused a slow further decline in the permeation rate of H_2 and N_2. However, heat treatment under O_2 at 700°C caused further reduction of the H_2 rate but increased the N_2 rate to the level measured immediately after deposition.

The results of thermal treatment of films deposited under wet conditions are shown in Figure 2.6. The N_2 and H_2 permeation rates decreased with each treatment. The H_2 permeation rate decreased to a lesser extent than for the case of the film deposited under dry conditions. The permeation rate of N_2 declined with wet N_2 treatment unlike the experiments with the film deposited under dry conditions. Wet O_2 treatment caused reduction of the N_2 permeation rate even at 700°C, again unlike the experiments with films produced under dry conditions.

As mentioned earlier, the changes in gas permeabilities are caused by the densification of the SiO_2 film material. This densification takes place by thermal treatment alone but is more pronounced in the presence of water vapor [2,3]. It has been suggested that densification by thermal treatment involves removal of silanol groups (Si-OH) in the SiO_2 film and formation of Si-O-Si bonds to close the channel. Water vapor seems to strongly catalyze the rearrangement of siloxane bonds and help dehydroxylation and thus densification (5).

The increase of N_2 permeation with wet N_2 treatment of films formed under dry conditions suggests microcrack formation during densification. Deposition under dry conditions may create tensile stresses in a SiO_2 film but subsequent thermal treatment of the stressed film with dry N_2 may cause

uniform densification, avoiding crack formation. In the absence of cracks, densification reduces the permeation rates of both H_2 and N_2. Wet N_2 treatment, on the other hand, decreases the permeation of hydrogen but increases the permeation of nitrogen. The reasons for this opposite direction of the change in N_2 permeation rate caused by dry and wet thermal treatments are unclear. One possible explanation can be sought in the uneven infiltration of water in the film creating regions of uneven shrinkage which results in the formation of microcracks. The formation of cracks in SiO_2 films was cited previously [6]. Deposition on silicon and even quartz results in cracking, especially when the film is thick. H_2 permeation through these microcracks makes a relatively minor contribution in view of the dominant contribution of diffusion through the nonporous material. But diffusion of nitrogen through the microcracks can become the major contribution in view of the negligible permeation through the nonporous material.

It has been found that the stress in CVD SiO_2 films could be decreased by the addition of water vapor to the reactant [7]. For films formed in the presence of water vapor, the decrease rather than increase of the N_2 permeation rate suggests that microcracks are not generated during the thermal treatment of this material. One possible explanation of this behavior is that water vapor during the reaction relieves the stresses in the film, allowing uniform densification upon subsequent thermal treatment.

The rapid decrease in permeability caused by heating in O_2 at 440°C can again be attributed to film densification. This finding is consistent with the results of a previous study showing that densification at 770°C was more rapid under air than under Ar [4]. The SiO_2 films tested in this latter study were pre-

pared by SiH_4 oxidation at O_2:SiH_4 ratios above 10. When this ratio fell below 4, the films were deficient in oxygen and contained an intermediate stoichiometric oxide Si_2O_3 [8] or a nonstoichiometric phase [9]. The O_2:SiH_4 ratio in our experiments varied spatially within the porous wall from extremely oxygen-rich on the one side of the tube to extremely silane-rich at the other side. It is likely therefore that the films contained oxygen-deficient regions that were oxidized and became denser during subsequent thermal treatment.

Evolution of film permeability during alternating periods of deposition and thermal treatment

A final experiment was carried out involving alternating intervals of deposition at 440°C in the presence of water vapor, and six-hour intervals of thermal treatment at 600°C under wet O_2. After each thermal treatment the temperature was decreased to 440°C and the permeation rates of H_2, N_2, and He were measured at that temperature. Figure 2.7 shows the evolution of gas flux as a function of cumulative deposition time. In 5 minutes of deposition, the flux of N_2 decreased drastically, while the fluxes of H_2 and He underwent a modest decline. Interestingly, the He:H_2 ratio, which was below unity before deposition, increased to 2 after 5 minutes of deposition. After 15 minutes of deposition (cumulative) and intervening periods of heat treatment, the H_2:N_2 ratio increased to 2800. After the last interval of deposition (15 minutes cumulative) and the last heat treatment period, the permeabilities of the three gases were measured at different temperatures. An Arrhenius plot of these measurements is shown in Figure 2.8. The N_2 permeation rate is very low and follows the Knudsen temperature dependence ($\propto T^{-\frac{1}{2}}$). The permeation rates of H_2 and He are activated with energies 26.4 and 6.8 kJ/mole respectively.

CONCLUSIONS

Films of SiO_2 deposited within the walls of porous Vycor tubes by dry or wet SiH_4 oxidation have been subjected to various thermal treatments that cause changes in permeation rates of H_2 and N_2. These changes depended on treatment temperature, gaseous atmosphere, and film type. Thermal treatment with dry N_2 slowly reduced the permeation rates of both H_2 and N_2. Treatment with H_2O-N_2 mixtures significantly decreased the flux of hydrogen. The same treatment increased the flux of nitrogen for those films that were deposited under dry conditions, and decreased the flux of nitrogen for the films deposited under wet conditions. Thermal treatment in oxygen had an even larger effect on the permeation rates. Heating under oxygen at temperatures as low as 440°C caused a rapid decrease in the permeation of both hydrogen and nitrogen. Deposition in the presence of water vapor followed by thermal treatment under H_2O-O_2 gave dense and relatively stable films with H_2:N_2 flux ratios above 2000.

REFERENCES

[1] G. R. Gavalas, C. Megiris and S. W. Nam, Deposition of H_2-Permselective SiO_2 Films. *Chem. Eng. Sci.*, in press (1989).

[2] B. Swaroop, "Low temperature densification of silica films," in Thin Film Dielectrics, Vratny (Ed.), The Electrochem. Soc., New York (1969).

[3] W. A. Pliskin, *J. Vac. Sci. Technol.*, **14**, 1064 (1977).

[4] W. Kern, RCA Rev., 37, 55 (1976).

[5] R. K. Iler, "The Chemistry of Silica," John Wiley and Sons, New York (1979).

[6] N. Goldsmith and W. Kern, *RCA Rev.*, **28**, 153 (1977).

[7] W. Kern, G. L. Schnable and R. B. Fisher, *RCA Rev.*, **37**, 3 (1976).

[8] E. Ritter, *Opt. Acta.*, **19**, 197 (1962).

[9] M. Nakamura, Y. Mochizuki, K. Usami, Y. Itoh and T. Nozaki, *J. Electrochem. Soc.*, **132**, 482 (1985).

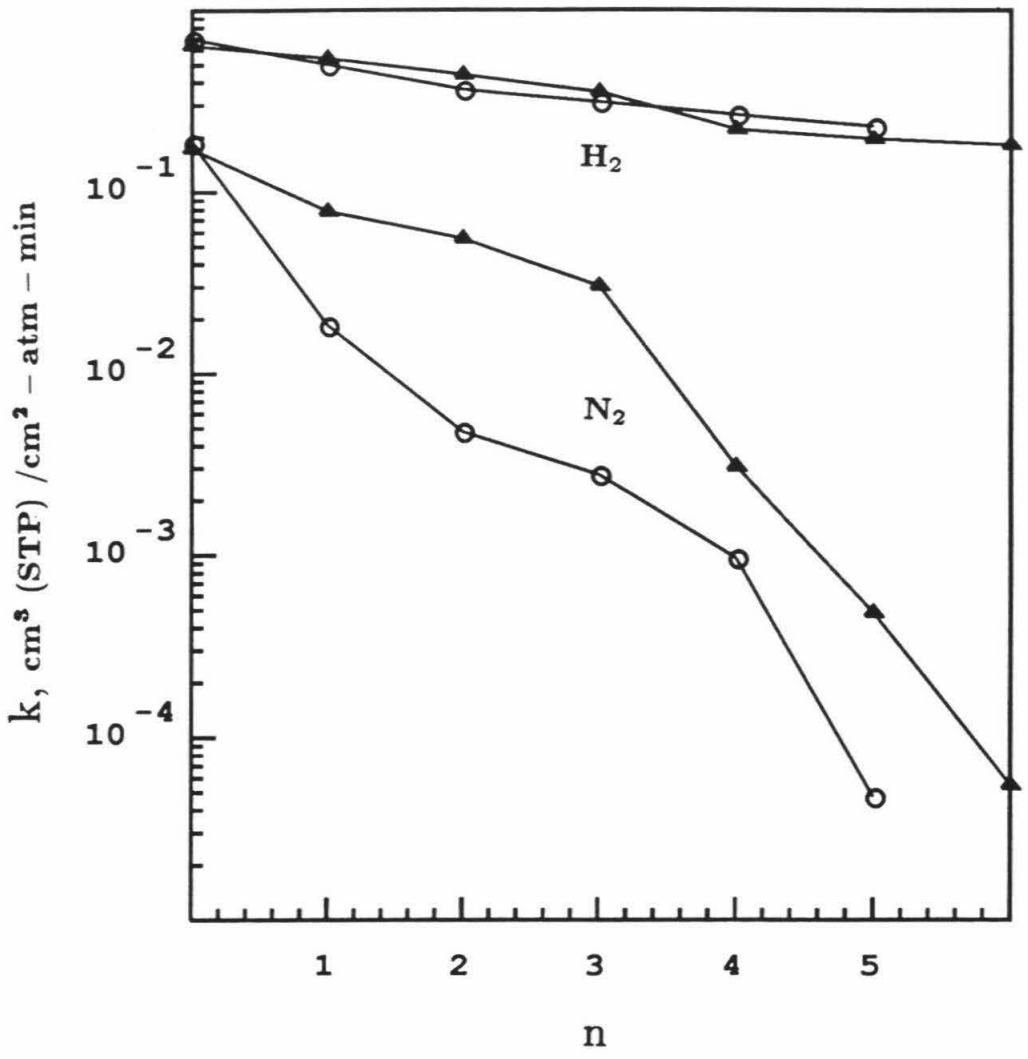

Figure 2.1 Evolution of H_2 and N_2 permeation rates after successive 5-minute deposition intervals. k : permeation coefficient ; n : number of deposition intervals ; △ : dry reaction ; ○ : humid reaction.

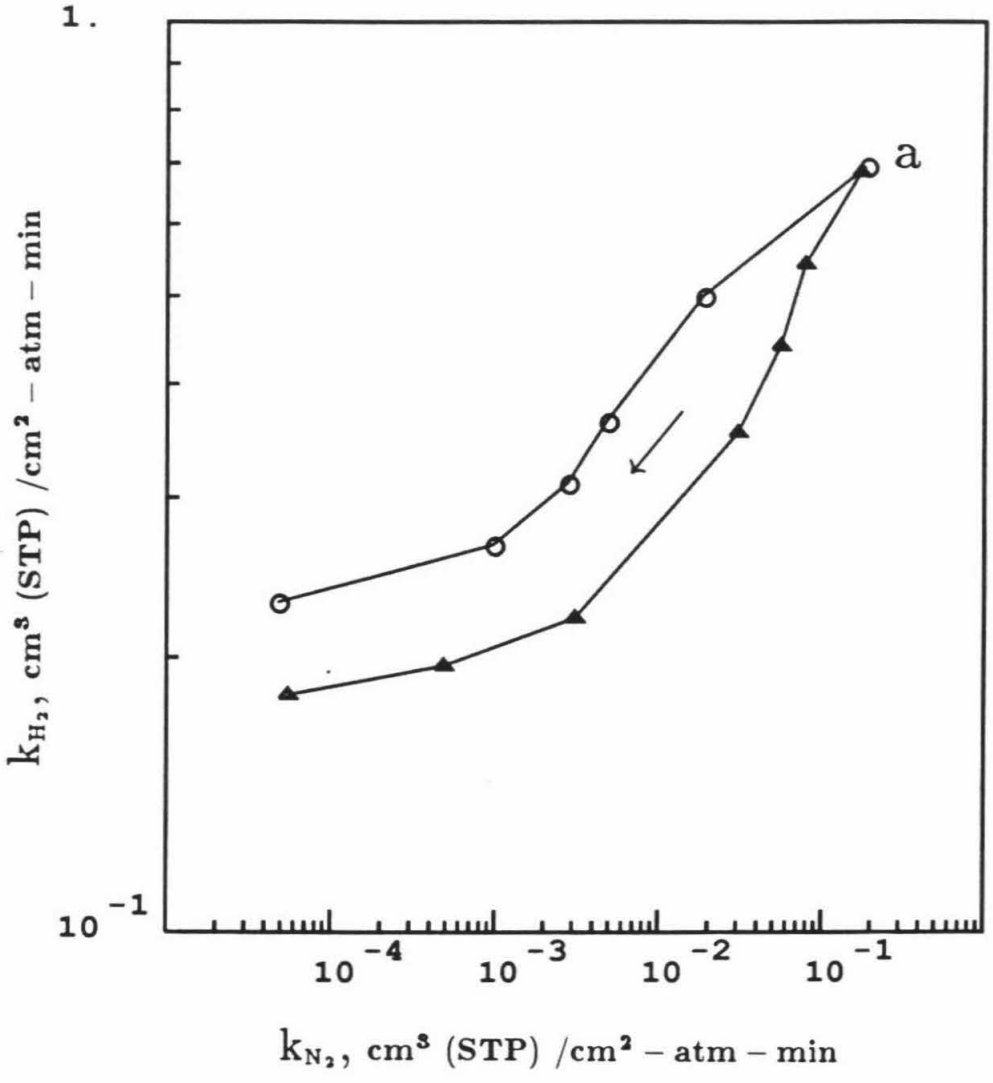

Figure 2.2 Evolution of H_2 and N_2 permeation rates after successive 5-minute deposition intervals. Arrow indicates the direction of deposition reaction. k_{H_2} : permeation coefficient of H_2 ; k_{N_2} : permeation coefficient of N_2 ; a : permeation coefficients before deposition ; △ : dry reaction ; ◯ : wet reaction.

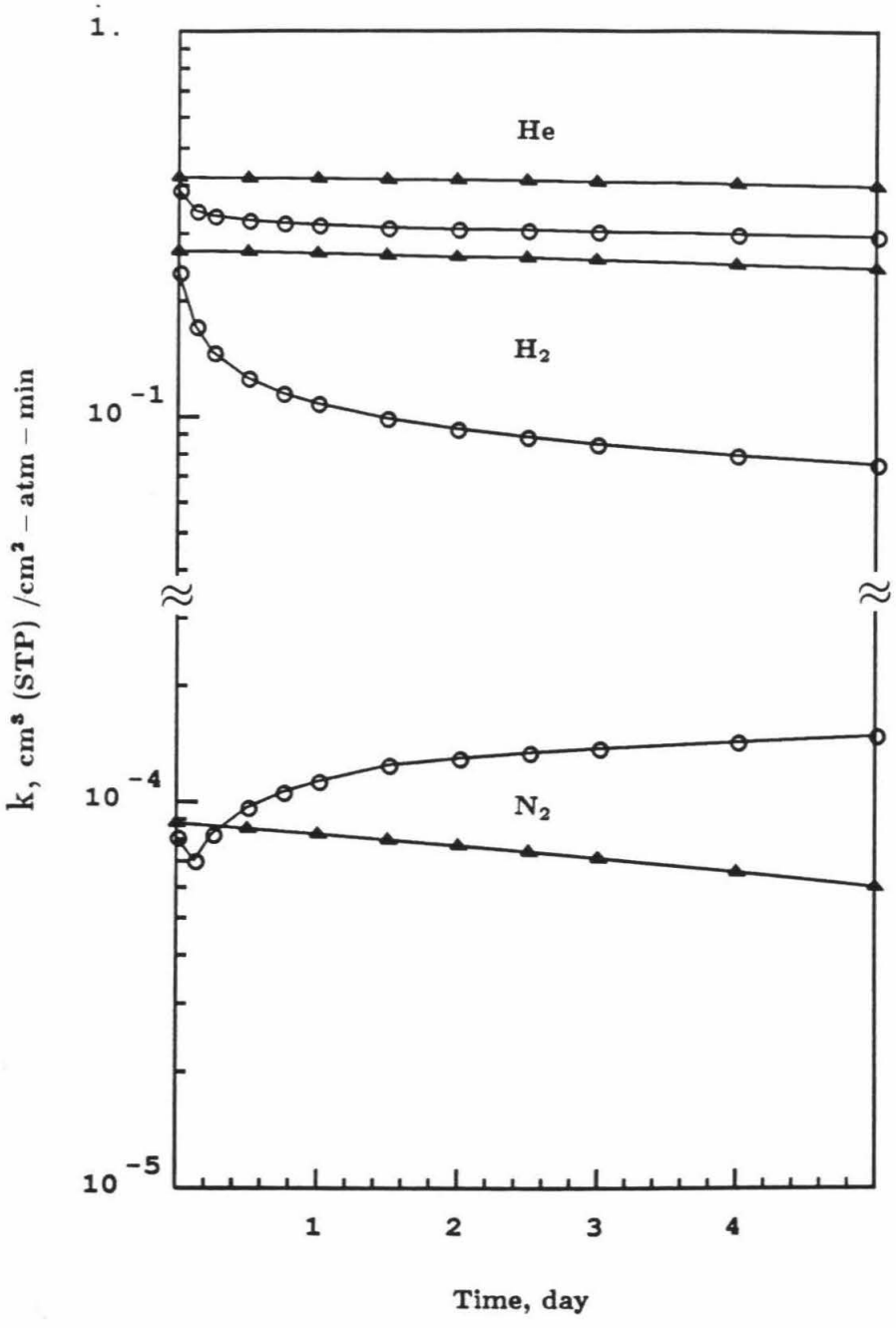

Figure 2.3 Permeation rates of gases during a 5-day thermal treatment period at 450°C. k : permeation coefficient ; △ : treatment without H_2O ; ○ : treatment with H_2O.

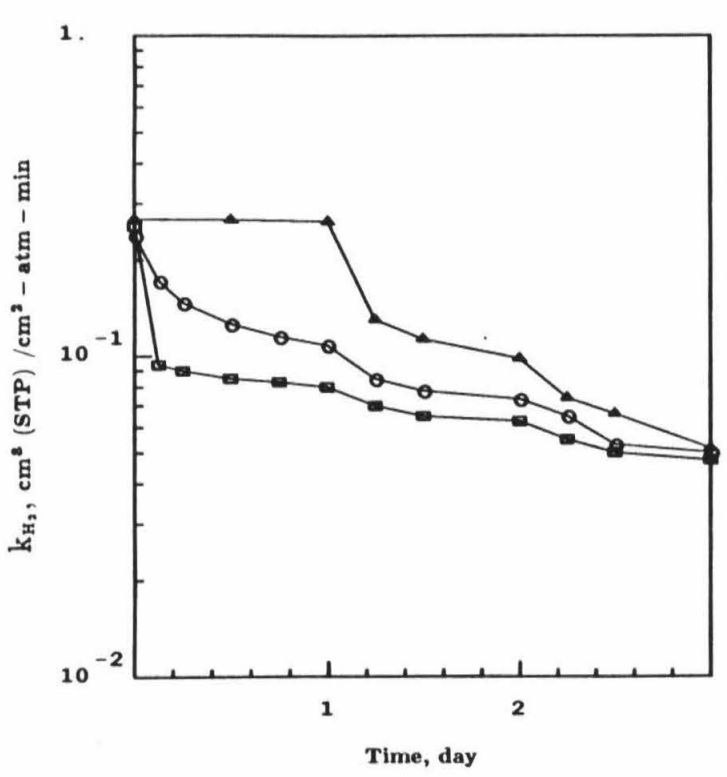

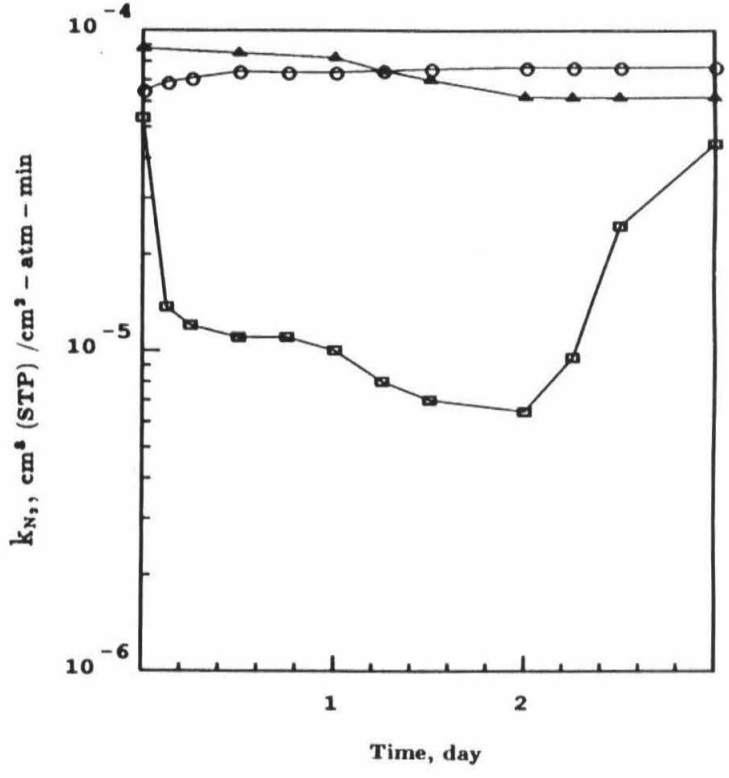

Figure 2.4 Permeation rates of gases during successive 1-day thermal treatments at 440, 600, and 700°C. Films were deposited under dry conditions. △ : treatment with dry N_2 ; ○ : treatment with wet N_2 ; □ : treatment with dry O_2.

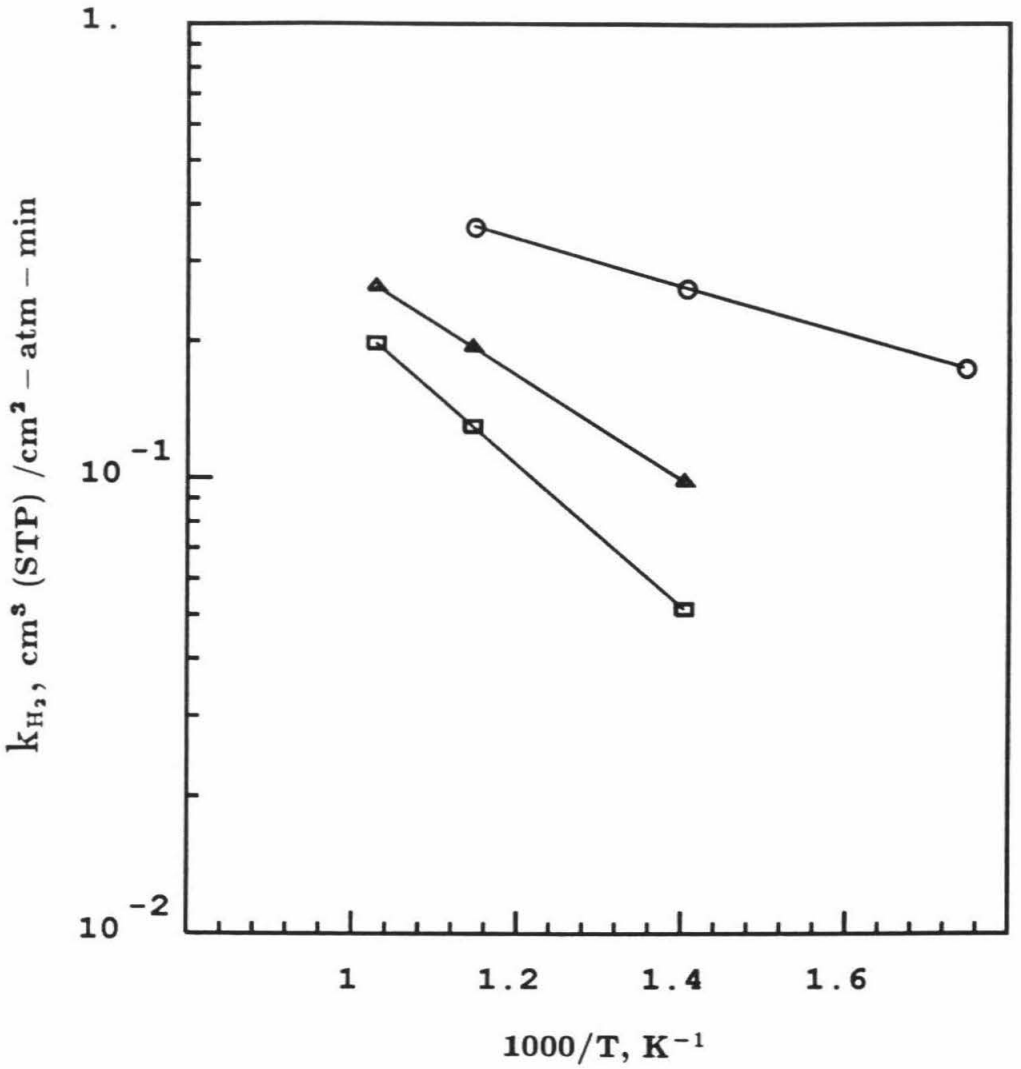

Figure 2.5 Permeation rates of H_2 during thermal treatment. Films were deposited under dry conditions. ○ : after 1 day treatment at 440°C ; △ : after 1 day treatment at 600°C ; □ : after 1 day treatment at 700°C.

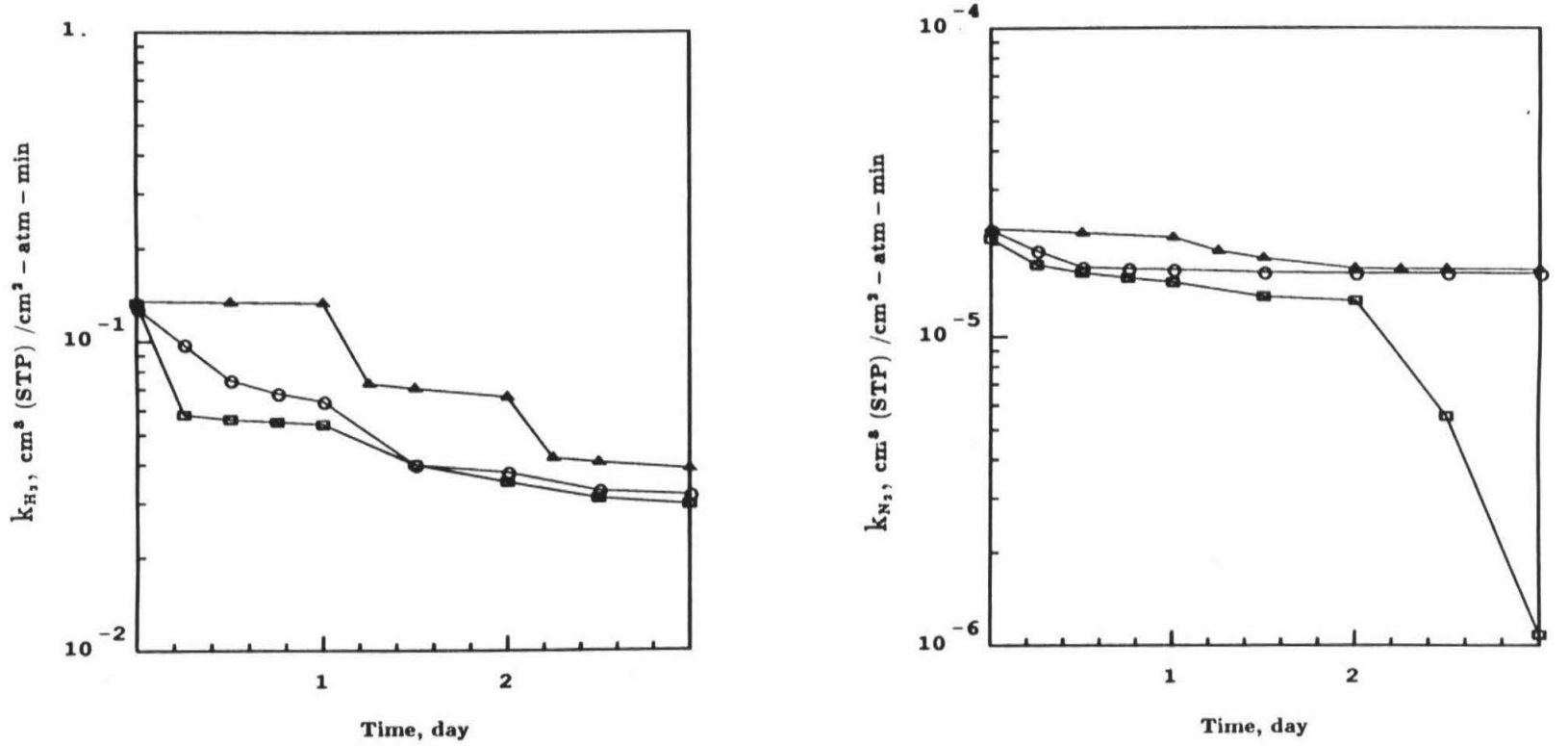

Figure 2.6 Permeation rates of gases during successive 1-day thermal treatments at 440, 600, and 700°C. Films were deposited under wet conditions. △ : treatment with dry N_2 ; ○ : treatment with wet N_2 ; □ : treatment with wet O_2.

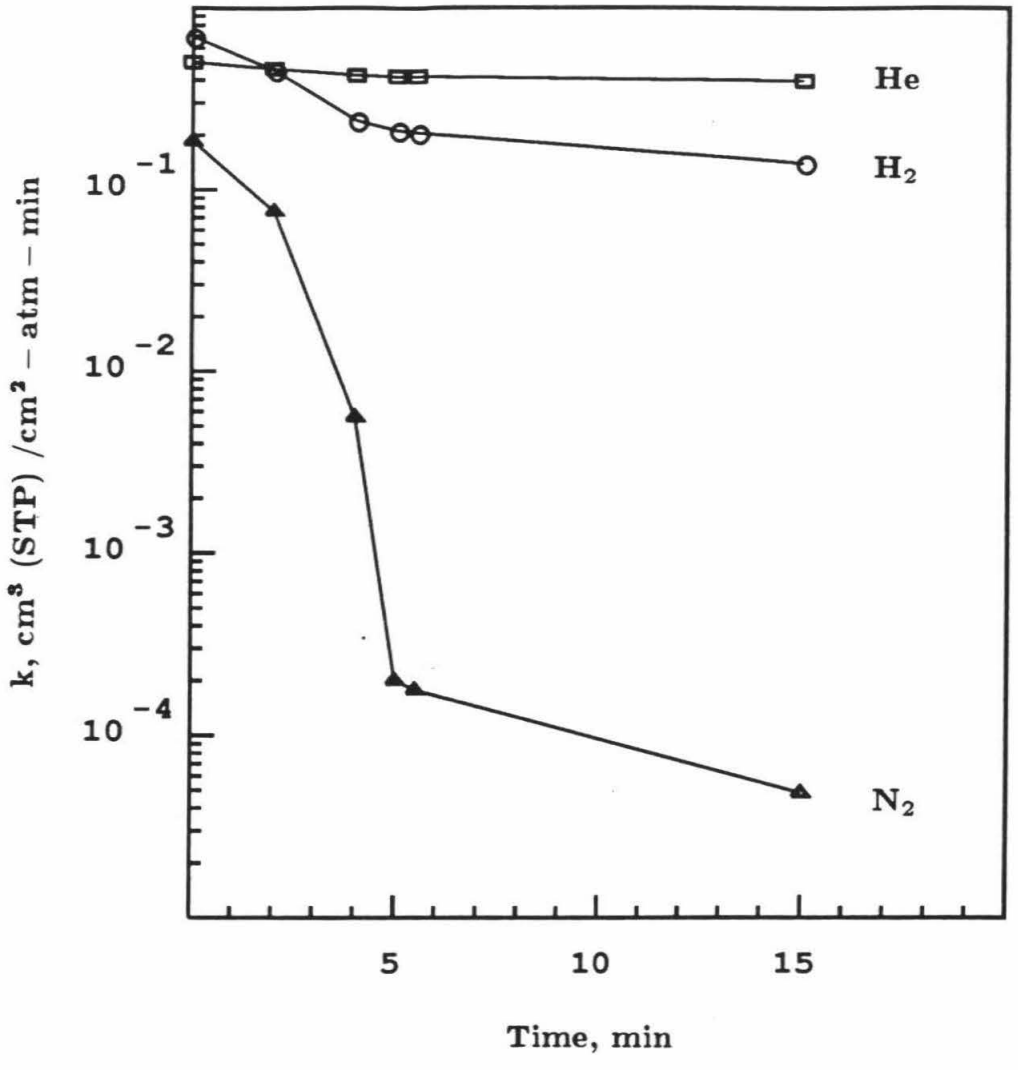

Figure 2.7 Evolution of film permeability during alternating periods of deposition and thermal treatment.

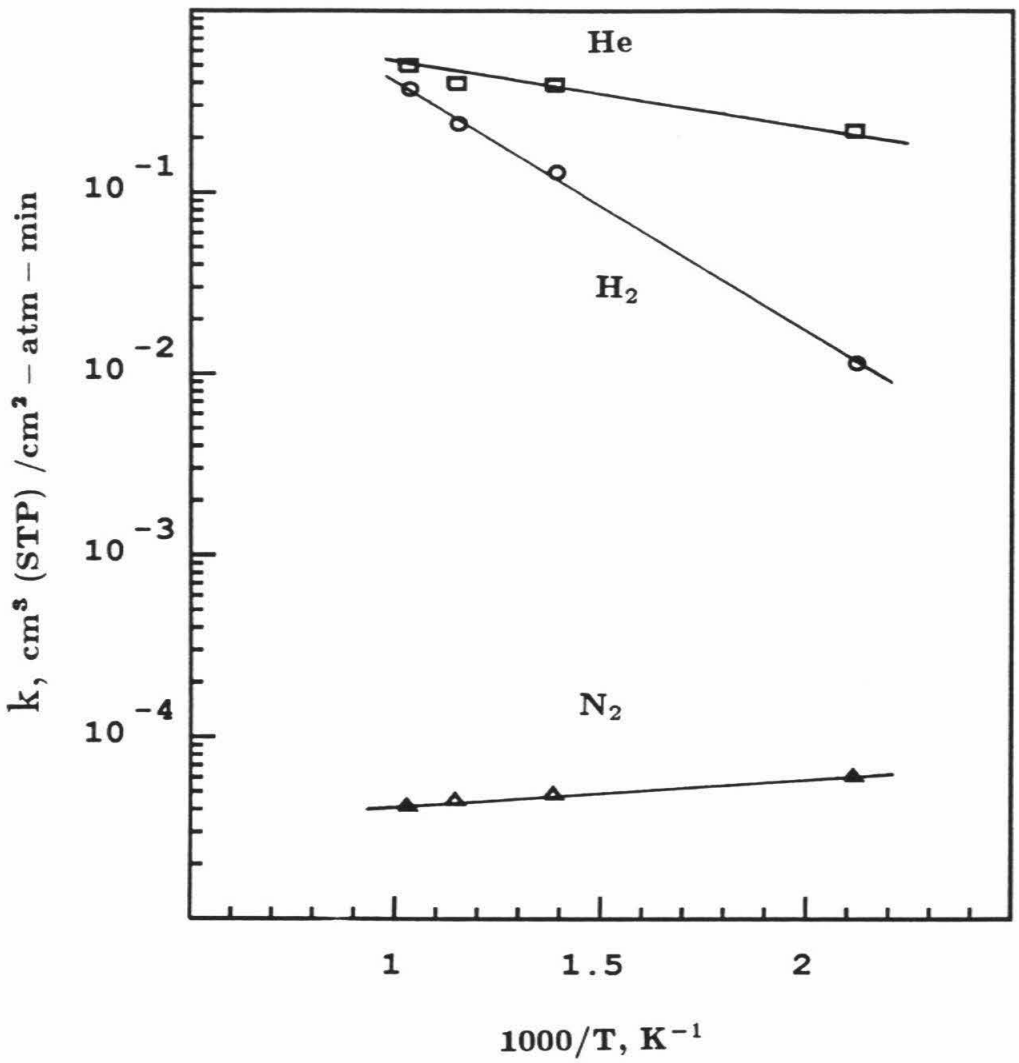

Figure 2.8 Permeation rates of H_2, N_2, and He vs. temperature.

CHAPTER V

Conclusions

The interaction of SO_2 with $\gamma - Al_2O_3$ and the deposition of H_2 permselective SiO_2 films have been investigated. The adsorption and oxidative adsorption of SO_2 on $\gamma - Al_2O_3$ have been examined at temperatures 500-700°C by Fourier transform infrared spectroscopy (FTIR) and thermogravimetric analysis (TGA). At temperatures above 500°C, most SO_2 adsorbed on the strong sites on alumina. The adsorbed SO_2 species was characterized by an IR band at 1065 cm^{-1}. The equilibrium coverage and initial rate of adsorption decreased with temperature suggesting a two-step adsorption. When $\gamma - Al_2O_3$ was contacted with a mixture of SO_2 and O_2, adsorption of SO_2 and oxidation of the adsorbed SO_2 to a surface sulfate characterized by broad IR bands at 1070 cm^{-1}, 1390 cm^{-1} took place. Sulfate formation was found to be reversible, but the reverse decomposition reaction took several hours even at 700°C. The results of a series of TGA experiments under different atmospheres ($SO_2 - O_2 - N_2$; $SO_2 - N_2$; $O_2 - N_2$; N_2) strongly suggest that surface SO_2 and surface sulfate involve the same active sites such that SO_2 adsorption is inhibited by already formed sulfate. The results also indicate a broad range of site strengths. SO_2 adsorbed on both weak and strong sites was involved in the oxidative adsorption at 700°C while SO_2 adsorbed on strong sites was mainly involved in the reaction at 500°C.

The desorption of adsorbed SO_2 and the reductive desorption of oxidatively adsorbed SO_2 have been investigated by microreactor experiments and thermogravimetric analysis (TGA). Temperature-programmed desorption (TPD) experiments of adsorbed SO_2 showed one broad SO_2 desorption peak. Temperature programmed reduction (TPR) experiments of adsorbed SO_2 showed that SO_2 was desorbed without significant reaction with H_2, when H_2 concentration was low, while considerable reaction occurred when 100% H_2 was used.

SO_2 adsorbed on the strong sites on alumina was reduced to sulfur and H_2S. The isothermal reduction experiments of oxidatively adsorbed SO_2 reveal that the rate of reduction is very slow below 550°C even with 100% H_2. The reduction product is mainly composed of SO_2. Small amounts of H_2S were produced at high temperatures, which seemed to be coming from the reaction of sulfur and H_2. TPR experiments of oxidatively adsorbed SO_2 showed that H_2S arose from a sulfate strongly chemisorbed on the surface.

Films of amorphous SiO_2 were deposited within the walls of porous Vycor tubes by SiH_4 oxidation in an opposing reactants geometry : SiH_4 was passed inside the tube while O_2 was passed outside the tube. The two reactants diffused opposite to each other and reacted within a narrow front inside the tube wall to form a thin SiO_2 film. Once the pores were plugged, the reactants could not reach each other and the reaction stopped. At 450°C and 0.1 and 0.33 atm of SiH_4 and O_2, the reaction was complete within 15 minutes. The thickness of the SiO_2 film was estimated to be about 0.1μm. Measurements of H_2 and N_2 permeation rates showed that the SiO_2 film was highly selective to H_2 permeation. The H_2:N_2 flux at 450°C varied between 2000-3000. Thermal annealing at 600°C somewhat reduced that selectivity. Thermal annealing in the presence of H_2O vapor further decreased the flux of hydrogen and increased the flux of nitrogen. Permeation of hydrogen is believed to occur through an activated diffusion mechanism.

Deposition of thin SiO_2 films within the wall of porous tubes can be used to make ceramic membranes for very selective hydrogen separation at high temperatures. Such membranes can be used to improve the conversion of equilibrium-limited reactions such as hydrogen sulfide decomposition. The opposing reactants technique could be applicable to the deposition of other oxide materials

by gas phase or liquid phase reactions.

Thin SiO_2 films were heat treated in different gas mixtures to determine their stability in functioning as high-temperature hydrogen permselective membranes. The films were formed within the walls of porous Vycor tubes by SiH_4 oxidation in an opposing reactants geometry. Film deposition was carried out at 450 °C in the presence and absence of water vapor. Immediately after formation, the films were highly selective to hydrogen permeation, having a H_2:N_2 permeability ratio of about 3000 : 1. The films were subsequently heat-treated at 450 - 700°C in dry N_2, dry O_2, N_2-H_2O, and O_2-H_2O mixtures. The permeation rates of H_2 and N_2 changed depending on the original conditions of film formation as well as on the heat treatment. Heating in dry N_2 slowly reduced the permeation rates of both H_2 and N_2. Heating in a N_2-H_2O atmosphere led to a steeper decline of H_2 permeability. But the permeation rate of N_2 increased or decreased according to whether the film deposition had been carried out in the absence or presence of H_2O vapor, respectively. Thermal treatment in O_2 caused a rapid decline of the permeation rates of H_2 and N_2 in films that were deposited under dry conditions. The decline was moderate in films deposited under wet conditions.